Haptic Steering Interfaces for Semi-Autonomous Vehicles

by

Akshay Bhardwaj

A dissertation submitted in partial fulfillment
of the requirements for the degree of
Doctor of Philosophy
(Mechanical Engineering)
in the University of Michigan
2021

Doctoral Committee:

Professor R. Brent Gillespie, Chair
Associate Research Scientist Tulga Ersal
Professor James Freudenberg
Professor Nadine B. Sarter

Akshay Bhardwaj

akshaybh@umich.edu

ORCID iD: 0000-0002-5261-3111

Acknowledgments

First and foremost, I would like to thank my advisor and mentor, Prof. Brent Gillespie. Thank you for providing me the guidance and freedom that I needed to complete this dissertation. I am grateful for all the opportunities you have given me over the years to grow as a scholar and person. Thanks for always pushing me to do better, being patient with me, and believing in me. Thanks also for giving me the opportunity to be a teaching assistant for your dynamic systems class, which was one of the most rewarding experiences of my time as a PhD student.

I would also like to thank my committee members—Prof. Nadine Sarter, Prof. Jim Freudenberg, and Dr. Tulga Ersal—who all have collaborated with me at one point or another. Thanks for providing inputs for my research and helping me write and revise my papers. Your unique perspectives and invaluable guidance have really helped me refine my ideas and this dissertation.

I am also grateful to my labmates and collaborators who have made this work possible. Thanks to Huckleberry Febbo, Yingshi Zheng, and Amirhossein Ghasemi for providing me the code to run the experiments presented in Chapter 2. Thanks to Xun Fu and Kunj Patel for helping me design the experimental apparatus, and thanks to Yidu Lu for helping me run the experiments presented in Chapter 3. Thanks to Dan Slavin, John Walsh, and Tan Zheng at the Ford Motor Company who helped me run the driving experiments presented in Chapter 4. Finally, thanks to Steven Cutlip for his input and assistance in producing simulation results in Chapter 5. Special thanks to friends and acquaintances who participated in the human subject experiments.

Many thanks to my sources of funding. This work was supported by the Toyota Research Institute, the Ford/U-M Alliance, and the Automotive Research Center at the University of Michigan. Their financial support enabled me to conduct my research and present my findings. Special thanks to the Ford/U-M Alliance, through which I also got a wonderful opportunity to work with the steering controls team at Ford that made the work presented in Chapter 4 possible.

I would also like to thank my friends in Ann Arbor who have been a great support system during my PhD. Steven, Abhishek, Lars, Sarah, James, Ilya, Robin, Alek, Tony, Alli – I am grateful that I got to know you. Thanks for all the fun times! I would also like to thank Deepak, Askari, and Abhimanyu, my college friends who are never far from me regardless of the time differences.

Finally, I am eternally grateful to my parents, Malti and Dayanand Bhardwaj, my brother, Mohit Bhardwaj, and my entire family in India for providing me unconditional love and support during my degree. Without them, none of this would be possible. This thesis is dedicated to them.

TABLE OF CONTENTS

LIST OF FIGURES

FIGURE

LIST OF TABLES

TABLE

ABSTRACT

Autonomous vehicles are predicted to significantly improve transportation quality by reducing traffic congestion, fuel expenditure and road accidents. However, until autonomous vehicles are reliable in all scenarios, human drivers will be asked to supervise automation behavior and intervene in automated driving when deemed necessary. Retaining the human driver in a strictly supervisory role, however, may make the driver complacent and reduce driver's situation awareness and driving skills which ironically, can further compromise the driver's ability to intervene in safety-critical scenarios. Such issues can be alleviated by designing a human-automation interface that keeps the driver in-the-loop through constant interaction with automation and continuous feedback of automation's actions. This dissertation evaluates the utility of haptic feedback at the steering interface for enhancing driver awareness and enabling continuous human-automation interaction and performance improvement in semi-autonomous vehicles.

In the first part of this dissertation, I investigate a driving scheme called Haptic Shared Control (HSC) in which the human driver and automation system share the steering control by simultaneously acting at the steering interface with finite mechanical impedances. I hypothesize that HSC can mitigate the human factors issues associated with semi-autonomous driving by allowing the human driver to continuously interact with automation and receive feedback about automation action. To test this hypothesis, I present two driving simulator experiments that are focused on the evaluation of HSC with respect to existing driving schemes during induced human and automation faults.

In the first experiment, I compare obstacle avoidance performance of HSC with two existing control sharing schemes that support instantaneous transfers of control authority between human and automation. The results indicate that HSC outperforms both schemes in terms of obstacle avoidance, maneuvering efficiency, and driver engagement. In the second experiment, I consider emergency scenarios where I compare two HSC designs that provide high and low control authority to automation and an existing paradigm that decouples the driver input from the tires during collision avoidance. Results show that decoupling the driver invokes out-of-the-loop issues and misleads drivers to believe that they are in control. I also discover a 'fault protection tradeoff': as the control authority provided to one agent increases, the protection against that agent's faults provided by the other agent reduces.

In the second part of this dissertation, I focus on the problem of estimating haptic feedback from

the road, or the road feedback. Road feedback is critical to making the driver aware of the state of the vehicle and road conditions, and its estimates are used in a variety of driver assist systems. However, conventional estimators only estimate road feedback on flat roads. To overcome this issue, I develop three estimators that enable road feedback estimation on uneven roads. I test and compare the performance of the three estimators by performing driving experiments on uneven roads such as road slopes and cleats.

In the final part of this dissertation, I shift focus from physical human-automation interaction to human-human interaction. I present the evidence from the literature demonstrating that haptic feedback improves the performance of two humans physically collaborating on a shared task. I develop a control-theoretic model for haptic communication that can describe the mechanism by which haptic interaction facilitates performance improvement. The model creates a promising means to transfer the obtained insights to design robots or automation systems that can collaborate more efficiently with humans.

CHAPTER 1

Introduction

1.1 Background and Motivation

Autonomous vehicles (AV) are predicted to have a significant impact on transportation. AVs are expected to reduce accidents, traffic congestion, parking needs, and fuel expenditure [1]. They are anticipated to bring significant national economic benefits and to make personal mobility accessible to those unable to drive [2]. AVs promise these benefits by taking the human out of the control loop and eliminating human faults from driving. Human faults in driving can arise from a number of reasons, such as, distraction, fatigue, impatience, and lack of information [3]. The automation system in an AV is capable of processing huge amounts of information more quickly, accurately, and tirelessly than human drivers which can enable it to remove human errors from driving [4].

However, albeit in different respects than human drivers, automation systems are also subject to faults and errors. Automation faults may arise from incorrect predictions, false activations and sensor dropouts [5,6]. A number of recent studies show that automation faults have resulted in more crashes per million miles driven than the crashes resulting from human faults [7–9]. This is despite the fact that AVs are still in the testing phase and are being driven at relatively low speeds. Based on public reaction to AV accidents, it is also likely that society would not tolerate automation faults at the same rates it currently tolerates human faults [5,10]. Therefore, until automation is fully reliable, human drivers will be required to intervene in automated driving.

Human intervention in automated driving results in so-called semi-automated or partially automated driving. Semi-automated driving can be explained using the levels of automation defined by the Society of Automotive Engineers (SAE) [11]. SAE describes six levels of automation based on the extent to which automation can support and assist driving tasks. Level 0 represents no automation and Level 5 represents full automation. Levels 1 through 3 are regarded as semi-automation whereas Level 4 is regarded as high automation [8]. The key difference between Level 4 and Levels 1-3 is that in Level 4 automation is responsible for serving as a "backup" during failures. On the other hand, Levels 1-3 place the fallback (or back-up) responsibility of the driving tasks on the human driver. In short, standard semi-automated driving puts the driver in a supervisory role

and expects the driver to remain available for immediate control take-over.

Generally, the capabilities that the human driver brings to semi-automated driving are complementary to the capabilities of automation systems. The human driver offers superior perception and judgment, is capable of making high-level and ethical decisions, brings rich prior experience, and brings an ability to generalize from one type of experience to another [4,12]. To improve safety in semi-automated driving, one might imagine a scheme that transfers driving authority to the human in situations where automation has a tendency to make faults and to automation where the human might be prone to errors. Ideally, human-automation team performance would exceed the performance of either human or automation acting alone and cognitive workload would be reduced for the human [13–15].

The problem of designing a scheme to support smooth authority transfers between human and automation is not new. Human-automation collaboration is prevalent in domains other than automotive engineering and the literature from these domains can help inform the design the human-automation interface in driving. Perhaps nowhere is human-automation teaming as old and as well-researched as it is in the aviation systems. Automation in aviation was first introduced in mid-Fifties in the form of auto-pilot, auto-throttle and flight director functions to reduce accidents due to human error [16]. Since then flight automation has significantly evolved to support various aspects of flying and has resulted in a significant drop in the number of accidents (see [16]). Apart from providing safety benefits, on-board automation has also resulted in dramatic reduction in pilot workload, operational costs, training costs, maintenance costs, and has improved job satisfaction, training flexibility, and operational capabilities for the pilots.

However, lessons from implementing automation in aviation systems also demonstrate that human-automation teams are prone to failures during transfers of control authority [17]. In particular, during control transitions, human operators are susceptible to misinterpreting and misappropriating responsibilities, and to losing vigilance and situation awareness [18]. Further, when working alongside highly automated systems, human operators are prone to human factors issues such as skill degradation, complacency and overreliance on automation's abilities [17,19]. Such issues lead to the misuse (overtrust) and disuse (distrust) of automation which can have an adverse effect on safety [20]. These unintended effects of adding automation are sometimes referred to as the "ironies of automation" in that rather than reducing problems for the human operator, adding automation can have a tendency to expand them [21].

Apart from aviation, human-automation collaboration issues have also been observed in maritime systems. In maritime operations, automation is frequently used to perform task allocation and path planning to reduce the workload for the human operator [22]. However, automation generated plans have been often found at odds with the human operator's expectations [23,24]. Even experienced human operators have encountered difficulties understanding automation's actions [22]. Moreover,

ship operators working with autopilot are experimentally shown to be prone to human factors issues such as skill degradation, automation complacency, and loss of situation awareness [22]. Some researchers however note that the reaction time required to return to a safe state is significantly larger in maritime systems resulting in a higher probability of saving accidents during automation failures than in the automotive and aviation systems [23].

In the manufacturing domain, human-automation collaboration has been demonstrated to reduce costs and increase both production quantity and quality [25,26]. In comparison to the other domains, the human operator is considered significantly more important in manufacturing because of their ability to interpret unplanned situations and handling complexity on the shop floor [27–29]. Automation is primarily regarded as a tool to extend human's cognitive capabilities, reduce human's physical and mental workload, and even improve worker's well-being [30–32]. But, like other domains, adding automation in manufacturing also results in additional physical and cognitive loads [33]. For example, a manufacturing robot collaborating with the human operator introduces the possibility of a collision which can adversely influence operational safety and technology acceptance [34]. Studies have shown that during production assembly, working alongside robots of a certain size and speed can increase the worker's stress and anxiety [35]. On the other hand, some researchers have found that an automation system that is transparent and that provides additional control to the operator can improve the worker's well-being and job satisfaction [31,36].

Human-automation collaboration has also become an indispensable part of the healthcare industry. In surgery, robots promise to enhance performance by automating tedious and difficult tasks and by improving surgeon's motor performance through stabilizing surgeon's tremor and enhancing the surgeon's sense of touch [37–39]. However, robots also fundamentally change the surgery task and impose new cognitive and physical demands on the surgeon and nurses [40,41]. During robotic surgery, in addition to performing the surgery task, surgeons become responsible for driving the robot which requires a higher degree of coordination and information from various sources and locations [42]. In robotic minimally invasive surgery, many visual cues for the surgeon are removed resulting in increased responsibilities for nurses who now have to continuously provide any missing information to the surgeon [43]. This added communication load opens up the possibilities for new failures or 'medical errors' which are directly or indirectly attributed to automation [44–46]. Due to safety concerns, researchers suggest that medical robots should most likely be never fully autonomous and that robots should only be designed to enhance surgeon's skills (and ideally extend their capabilities) but never take away the control completely from the human operator [42].

Synthesizing the literature from various domains, over the past three decades, researchers have proposed various guidelines for designing human-automation teaming schemes that can alleviate human factors issues in automation design [47,48]. Abbink et al. in [13] combined and rephrased

the guidelines appearing in the literature and put forth four design guidelines: "the human operator should (1) always remains in control [...]; (2) receive continuous feedback about the automation boundaries and functionality; (3) continuously interact with the automation; and (4) benefit from increased performance and/or reduced workload." These guidelines echo the ideas of human-centered automation design [47,48] which state that the human must always be in control and continuously interact with automation. The guidelines ensure that the human operator is aware of the intentions and limitations of the automation system and can utilize this information to decide whether to relinquish control to automation or to take over control from automation.

In vehicles, one way to provide continuous feedback of automation's actions to the driver is by combining the capabilities of human and automation at the steering wheel. Naturally, driving involves control through the steering wheel. The steering wheel can therefore act as an interface through which the human driver can both continuously exert control and receive feedback about automation action. By working simultaneously at the common interface, the human driver and automation system can then share the steering control and can together determine the final steering angle and vehicle trajectory. This approach to human-automation teaming is called shared control and has been investigated in a number of studies in the past two decades [49–53].

To enable constant interaction between human and automation during shared control, steering can be shared through haptic feedback. This scheme of control sharing is called haptic shared control (HSC), and it derives its inspiration from two humans cooperating on a manual task. In haptic shared control, the driver, the automation, and the vehicle (tires) are all coupled to one another through the steering wheel. The driver can simultaneously exert control and extract information about the automation action and tire-road interaction through haptic feedback. Automation acts on the steering system through a motor with a finite mechanical impedance roughly matching the driver's biomechanical impedance [13,54]. The human driver can override the automation command by increasing their steering grip thereby increasing their biomechanical impedance [55] or can acquiesce to the automation command by assuming a relaxed grip and reducing their impedance. The final steering maneuver in HSC depends on the actions and relative impedance of both the driver and automation system.

Haptic shared control satisfies a majority of human-automation interaction design guidelines that have appeared in the literature [13,47,48]. In particular, HSC can meet all four design guidelines defined by Abbink et al. that we mentioned earlier [13,18]. In HSC, the driver always remains in control of the vehicle. The driver continuously interacts with the automation system and receives constant feedback about automation's actions and intentions through haptic feedback. Additionally, the driver can negotiate driving authority with automation simply through muscle action and can do so smoothly and intuitively. A number of studies in the past have demonstrated the benefits of employing HSC in the automotive domain. HSC has been shown to improve driving performance in

terms of lane following [56], curve negotiation [51], lane changing [57], and reaction times [58].

Existing studies on HSC predominantly focus on evaluating its advantages in comparison to either conventional driving (with no haptic feedback) [12,18,50,51] or to other HSC designs [59,60]. Only a few studies compare HSC with alternative control sharing schemes and even fewer evaluate the response to faults of different control sharing schemes [61–63]. Evaluation of HSC with respect to the available driver-automation control sharing schemes can help understand the long-term benefits of HSC and can accelerate its adoption in commercial vehicles. Moreover, comparing performance during driver and automation faults can help determine the sensitivities of different control sharing methods to unanticipated scenarios on the road. The core of this dissertation is focused on the design and evaluation of HSC with respect to control sharing schemes currently available in commercial vehicles, especially in light of known human factors issues.

This dissertation evaluates the utility of haptic feedback at the steering interface for enhancing driver awareness and enabling continuous human-automation interaction and performance improvement in semi-autonomous vehicles. The dissertation focuses on four different research problems in the area of haptic interaction. The following subsections describe the specific motivation behind each problem.

1.1.1 Continuous versus Discrete Authority Transitions

In the first problem in this dissertation, I will compare the performance of HSC with control sharing schemes that support instantaneous transfer of control authority between human and automation. The transitions of control authority in HSC are continuous and occur over a period of time, which can make them intuitive to initiate. However, continuous transitions can be disadvantageous in scenarios in which fast and instantaneous shifts of control transfer might be necessary to ensure safety [61,62,64]. For example, during automation faults in semi-autonomous driving, drivers might want the option to disengage the automation system with a simple button press or other trigger. Such schemes of control sharing are available in commercial vehicles and are called discrete control sharing schemes in this dissertation, in contrast to continuous control sharing schemes such as haptic shared control where the authority transitions are continuous. In this dissertation, I will compare the performance of continuous and discrete control sharing schemes in the context of human and automation faults.

1.1.2 Coupled versus Decoupled Steering Interfaces

In a second related research problem, I will compare the performance of high and low automation impedance HSC with a scheme that decouples the driver during emergency situations. In emergency collision avoidance scenarios, drivers tend to reduce the efficiency of automation-initiated steering

maneuvers due to their slow reaction times [65,66]. One way to reduce the influence of driver input on automation-initiated maneuvers is by decoupling the driver and the steering wheel from the tires using a steer-by-wire system [67,68]. Another way is to keep the driver coupled with HSC but choose a large value of mechanical impedance (amount of control authority) in the automation design to attenuate driver input instead of completely removing it. However, high automation impedance may cause driver discomfort and even injury [62]. On the other hand, a low automation impedance HSC might be more comfortable to operate but may not suppress driver input [61]. In this dissertation, I will investigate the effects of automation impedance and driver decoupling on driving performance in emergency scenarios.

1.1.3 Road Feedback Estimation on Uneven Roads

The third research problem is focused on estimating haptic feedback arising from tire-road interaction. While this problem is not directly related to automation design, it is related to the design of driver assist systems in semi-autonomous vehicles. The haptic feedback from the road, or road feedback, plays a critical role in improving a driver's awareness of the state of the vehicle, the road conditions, and the environment [69–71]. As a result, a wide variety of driver assist systems use the estimates of road feedback in their control design [69,71–75]. Road feedback arises from tire-road interaction primarily in response to the steering angle applied by the driver and the variations in road profile. It can usually be expressed as a fraction of 'rack force' which is defined as the force transmitted from the tires to the steering rack of a vehicle, making the problems of estimating road feedback and rack force equivalent. Conventional methods of estimating rack force are only applicable for driving on flat roads [69,76–78]. In this dissertation, I will fill this research gap by presenting models that can be used to estimate road feedback on uneven roads.

1.1.4 Modeling Human-Human Haptic Communication

The final research problem is focused on yet another separate problem which aims at investigating how two humans physically interact with each other. The problem of designing an intuitive automation system that can cooperate with humans can be interpreted in a broader sense by understanding how two humans perform joint action, that is, how they coordinate their actions to produce a joint outcome. Whether it is dancing with a partner or moving a piece of furniture, humans are well known to coordinate their actions smoothly and accurately with each other [79]. The perceptual, cognitive, and motor processes that enable two humans to coordinate their actions with each other are complicated and have received increasing attention during the last decade in the fields of cognitive psychology and neuroscience [80,81].

Taking inspiration from the joint action literature, several researchers in haptics have tried to

investigate the role of haptic feedback in joint task performance. A number of studies have shown that haptic feedback can improve shared task performance between two humans [82–85]. However, this evidence remains strictly empirical without any investigation into the underlying mechanism by which haptic interaction facilitates performance improvement [86,87]. Yet insights into the mechanism enabling the performance improvements in human-human haptic interaction can be helpful in designing robotic systems that can collaborate efficiently with the human user or, in particular, in designing automation systems that can collaborate more efficiently with the human driver. In this dissertation, I will present a control theoretic model for haptic communication to describe the means by which haptic interaction between human and automation might improve driving performance. Note that the fields of joint action and human-human interaction are broader than the field of human-automation interaction. Therefore, the scope for this last research problem is wider than haptic shared control or human-automation interaction, and the results can in general be applicable to a wider variety of domains such as physical human-robot interaction, manual control, and psychophysics.

1.2 Contributions

This dissertation has four contributions.

The first contribution is the experimental findings demonstrating that driving performance is improved when the transitions of control authority between human and automation are continuous. In collaboration with the researchers at the Automated Modeling Lab at U-M, I conducted a driving simulator study with 11 participants in a within-subjects design to compare the obstacle avoidance performance between continuous and discrete control sharing schemes during human and automation faults. I implemented one continuous (HSC) and two discrete control sharing schemes under which the human would share control with the automation. In the first discrete control sharing scheme the transitions were initiated by the driver and in the second scheme the transitions were initiated by the automation. The findings indicated that the continuous control sharing scheme (HSC) supported the best overall team performance. Moreover, during automation faults, the team performance suffered most under the discrete control sharing scheme with automation-initiated transitions. On the other hand, during human faults, the performance was the lowest under the discrete scheme with driver-initiated transitions.

The second contribution is the experimental findings demonstrating the existence of a 'fault protection tradeoff': as the control authority provided to one agent increases, the protection against one agent's faults provided by the other agent reduces. In collaboration with the researchers at the THInC Lab at U-M, I designed a driving simulator study with 64 participants in a between-subjects design where I compared four steering interface design schemes in their ability to enable emergency

obstacle evasion during induced driver and automation faults. The drivers were either provided 1) no driving authority by decoupling their steering inputs from the tires, or a partial driving authority by keeping them coupled using HSC with a 2) low or 3) high automation impedance, or 4) full driving authority by removing the automation assistance. A model to describe physical driver-automation interaction was also developed to derive further insights into the differences in driver behavior across the four conditions. The results highlighted the fault protection tradeoff and showed that decoupling the drivers invoked out-of-the-loop issues and misled the drivers to believe that they were in control. Moreover, coupled drivers in the high impedance HSC group applied larger steering effort than the drivers in other conditions.

The third contribution is the development and validation of road feedback (rack force) estimators for driving on uneven roads. Using sensed steering angle and road profile inputs, the developed estimators enable road feedback estimation while driving on road slopes, cleats, and potholes, and produce independent estimates of the primary components of road feedback: road feedback due to steering angle and road feedback due to road profile. In particular, I developed three vehicle and tire dynamics based rack force estimators and, with help from the project collaborators at the Ford Motor Company, compared their performance by performing driving experiments on uneven roads. I also presented results from a simulation study to demonstrate that the developed estimators are capable of estimating the components of rack force.

The fourth contribution is a simplest competent control-theoretic model for haptic communication that is aimed at describing the performance improvement observed in human-human interaction. In collaboration with my colleagues at the HaptiX Lab at U-M, I performed a simulation study where I modeled human-human haptic communication through an object using internal force. Taking inspiration from [86], I adopted the McRuer Crossover model [88] to describe the tracking behavior of each human within the interacting human-human team. The results uncovered a haptic communication pathway that supported a means to describe how two agents acting together could outperform the two agents without haptic feedback or either agent acting alone, even when either agent acts only on half the mass. The results also suggested a mechanistic explanation for how the individual behavior could change due to haptic interaction. The fourth contribution is completely theoretical in nature and the results are yet to be validated through actual human subject experiments.

1.3 Dissertation Overview

This dissertation focuses on the design and evaluation of steering interfaces for semi-automated vehicles. The overarching aim is to evaluate the use of haptic feedback in the axis of steering as a means to improve driver awareness and enable continuous human-automation interaction in semi-autonomous vehicles. Each of Chapters 2 to 5 corresponds to one of the contributions listed in

Section 1.2. The chapters have been adapted from previously published manuscripts but much of the published content has been expanded and reorganized in order to improve the coherence and structure of this dissertation.

In Chapter 2, I compare the performance of HSC with two discrete control sharing schemes. I also evaluate all three control sharing schemes in situations involving human and automation faults. In Chapter 3, I investigate the effects of automation impedance and driver decoupling on driving performance in emergency scenarios. I also develop a model to describe physical driver-automation interaction that contributes meaningful insights to the analysis of the results.

In Chapter 4, I develop models that can be used to estimate rack force, and hence road feedback, for driving on a wide variety of road profiles, such as road slopes, cleats, and potholes. I also present a method to estimate rack force due to the driver's applied steering angle independent of rack force arising from road profile variations. In Chapter 5, I develop a theoretical model for haptic communication as a first step towards describing the performance improvement observed in human-human haptic interaction. I present simulation results that are supported by experiments conducted by researchers in past, and present future steps to experimentally validate the results.

Finally, in Chapter 6, I present concluding remarks and limitations of the dissertation and suggest future work.

CHAPTER 2

Continuous versus Discrete Authority Transitions during Obstacle Evasion

2.1 Introduction

Self-driving cars promise to eliminate accidents caused by human errors by removing human drivers from the control loop. Undeniably, vehicle automation is capable of faster response times, is able to handle greater amounts of information, and is able to process information more quickly and in a more repeatable fashion than human drivers. However, automation is subject to faults and misses as well, even if these rates have not been established given the short time self-driving cars have been on the road. It is also likely that society will not tolerate automation faults at the same high rates it currently tolerates human faults. Human drivers are therefore retained in a supervisory role or asked to remain available for immediate control take-over, oftentimes without warning [11]. Indeed, until self-driving cars are reliable in all foreseeable and even unforeseeable situations on the road, occasions will arise in which control must be transferred back to a human driver, perhaps on short notice.

Humans bring capabilities for driving a vehicle that are in large part complementary to the capabilities of automation systems. The human driver offers superior perception and judgment, is capable of making high-level decisions, brings rich prior experience, and brings an ability to generalize from one type of experience to another. To combine the capabilities of human and automatic drivers, one might imagine a scheme in which control authority is given to whichever agent outperforms the other in each traffic situation or time interval on the road. Ideally, safety would be guaranteed and the addition of automation would free attention for the human driver. However, a clean division and means of transitioning control authority is difficult to find.

Various schemes for combining the capabilities of human and automatic drivers have been proposed, differing primarily according to the manner in which control authority is transitioned between the two agents. Most commonly, transitions involve complete transfers of control authority that take place at discrete instants of time. That is, control authority is transferred as a lumped whole from human to automation system or back to human. These schemes are discrete control sharing schemes in this chapter. In such schemes, transfers may be initiated by the human driver, by

the automation system, or by a separate arbitration algorithm [89–91].

In one common discrete control sharing scheme, which I call *Autopilot* in this chapter, the human driver initiates the transitions, engaging and disengaging automatic control with a button-press or other trigger. For example, cruise control is conventionally engaged with a button press and disengaged with another button press or tap on the brake. Flight automation systems are likewise engaged by the pilot at discrete instants of time. In a second discrete control sharing scheme, which I call *Active Safety*, it is the automation system that initiates a transition of control authority. For example, automated emergency braking can be initiated when the automation system detects an impending collision for which human reaction time is too short [92]. Active safety systems have also been proposed that decouple the steering rack from the steering wheel during avoidance maneuvers [93,94].

However, smooth transfer of control authority between an automation system and human is notoriously difficult. From experience in deploying automation in aviation systems, we know that human/automation teams are particularly prone to errors during transfers of control authority [17]. Issues surrounding control transfer include a protracted time interval required for full transfer, mis-interpretation or mis-appropriation of responsibility (called mode errors), and incomplete understanding of vehicle or environment state (loss of situation awareness) [20,95,96]. Transitions involving such issues are often called "bumpy", and are implicated in compromises to safety [97,98].

To support smooth transfers of authority and harness the complementary features of human and automatic control, researchers have proposed various schemes under which control may be continuously shared between human and automation. Rather than complete transfers of control authority that occur at discrete instants of time, these schemes attempt to form a cooperative team that involves the human and automation system working together simultaneously. Such schemes are called continuous control sharing schemes in this chapter. With a continuous control sharing scheme it is ideally expected that the team performance would exceed the performance of either agent acting alone and cognitive workload would be reduced for the human [13–15,47,48,99].

The continuous control sharing scheme called *Haptic Shared Control* takes its inspiration from two humans cooperating on a manual task, for example moving a piece of furniture [49,56]. In continuous shared control of steering, the automation system acts through an instrumented and motorized steering wheel, but by design acts with a mechanical impedance that is roughly matched to the impedance of the human driver. The human driver can increase the impedance by increasing the steering grip and co-contracting the muscles to override the automation system, and can reduce the impedance by decreasing the steering grip and relaxing the muscles (while keeping hands on the wheel) to yield control to the automation system. Whether active or relaxed, the human driver can monitor the actions of the automation system through haptic feedback [13,59,100,101]. At all times, the final steering maneuver in *Haptic Shared Control* depends on the actions and the relative

impedance of both the human driver and the automation system. The automation is generally designed to have a constant finite impedance but it can also be equipped with the ability to vary its impedance and to adjust its relative driving authority [49,100].

While the underlying processes and degrees may differ, it is clear that both human drivers and automation systems are subject to misses, faults, or errors. A given scheme for combining human and automatic control must be robust to unanticipated conditions, misses, faults, and errors. As Bainbridge [21] noted, adding automation may expand rather than reduce problems for the human operator, especially when faults occur.

Operators left with the task of monitoring the driving situation and automation behavior are challenged precisely where their skills are poor—in maintaining vigilance [102]. Taking over control from an automation system in unexpected conditions usually requires additional cognitive rather than manual skills, and skills that may be difficult to develop and maintain [21]. Few studies have compared the response to faults of different control sharing schemes. Yet studies comparing performance across schemes are critical to determine gross sensitivities to unexpected conditions. Because faults are often sudden occurrences, schemes that support rapid transitions such as button presses may hold advantages. On the other hand, schemes that use the steering wheel as the interface for changing the balance of control authority rather than a button press might support smoother or earlier transitions.

For example, according to Itoh et al. [103], control sharing methods like *Haptic Shared Control* are effective at supporting smooth shifts of authority during automation-induced faults. The hypothesized mechanism is that the haptic feedback present in *Haptic Shared Control* enables the human driver to quickly understand and fix automation errors or faults by modulating their impedance [103]. In a 2016 survey conducted by Wolf on 1000 respondents [10], it was found that a majority of human drivers would not wish to completely relinquish control to an automation system. *Haptic Shared Control* also fulfills this requirement by giving neither the human nor the automation system full authority at any point of time while driving.

A majority of *Haptic Shared Control* designs are only concerned with human automation cooperation at the "operational level" (or the "control level") [104,105]. In automotive systems, cooperation at the "operational level" involves collaboratively generating a trajectory or a path using both the automation and driver inputs to determine the final steering wheel angle [104]. Although such embodiments of *Haptic Shared Control* still provide a smooth shift of authority during driving, they can suffer from conflicts between the driver and the automation that arise when there is a difference between the actions and intentions of the human driver and the automation system. Conflicts are undesirable as they can cause annoyance, can deteriorate driving performance and, in worst-case scenarios, can result in accidents [103,104].

Even though the conflicts can be dangerous, Itoh et al. [103] maintain that neither human nor

machine should be given the full authority during driving and that control should still be shared. One way to manage conflicts while also sharing control is to perform cooperation at a higher "tactical" level as suggested in [104,105]. For example, in [101], Mars et al. integrated the design of *Haptic Shared Control* system with a driver model that led to fewer conflicts and more agreements between the driver and the automation [106].

The surveys in [89] and [90] review the literature on control sharing schemes such as *Autopilot* and *Active Safety* that have appeared in commercialized vehicles. but do not include an assessment of schemes like *Haptic Shared Control* in which control authority is graded on a continuum between human and automation. Rather than comparing performance across schemes, studies on control transitions appearing to date have investigated the dependence of performance under one scheme to variation in certain parameters. For example, Ericksson and Stanton [107] found less erratic driver steering input in the first 20 seconds after taking over from automation in self-paced conditions than in automation-paced conditions. Desmond et al. [108] found similar degraded performance in the first 20 seconds after resuming control from automated driving following an automation failure compared to compensating for a wind gust in manual driving.

In this chapter I pit the schemes *Autopilot*, *Active Safety* and *Haptic Shared Control* against one another in a simulated driving scenario in which faults occur at fixed rates but at unpredictable times. Faults are induced simply by making obstacles invisible to either the human driver or the automation system. Similar to the implementation in [94,104] the automation system is based on Model Predictive Control (MPC) and takes the current steering angle as an input to plan a path that conforms to the intention of the human driver to reduce conflicts. In Section 2.2 I present the details of the MPC-based automation system and the driving simulator and elaborate on the implementation of *Autopilot*, *Active Safety* and *Haptic Shared Control*. I describe an experiment in which I asked 11 participants to drive with the assist of the automation system under these three control sharing schemes. To establish baseline performance, I also asked the same participants to drive the course independently (*Manual Control*). The automation system also drove the course independently (*Automatic Control*). In Section 2.3 I present experimental results followed by a discussion of the results and conclusion in Sections 2.4 and 2.5 respectively.

2.2 Methods

2.2.1 Participants

Eleven test participants (10 male and 1 female) between the ages of 23 and 40 years were recruited for the study. Participants did not receive compensation. All participants had normal or corrected-to-normal vision and signed informed consent in accordance with University of Michigan human participant protection policies.

Each participant was instructed on the four conditions *Manual Control*, *Active Safety*, *Autopilot*, and *Haptic Shared Control* and given a chance to familiarize themselves with these conditions in a training session up to 15 minutes long. The name of each condition was displayed on the corner of the screen during each run. Each participant was asked to complete the four experimental conditions with three repetitions each. The order of conditions including repetitions was randomized. The vehicle speed was set constant at 10 m/s, and each test run was about 90 s long.

Participants were informed about the existence of obstacles that would be invisible to them or not detected by the automation system. They were instructed that the automation system might be able to help them avoid obstacles that were invisible to them and that they might be able to avoid obstacles that were not detected by the automation system.

2.2.2 Apparatus

A low-fidelity fixed-base driving simulator was developed featuring a motorized steering wheel (see Fig. 2.1). A DC motor (AmpFlow A28-150, Belmont, CA) was coupled to the steering wheel (Speedway 38 cm solid aluminum wheel, Lincoln, NE) through a timing belt with a 72:15 mechanical advantage, making up to 66 Nm torque available to be imposed on the human driver. A 10,000 count per revolution optical encoder (US Digital HB6M, Vancouver, WA) was attached to the steering shaft and the motor was equipped with a 2048 count per revolution optical encoder (US Digital HB6M). In addition, the steering wheel was equipped with a red button within easy reach of a participant's thumb on the steering wheel. The virtual driving environment was displayed on a 50 cm LCD Widescreen monitor positioned about 140 cm from the participant.

The computational hardware supporting the driving simulator included two computers: a PC (Intel Core i7-3770) to support the automation system and a second PC (Intel Core i5) to support the vehicle model, virtual driving environment, and control of the motorized steering wheel. Additional Arduino micro-controllers (Arduino Mega 2560) supported encoder reading and production of pulse-width-modulated (PWM) signals for the motor amplifier (Robot Power OSMC, Olympia, WA). The Arduino code was cycled at 350 Hz. The two PCs communicated every 10 ms through a dedicated User Datagram Protocol (UDP) link. The automation computer received vehicle states including steering angle and obstacle positions and responded with a steering angle setpoint. Data including vehicle position and heading, steering wheel angle, obstacle positions, and motor commands were logged at 100 Hz. The graphical display was rendered at 20 Hz.

The virtual environment was adapted from [109]. It was created using the Matlab-Simulink Virtual Reality Toolbox, and appeared as shown in Fig. 2.2. It contained a notional High Mobility Multipurpose Wheeled Vehicle (HMMWV) and a road with various landmarks that provided motion cues during driving. The vehicle traveled at a constant speed of 10 m/s, and neither the participant nor the automation system had any control over speed. The road (in gray) was 8 m wide with a

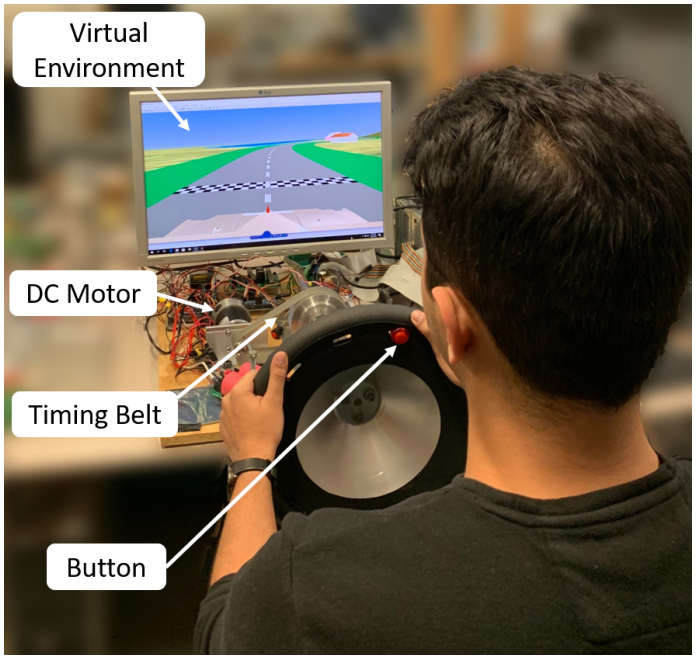

Figure 2.1: Fixed base driving simulator: experimental setup.

white dashed centerline. Shoulders of 6 m width (in dark green) were located on either side of the road. The entire track was 850 m long, with 5 left turns and 4 right turns. An overview of the track is shown in Fig. 2.2 (A). Ten cylindrical obstacles with a 2 m diameter and 0.5 m height were distributed along the track's centerline at intervals that were set randomly between 40 and 50 m. A red notch was visible on the vehicle's hood as a center reference.

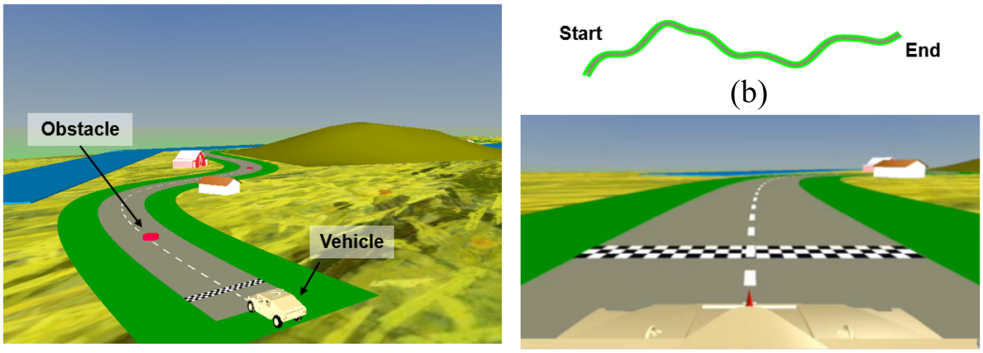

(a) (b) (c)

Figure 2.2: (a) Vehicle, track, landmarks, and obstacles in the virtual environment; (b) An overview of the track; (c) Scene visible to participants.

2.2.3 Automation System Design

Model Predictive Control (MPC) was used to develop an automation system capable of steering the vehicle along the track centerline while avoiding obstacles. The nonlinear MPC formulation described in [110,111] was adopted and was designed by my collaborators Huckleberry Febbo and Yingshi Zheng. Inputs to the controller included the vehicle's state, the position and size of the obstacles, and data describing the track. To capture the dynamics of the vehicle, the 3 degrees of freedom dynamic model developed in [112] was used. This vehicle model has seven states and uses a pure-slip Pacejka tire model [113] to calculate the lateral forces on the tires. The states include the vehicle's global position (x, y), lateral speed $V(t)$, yaw rate $\omega_z(t)$, heading angle $\Psi(t)$, steering angle $\delta(t)$, and longitudinal speed $U(t)$; the control input is the steering rate $\dot{\delta}(t)$. To prevent rollover, the vertical loads on the tires were constrained to be greater than 1000 N. Load transfer effects were accounted for in the vertical tire force computations.

The cost function included two terms: a first term to minimize the steering rate control effort $\dot{\delta}(t)$ and a second term to minimize the distance between position coordinates of the vehicle (x, y) and the coordinates of a closest target point on the track centerline (x_t, y_t). The cost function is expressed as follows:

$$\begin{aligned} J =& w_{\dot{\delta}} \int_{t_0}^{t_0+t_p} \dot{\delta}(t) \mathrm{d}t \\ &+ w_{\text{path}} \int_{t_0}^{t_0+t_p} (x(t) - x_t(t))^2 + (y(t) - y_t(t))^2 \mathrm{d}t, \end{aligned} \tag{2.1}$$

where $w_{\dot{\delta}}$ and w_{path} were constant weighing terms set to 0.05 and 10.0, respectively, t_0 indicated the time at which each MPC computation began, and t_p encoded a time horizon of 6 s.

Elliptical hard constraints ensured that the vehicle avoided collisions with perceived obstacles [111]. These obstacle avoidance constraints were expressed as

$$\begin{aligned} (x(t) - \mathbf{x_{obs}}[i])^2 + (y(t) - \mathbf{y_{obs}}[i])^2 > (r_{\text{obs}} + sm)^2, \\ i = 1, 2, \ldots Q, \end{aligned} \tag{2.2}$$

where r_{obs} is the obstacle radius, sm is a safety margin that accounts for the vehicle's size and Q is the total number of obstacles. The vectors $\mathbf{x_{obs}}$ and $\mathbf{y_{obs}}$ contain the position and radii of the obstacles that are shown to the automation system.

At the beginning $t = t_0$ of computations, the states of the vehicle, steering angle θ, and coordinates of obstacles visible to automation were sent from the driving simulator computer to the automation computer over the network connection. At $t = t_0 + t_s$, where $t_s = 0.3$ s, the computed cost-minimizing steering trajectory θ_{A} was passed back to the driving simulator and

used as a setpoint trajectory for the steering wheel. While this setpoint trajectory was used for a period of another $t_s = 0.3$ s, the vehicle state and steering angle were sampled again and the prediction horizon was shifted forward in time. Using the new values, the next cost-minimizing steering trajectory was delivered with the next iteration of the MPC algorithm.

A simple proportional-integral (PI) control law was used to generate the motor command torque τ_{A} as a function of the setpoint trajectory θ_{A} generated by the automation system and the current steering angle θ:

$$\tau_{\mathrm{A}}(t) = k_{\mathrm{p}}(\theta_{\mathrm{A}}(t) - \theta(t)) + k_{\mathrm{i}} \int_{t_{\mathrm{eq}}}^{t} [\theta_{\mathrm{A}}(T) - \theta(T)]dT, \tag{2.3}$$

where k_{p} and k_{i} are the proportional and integral gains. t_{eq} is defined as the time instant at which the steering angle $\theta(t)$ was found to be equal to the set-point trajectory $\theta_{\mathrm{A}}(t)$ for at least five consecutive sampling instances. At t_{eq}, the integral term in the control law was reset to zero to prevent unnecessary accumulation of past errors in the commanded torque. Finally, the steering controller command τ_{A} was passed to the Arduino micro-controller where a PWM signal was generated and applied to the motor amplifier that produced the command torque at the motor.

2.2.4 Experimental Conditions

The experiment involved three conditions in which control was shared between a human and automation, called *Active Safety*, *Haptic Shared Control*, and *Autopilot*. In addition, I included two conditions in which control was given in whole (without transitions) to either the human, called *Manual Control*, or the automation, called *Automatic Control*.

Under each condition, participants were asked to follow the road, keeping as close as possible to the centerline, but to avoid obstacles. Obstacles were invisible until the vehicle was within 40 meters range. Therefore, with a constant speed of 10 m/s, the participant had about 4 s to recognize and avoid an obstacle.

Ten obstacles were encountered on each run, though 2 obstacles chosen at random were made invisible to the driver (by not showing them on the monitor). These events were termed "Human Faults". Another 2 obstacles on each run were not detected by the automation system (their coordinates were not passed to the automation computer). These events were termed "Automation Faults". That is, of the 10 obstacles encountered in each run, only 6 were "No Fault" obstacles while 2 were "Human Fault" and another 2 were "Automation Fault" obstacles. The particular obstacles falling into each of these three bins were randomized in each run. The driver was informed that 2 of the 10 obstacles would not be visible on the screen but would be detected by the automation system and of the remaining 8 visible obstacles, 2 would not be detected by the automation.

Table 2.1: Steering Control Parameters for the Control Conditions

Control Condition	k_p (V/rad)	k_i (V/rad/s)
Manual Control	–	–
Active Safety	55	100
Haptic Shared Control	40	80
Autopilot	40	80
Automatic Control	40	80

2.2.4.1 *Manual Control*

In the *Manual Control* condition the driver was solely responsible for steering the vehicle; the automation system was not involved. The only torque feedback that the driver received from the motorized steering wheel was a self-aligning torque associated with the simulated tire-road interaction.

2.2.4.2 *Automatic Control*

To characterize the performance of the automation system alone, the MPC-based automation system described above in Section 2.2.3 drove the course without any human intervention. The automation system acted on the physical steering wheel through the motor, producing a steering trajectory that included the influence of the simulator hardware dynamics and PI control. The control gains listed in Table 2.1 were used.

2.2.4.3 *Active Safety*

In the *Active Safety* condition, the automation system took over complete control in the presence of obstacles that it detected and deemed likely to be hit without intervention. The automation system utilized the MPC algorithm described in Section 2.2.3. The gains in Table 2.1 rendered the automation desired steering angle with a high impedance and ensured that the automation system could wrest control from the driver whose hands remained on the steering wheel. The automation system in the active safety condition was not designed to bring the vehicle back to the path after passing the obstacle. In fact, once the vehicle successfully avoided a given obstacle, the automation system turned off and the driver became responsible for steering the vehicle back to the centerline.

2.2.4.4 *Autopilot*

The *Autopilot* system utilized the same automation system as the *Automatic Control* system, except in this case the human was charged with monitoring system performance and intervening if they thought the automation system did not recognize an obstacle. The human could intervene by

grasping the steering wheel and pressing the red button to disengage the automation system. That is, when the red button was pressed, the control task was given completely to the human. After driving around the obstacle in question the human driver could re-engage *Automatic Control* by pressing the red button again. A symbol on the screen indicated whether the automation system was engaged or disengaged. When the automation system was engaged, the motor acted on the steering wheel with the PI gains shown in Table 2.1. During such periods, the participant could either relax and let the motor action determine the steering trajectory or could let go of the steering wheel.

2.2.4.5 *Haptic Shared Control*

In the *Haptic Shared Control* condition, the participant kept both hands on the steering wheel and was free to act at any time. Likewise, the automation system was free to apply torque throughout a run. When the driver decided to take over control, they could increase their impedance and impose higher torques on the steering wheel. Conversely, the driver could yield control to the automation system by decreasing their impedance (relaxing) and applying a lower torque on the steering wheel. As in the other conditions, the automation system used the vehicle states as inputs to its MPC algorithm to generate control action using the motor coupled to the steering wheel. The steering controller gains were selected so that the participant could easily override, or "edit" the automation system's command (see Table 2.1).

2.2.5 Performance Metrics

Three metrics were defined to quantify driving performance and enable comparison across conditions and participants. The first metric, Obstacle Hits, was simply the number of obstacle collisions that occurred within a given run. Another two metrics, called Approach Distance and RMS Lateral Deviation, were defined to characterize driving performance around the obstacles that were successfully avoided as shown in Fig. 2.3. Both Approach Distance and RMS Lateral Deviation were defined with reference to points A and B, A being the point at which the vehicle trajectory first deviates by more than 1 m from the centerline, and B the point at which the vehicle trajectory arrives again within 1 m of the centerline (see Fig. 2.3). The Approach Distance is defined as the distance along the centerline from point A to the center of the obstacle O. For each point sampled at 10 ms along the vehicle trajectory, the closest point on the centerline was interpolated. Lateral deviation was then defined as the closest distance to the centerline, for each evenly sampled point on the vehicle trajectory. The RMS Lateral Deviation was the root mean square of the lateral deviation between points A and B. Note that Approach Distance and RMS Lateral Deviation were computed only for obstacles that were not hit.

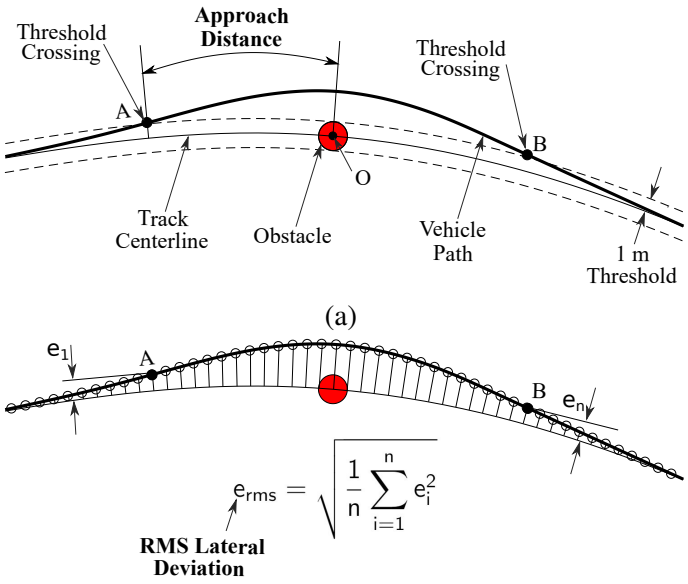

Figure 2.3: A typical obstacle avoidance trajectory taken by a participant is used to define the performance metrics Approach Distance and RMS Lateral Deviation. (a) The track centerline and vehicle path are used to define the location of points A and B that lie on the vehicle path at a lateral distance of 1 m from centerline when the vehicle approaches and departs the obstacle. The distance between point A and obstacle center O along the centerline is defined as the Approach Distance. (b) Starting at point A on the vehicle path, the lateral deviation is denoted by e_1, then e_2 and so on until the lateral deviation at point B is denoted by e_n. RMS Lateral Deviation is then the root mean square of the values of lateral deviation between points A and B.

2.2.6 Data Analysis

The present study employed a 3×3 factorial design, with the two factors being: Control Sharing Condition (*Active Safety*, *Haptic Shared Control*, and *Autopilot*) and Fault Type (No Fault, Human Fault, and Automation Fault). The Control Sharing condition was varied between trials and the Fault condition was varied within trials. The dependent measures were: (1) the percentage of Obstacle Hits, (2) the RMS Lateral Deviation, and (3) the Approach Distance. Data analysis was performed using Generalized Linear Mixed Modeling method in IBM SPSS Statistics version 25. The Obstacle Hit metric was analyzed using the binary logistic regression procedure whereas the RMS Lateral Deviation and Approach Distance were analyzed using the linear modeling procedure. The Control Sharing condition and Fault Type were chosen as independent factors. A p-value of 0.05 was set to determine significance. Post-hoc, sequential Bonferroni method was applied to determine significant differences.

2.3 Results

2.3.1 Obstacle Hits

Each of the eleven participants and the automation system, when driving by themselves, were able to drive the course keeping close to the centerline and without hitting obstacles. And as expected, without seeing or detecting obstacles, the eleven participants and the automation system drove right through the obstacles located on the centerline. Thus the best case scenario for forming a human-automation team under conditions in which at least one agent saw every obstacle could be expected to produce perfect performance. However, this was not the case.

Table 2.2: Obstacle Hits for each Control Sharing Condition separated by Fault Conditions

	No Fault		Human Fault		Automation Fault		**All Fault Conditions**	
	Obstacles Hit	%Hits	Obstacles Hit	%Hits	Obstacles Hit	%Hits	**Obstacles Hit**	**%Hits**
Active Safety	3/198	1.5%	19/66	28.8%	0/66	0%	**22/330**	**6.7%**
Haptic Shared Control	1/198	0.5%	3/66	4.5%	2/66	3%	**6/330**	**1.8%**
Autopilot	5/198	2.5%	4/66	6.1%	1/66	1.5%	**10/330**	**3%**
All Control Conditions	**9/594**	**1.5%**	**26/198**	**13.1%**	**3/198**	**1.5%**	**38/990**	**3.8%**

Table 2.3: Obstacles Hits for Baseline Conditions separated by Fault Conditions

	No Fault		Human Fault		Automation Fault		**All Fault Conditions**	
	Obstacles Hit	%Hits	Obstacles Hit	%Hits	Obstacles Hit	%Hits	**Obstacles Hit**	**%Hits**
Manual	0/264	0%	66/66	100%	–	–	**66/330**	20%
Automatic	0/24	0%	–	–	6/6	100%	**6/30**	20%

As shown in Table 2.2 and Table 2.3, a lower percentage of obstacles were hit in the three Control Sharing conditions in comparison to the 20% obstacles that were hit in both the *Manual Control* and the *Automatic Control* conditions. Considering only Fault Conditions, in the *Manual Control* condition, 100% of the obstacles that simulated Human Faults were hit whereas only 4.5% were hit in the *Haptic Shared Control*, 6.1% were hit in the *Autopilot*, and 28.8% were hit in the *Active Safety* condition. Likewise, in the *Automatic Control* condition 100% of the obstacles that simulated Automation Fault were hit whereas only 3% were hit in the *Haptic Shared Control*, 1.5% were hit in the *Autopilot*, and no obstacles were hit in the *Active Safety* condition. Between control sharing conditions, the *Active Safety* condition resulted in the highest percentage of obstacle hits (6.7%) whereas the *Haptic Shared Control* condition resulted in the lowest percentage of hits (1.8%). On the other hand, between Fault Conditions, Human Fault resulted in the highest percentage (13.1%) whereas both Automation Fault and No Fault resulted in an equal percentage of hits (1.5%).

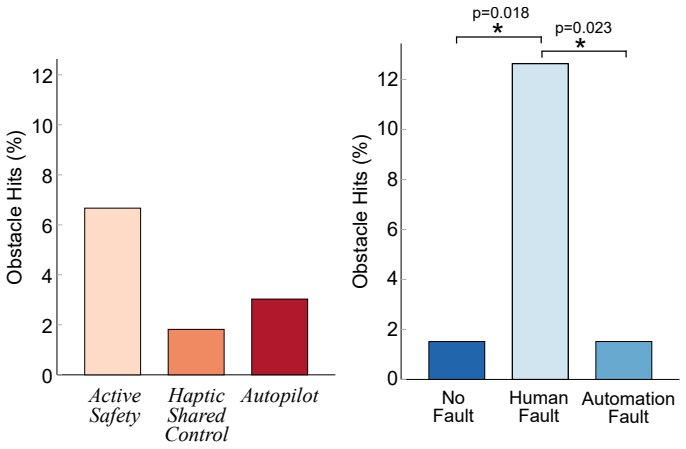

(a) (b)

Figure 2.4: (a) Percent obstacle hits by Control Condition, (b) Percent obstacle hits by Fault Condition. The asterisks on the lines linking two bars indicate a significant difference between two conditions.

Analysis on the Obstacle Hit data indicated that the Control Sharing condition was not a significant predictor of an obstacle hit ($F(2, 981) = 0.923, p = 0.398$). Fault Condition, on the other hand, had a significant main effect on the likelihood of a hit ($F(2, 981) = 6.555, p = 0.001$). Post-hoc comparisons indicated that the possibility of an obstacle hit for the Human Fault condition was significantly higher than for both the Automation Fault ($p = 0.023$) and for the No Fault ($p = 0.018$) conditions (also indicated in Fig. 2.4 (b)). However, since the interaction effect between Fault Condition and Control Sharing condition was also found to be significant ($F(4, 981) = 2.579, p = 0.036$), it was difficult to generalize the effect of Fault Condition on all control conditions. To further understand this, I looked at the simple main effect of Control Sharing condition on obstacle hits for each of the three Fault Conditions and of Fault Condition on obstacle hits for each of the three Control Sharing conditions.

The analysis showed that only for the Human Fault condition, Control Sharing condition had a significant effect on the likelihood of a hit ($F(2, 981) = 7.265, p = 0.0007$). Post-hoc sequential Bonferroni test revealed that for the Human Fault condition, *Active Safety* had a higher likelihood of an obstacle hit than *Autopilot* ($p = 0.001$) and *Haptic Shared Control* ($p = 0.0007$) conditions. For any other Fault Type, the Control Sharing Condition had no effect. Likewise, only for the *Active Safety* condition, the Fault Condition had a significant effect on obstacle hits ($F(2, 981) = 10.032$ $, p < 0.0005$). Post-hoc test revealed that for *Active Safety*, the Human Fault condition was found to result in a higher number of hits than Automation Fault ($p < 0.0005$) and No Fault ($p < 0.0005$) conditions. The results of post-hoc tests for the simple main effects analysis are summarized in Figure 2.5. Hence the main effect of Fault Type was only due to the large number of hits in the *Active Safety* condition for Human Fault and therefore this effect could not be generalized to the

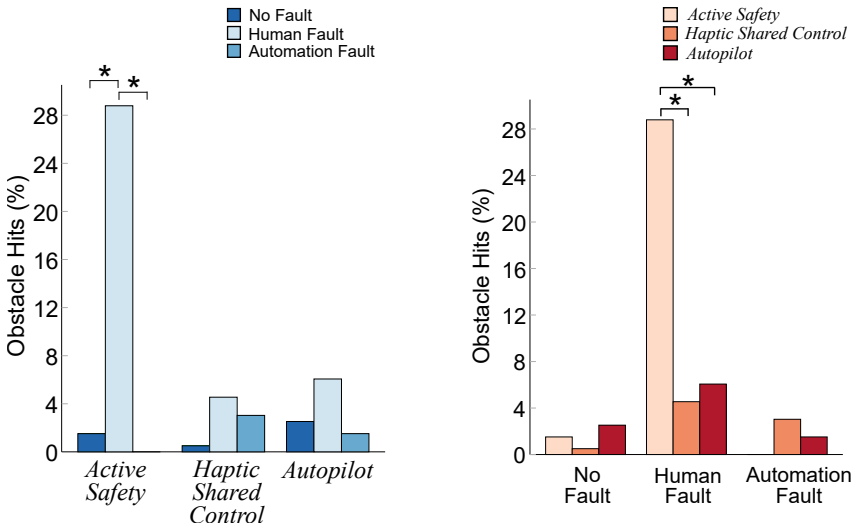

Figure 2.5: Percent Obstacle Hits (a) for each Fault Condition grouped by Control Condition and (b) for each Control Condition grouped by Fault Condition. The asterisks on the lines linking two bars indicate a significant difference between two conditions.

Haptic Shared Control and *Autopilot* conditions.

2.3.2 RMS Lateral Deviation

The RMS Lateral Deviation was used to gauge which control sharing condition resulted in the most "efficient" maneuver around the obstacles. The means of RMS Lateral Deviation are presented in Table 2.4 for all the Control Sharing conditions including *Manual* and *Automatic* conditions. As mentioned earlier, the RMS Lateral Deviation was only computed for obstacles that were successfully avoided. Therefore a lower value of RMS Lateral Deviation for a condition indicates that the participant found it relatively easier to use that control scheme to make an efficient maneuver around the obstacle. This becomes more apparent when we look at the trajectories presented in Fig. 2.6 and compare them with the numbers in Table 2.4. A lower mean value of RMS Lateral Deviation for a condition in Table 2.4 corresponds to a lower spread (indicated in grey) of trajectories for that condition in Fig. 2.6, and to an average trajectory (indicated by black solid line) that deviates less from the centerline.

Since the case of Automation Fault was not possible in the *Manual Control* condition (because automation was absent), and the case of Human Fault - which resulted in hits - was removed while computing the metric, only the case of No Fault was pertinent for the *Manual Control* condition. Likewise, only the case of No Fault was pertinent for the *Automatic Control* condition. Looking at the means presented in Table 2.4, in the No Fault case, RMS Lateral Deviation values with *Haptic Shared Control* and *Autopilot* were lower than *Manual Control* condition and was similar to the

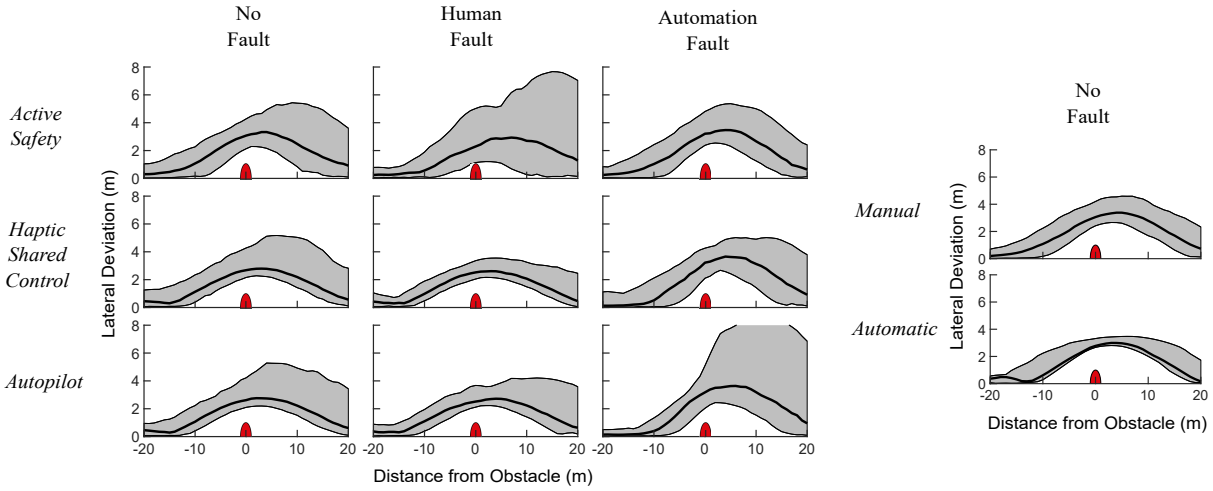

Figure 2.6: Plots depicting driving trajectories around the obstacles computed across all 11 participants for each control condition and fault condition. The black solid line indicates the 50th percentile of lateral deviation. Two traces enveloping the black solid line shade the 5th to 95th percentile intervals for the lateral deviation. Obstacles are shown to scale by red half ellipses.

Table 2.4: Means and Standard Errors (S.E.) of RMS Lateral Deviation for all Control Conditions separated by Fault Conditions

	No Fault		Human Fault		Automation Fault		**All Fault Conditions**	
	Mean	S.E.	Mean	S.E.	Mean	S.E.	**Mean**	**S.E.**
Active Safety	2.71	0.07	2.83	0.12	2.69	0.10	**2.74**	**0.07**
Haptic Shared Control	2.41	0.07	2.17	0.10	2.87	0.10	**2.48**	**0.07**
Autopilot	2.40	0.07	2.33	0.10	3.15	0.10	**2.63**	**0.07**
All Control Conditions	**2.51**	**0.05**	**2.44**	**0.08**	**2.90**	**0.08**	2.62	0.06

	No Fault	
	Mean	S.E.
Manual	2.63	0.025
Automatic	2.41	0.063

Automatic Control condition whereas RMS Lateral Deviation with *Active Safety* was higher than all other control conditions. These observations indicate that sharing control using schemes such as *Haptic Shared Control* and *Autopilot* can indeed maintain or reduce RMS Lateral Deviation when compared with *Automatic* and *Manual* driving.

Unlike Obstacle Hits, the Control Sharing Condition significantly affected the RMS Lateral Deviation ($F(2, 915) = 7.709, p < 0.0005$). As shown in Fig. 2.7 (a), between the three Control Sharing conditions, *Haptic Shared Control* had significantly lower RMS Lateral Deviation and consequently better maneuvering efficiency than *Active Safety* ($p < 0.0005$) and *Autopilot* ($p = 0.049$). Fault Condition also had a main effect on RMS Lateral Deviation ($F(2, 915) = 26.04, p < 0.0005$) and, as shown in Fig. 2.7 (b), the RMS Lateral Deviation for the Automation Fault condition was significantly higher compared to the Human Fault ($p < 0.0005$) and No Fault ($p < 0.0005$) conditions. The effect of interactions on the RMS Lateral Deviation was also found to be significant ($F(4, 915) = 9.83, p < 0.0005$). Simple main effects analysis showed that the Control Sharing

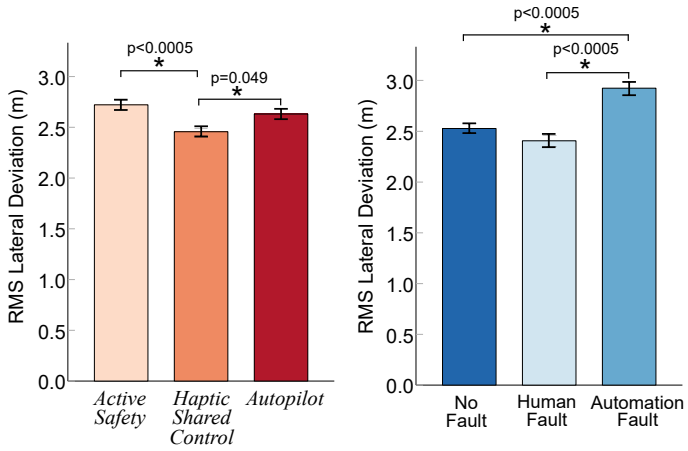

(a) (b)

Figure 2.7: Mean RMS Lateral Deviation. The RMS Lateral Deviation is defined in Fig. 2.3. (a) Mean RMS Lateral Deviation for the three control conditions, (b) Mean RMS Lateral Deviation for the three Fault Conditions. Error bars are $\pm$ 1 standard error of the mean. The asterisks on the lines linking two bars indicate a significant difference between two conditions along with the respective p values.

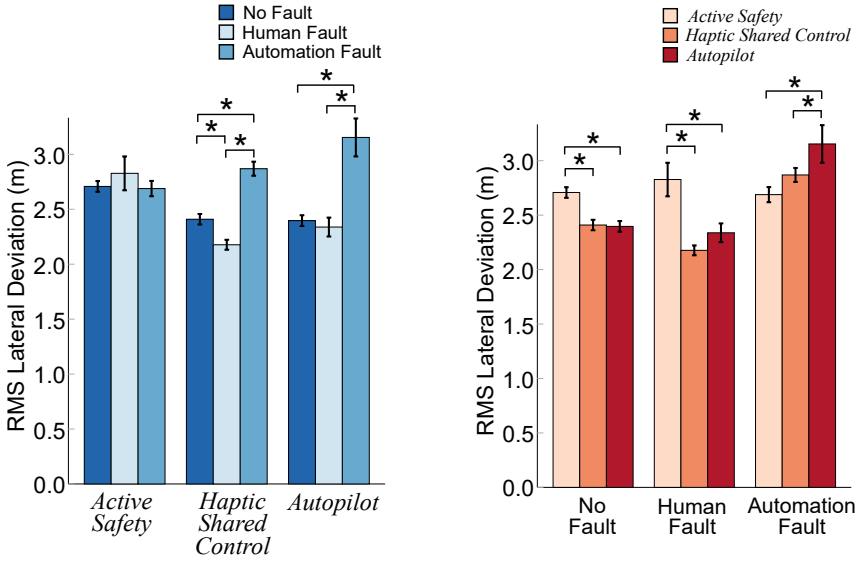

(a) (b)

Figure 2.8: Mean RMS Lateral Deviation (a) for each Fault Condition grouped by Control Condition and (b) for each Control Condition grouped by Fault Condition. Error bars are $\pm$ 1 standard error of the mean. The asterisks on the lines linking two bars indicate a significant difference between two conditions.

Condition had a significant effect on RMS Lateral Deviation for each Fault Condition: Human Fault ($F(2, 915) = 11.681, p < 0.0005$), Automation Fault ($F(4, 915) = 6.727, p = 0.001$), and No Fault ($F(4, 915) = 12.125, p < 0.0005$). Moreover, Fault Condition had a significant effect on

RMS Lateral Deviation for *Autopilot* ($F(2, 915) = 29.284$, $p < 0.0005$) and *Haptic Shared Control* ($F(4, 915) = 6.727, p = 0.001$) conditions.

Post-hoc analysis indicated that *Active Safety* had significantly better maneuvering efficiency than *Autopilot* ($p = 0.0009$) around the obstacles that simulated Automation Faults whereas *Autopilot* had significantly better maneuvering efficiency than *Active Safety* around the obstacles that simulated Human Faults ($p = 0.0008$) and in the cases of No Fault ($p < 0.0005$) (Fig. 2.8 (b)). However, overall differences (averaged over three fault conditions) between *Active Safety* and *Autopilot* were found to be insignificant ($p = 0.087$) (Fig. 2.7 (a)). Other significant differences resulting from the post-hoc tests for the simple main effects analysis are summarized in Fig. 2.8.

2.3.3 Approach Distance

The Approach Distance was used to gauge the human driver's preparedness to give up or take over the driving authority during obstacle avoidance. The value of approach distance indicated how early the human-automation team deviated from the track to avoid the obstacle. For instance, a lower approach distance implied that during obstacle avoidance, the human-automation team took more time to deviate from the track. However, since the behavior of automation near the obstacles was fixed, a lower Approach Distance indicated that the human driver was primarily responsible for the additional delay in deviating from the track. In particular, the driver was either unprepared to take over the driving authority or was unprepared to give away the driving authority to automation which resulted in late deviation from the track. The means of Approach Distance for all conditions are summarized in Table 2.5. Note that the mean Approach Distance for a condition corresponds to the Approach Distance value of the mean driver trajectory for that condition in Fig. 2.6.

Table 2.5: Means and Standard Errors (S.E.) of Approach Distance for all Control Conditions separated by Fault Conditions

	No Fault		Human Fault		Automation Fault		**All Fault Conditions**	
	Mean	S.E.	Mean	S.E.	Mean	S.E.	**Mean**	**S.E.**
Active Safety	11.52	0.47	8.98	0.70	11.00	0.62	**10.50**	**0.47**
Haptic Shared Control	12.12	0.47	11.92	0.62	9.73	0.62	**11.25**	**0.45**
Autopilot	11.62	0.47	11.24	0.62	8.30	0.63	**10.39**	**0.46**
All Control Conditions	**11.75**	**0.31**	**10.72**	**0.48**	**9.68**	**0.47**	**10.72**	**0.41**

	No Fault	
	Mean	S.E.
Manual	11.38	0.26
Automatic	10.32	1.12

Looking at the means of Approach Distance presented in Table 2.5, we see that out of all Control Conditions, the *Haptic Shared Control* condition had the highest Approach Distance whereas the *Automatic Control* had the lowest Approach Distance value. Note that the Approach Distance was low in *Automatic Control* condition not because automation was "unprepared" but because it was designed to minimize the lane keeping error. Therefore, the Approach Distance metric only

indicates the behavior of automation near the obstacles but does not tell much about the performance of automation in the *Automatic Control* condition. The second highest mean Approach Distance after the *Haptic Shared Control* condition was seen in the *Autopilot* condition which was followed by the *Active Safety* and the *Manual* condition. These observations indicate that sharing control using any scheme increases the Approach Distance when compared with *Automatic* and *Manual* driving.

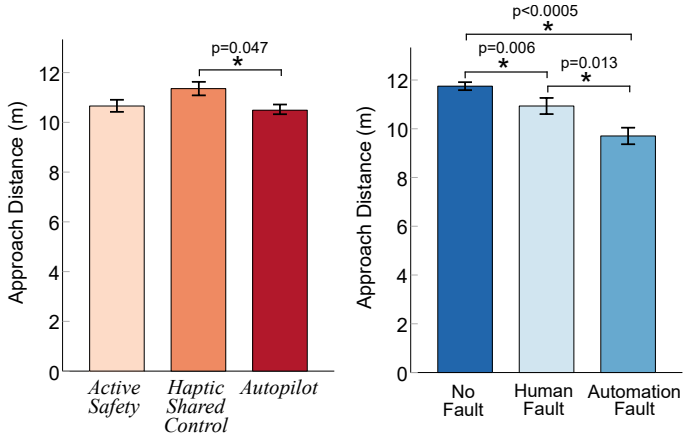

(a) (b)

Figure 2.9: Mean Approach Distance. The Approach Distance is defined in Fig. 2.3. (a) Mean Approach Distance for the three Control Sharing Conditions (b) Mean Approach Distance for the three visibility conditions. Error bars are $\pm$ 1 standard error of the mean. The asterisks on the lines linking two bars indicate a significant difference between two conditions along with the respective p values.

The results for the analysis of Approach Distance are summarized in Fig. 2.9 and Fig. 2.10. The effect of control condition on Approach Distance was found to be statistically significant ($F(2, 915) = 3.43, p = 0.033$). Through the post-hoc tests it was found that the mean Approach Distance for the *Haptic Shared Control* condition was significantly higher than the *Autopilot* condition ($p = 0.047$). The Fault condition also had a significant effect on Approach Distance ($F(2, 915) = 21.07, p < 0.0005$). The post-hoc tests revealed that all three Fault conditions were significantly different from each other. The Automation Fault condition was found to have a significantly lower Approach Distance than the Human Fault ($p = 0.013$) and the No Fault ($p < 0.0005$) conditions. Furthermore, Approach Distance for the Human Fault condition was significantly lower than the No Fault condition ($p = 0.006$). Finally, the effect of interaction of the independent factors was also found to be significant ($F(2, 915) = 6.67, p < 0.0005$). Through simple main effect analysis, it was found that Control Sharing Condition had a significant effect on Approach Distance both for Human Fault condition ($F(2, 915) = 7.618, p = 0.0006$) and for Automation Fault condition ($F(2, 915) = 7.34, p = 0.0008$). Post-hoc tests for Control Condition

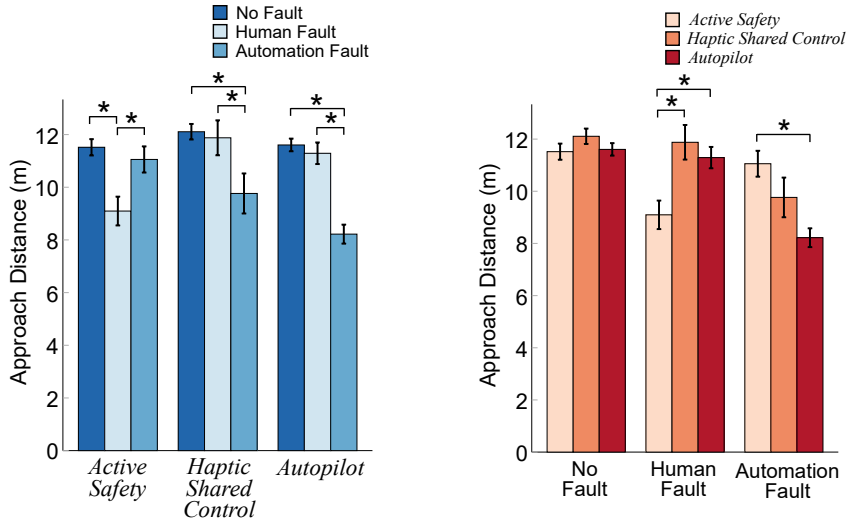

Figure 2.10: Mean Approach Distance (a) for each Fault Condition grouped by Control Condition and (b) for each Control Condition grouped by Fault Condition. Error bars are $\pm$ 1 standard error of the mean. The asterisks on the lines linking two bars indicate a significant difference between two conditions.

further revealed that in the case of Automation Faults, the *Autopilot* condition had significantly lower Approach Distance than the *Active Safety* ($p < 0.0005$) condition. In the case of Human Faults however, the *Active Safety* condition had significantly lower Approach Distance than both the *Autopilot* ($p = 0.007$) and the *Haptic Shared Control* ($p < 0.0005$) conditions. These results are summarized in Fig. 2.10 (b). Fault Condition also had a significant effect on the Approach Distance for all the Control Sharing Conditions. The post-hoc results for Fault Conditions are summarized in Fig. 2.10 (a).

2.4 Discussion

In this chapter my goal was to compare the obstacle avoidance performance of human/automation teams under three Control Sharing Conditions in the presence of simulated *faults*. Faults were simulated by partitioning the visibility of obstacles among the human driver and the automation system. That is, certain obstacles were visible to the automation but invisible to the human (Human Fault), certain obstacles were visible to the human but invisible to the automation (Automation Fault) while the rest were visible to both human and automation (No Fault). Performance under the three Control Sharing Conditions and under the three Fault Conditions were then analyzed in a 3$\times$3 study. To further understand the role of each agent in the Control Sharing Conditions, they were compared against two baseline driving conditions that did not involve any control sharing: *Manual Control* and *Automatic Control*. All analyses were undertaken on three performance metrics

that focused on distinct aspects of the obstacle avoidance task. The Obstacle Hits metric was used to compare driving safety; higher obstacle hits corresponded to lower safety. Approach Distance was used to gauge the human driver's preparedness to give up or take over driving authority during obstacle avoidance; a lower approach distance indicated that around the obstacle the human driver was either unprepared to take over the driving authority or was unprepared to give away the driving authority to automation. Finally, RMS Lateral Deviation was used to compare the driver's maneuvering efficiency around the obstacle; lower RMS lateral deviation indicated that the maneuver was performed more efficiently without excessive lateral deviation from the centerline.

In terms of Obstacle Hits, two agents driving together were found to be better than either agent driving alone. With only one agent driving (as in the Manual and Automatic baseline conditions), a fault led unconditionally (100%) to an obstacle hit. With two agents sharing control, between 0% and 28.8% of faults led to an obstacle hit, depending on the Fault Condition and the Control Sharing Condition (see Table 2.2). In one sense this was encouraging, but in another quite disappointing. If each obstacle was seen by at least one agent in the Control Sharing Conditions, and each agent acting alone was capable of avoiding No Fault obstacles, as established in the baseline conditions, one might have expected zero obstacles to be hit in the Control Sharing conditions. It appears that transitions of control and an associated need for time to acquire situation awareness, communication, or negotiation between the two agents led to difficulties in handling Human Fault or Automation Fault obstacles.

But note further, adding a second agent had an alarming effect on the perfect single-agent record for No Fault obstacles, as between 0.5% and 2.5% of No Fault obstacles were hit in the Control Sharing Conditions. Like a back-seat driver may be blamed for distracting and inducing errors rather than helping, adding automation can be blamed for inducing errors. For that matter, adding a human to automatic driving might also be blamed for inducing automation errors.

In contrast, adding a second agent seemed to enhance the Approach Distance. This is supported by Table 2.5 where it can be observed that, for the No Fault Condition, all Control Sharing conditions had higher values of Approach Distance than the baseline conditions. Moreover, the *Manual* condition had a larger Approach Distance than the *Automatic* condition. This indicates that when faced with an obstacle, human drivers preferred to deviate earlier from the center-line than the automation system. Recall that the automation was designed to have a lower approach distance to minimize the deviation from the center-line. For the Control Sharing conditions, this might mean that while sharing control, the participants most likely reacted before the automation to avoid an obstacle. Likewise, as shown in Table 2.4, adding a second agent with the *Haptic Shared Control* and the *Autopilot* conditions also reduced or maintained the RMS Lateral Deviation, and therefore improved or maintained the maneuvering efficiency over the baseline conditions. In addition, since the *Automatic Control* condition had lower RMS Lateral Deviation than the *Manual* condition it is

likely that the participants let the automation be more active in *Haptic Shared Control* and *Autopilot* while maneuvering around the obstacle. On the other hand, since RMS Lateral Deviation for the *Active Safety* condition was higher than the baseline conditions it might indicate that the human was still more involved during the obstacle avoidance maneuver than the automation system, which resulted in reduced maneuvering efficiency. Note, however, that the baseline conditions could not be statistically compared with the control sharing conditions because they had different levels of Fault Conditions. Therefore these results merit further exploration in future studies.

Looking at Obstacle Hits across Control Sharing and Fault conditions, it was found that significantly more Human Fault obstacles were hit in the *Active Safety* condition than in the *Haptic Shared Control* or *Autopilot* conditions. It was observed that during the Human Fault condition in *Active Safety*, when the automation intervened to avoid the obstacle, the participants were oftentimes unwilling to let go of the steering wheel and give away the driving authority to automation. As a result, they either inadvertently crashed into an obstacle that they could not see or reacted very late and barely avoided the obstacle with an inefficient and potentially unsafe maneuver around the obstacle (see Fig. 2.6). Consequently, in the condition of Human Faults, *Active Safety* produced significantly more obstacle hits, lower Approach distance and larger RMS Lateral Deviation than the other two control sharing conditions. On the other hand, during the Human Fault condition in *Autopilot*, since the automation was already performing the driving task, the participants did not intervene and simply let the automation avoid the obstacle.

In contrast, in the case of Automation Faults, the *Autopilot* condition resulted in significantly larger RMS Lateral Deviation than the *Active Safety* condition and the *Haptic Shared Control* condition, and significantly lower Approach Distance than the *Active Safety* condition. For Automation Faults in *Autopilot*, the participants were found unprepared to take over the driving authority; they took additional time to acknowledge that the automation had failed and to press the button to take over the driving authority. This delay also resulted in more inefficient and uncontrolled obstacle avoidance maneuvers as shown in Fig. 2.6. Such a delay was absent in *Active Safety* where the participants were already performing the driving task and were not required to take over control from automation to avoid the obstacle (similar to *Manual* driving).

Contemporary research on transitions in control indicate that externally-paced (automation initiated) transitions lead to reduced performance relative to human-paced transitions in human takeovers from automation. Reduced performance is associated with lower "levels of control", in particular so-called "scrambled control", characterized by urgent selection of control actions seemingly at random [107,114]. Note that in this study I investigated urgent human-paced takeovers from automation (*Autopilot*) and urgent externally-paced takeovers from human drivers (*Active Safety*). These takeovers were all necessary because of fault conditions induced artificially at constant high rates but at random times. Faults were not accompanied by alarms or announcements.

Extensions to the current study could be undertaken to determine the effects of factors such as the time required to press a button or the potential delays associated with committing to transition when that transition takes the form of a lumped or total transfer of control authority.

Between *Active Safety* and *Autopilot*, we therefore see a reduction in overall driving performance (higher hits, higher RMS Lateral Deviation, lower Approach Distance) when the primary agent responsible for lane keeping cannot see the obstacle: *Active Safety* does not perform well when the primary driver, human, cannot see the obstacle and *Autopilot* does not perform well when the primary driver, automation, cannot see the obstacle. In other words, it can be said that *Active Safety* behaves similar to the *Manual* condition whereas *Autopilot* behaves similar to the *Automatic* condition. This observation is further reinforced by Table 2.4 where the mean RMS Lateral Deviation for *Active Safety* is closer to *Manual* condition and for *Autopilot* is closer to *Automatic* condition. This indicates that even though *Active Safety* and *Autopilot* conditions are designed to support control sharing between human and automation, they apparently still perform similar to single agent driving schemes.

Theoretically, therefore, driving performance could still be enhanced by increasing the involvement of the secondary agent in the primary driving task. This was facilitated in the *Haptic Shared Control* condition by having the driver actively hold the steering wheel while the automation performed the lane keeping task. The results showed that overall, averaging over all fault conditions, *Haptic Shared Control* had significantly lower RMS Lateral Deviation than both *Active Safety* and *Autopilot* conditions and had significantly higher Approach Distance than the *Autopilot* condition and higher (if not "significantly" higher) Approach Distance than the *Active Safety* condition. Moreover, for each individual Fault Condition, with respect to the three metrics, the driving performance with *Haptic Shared Control* was never significantly lower than the *Active Safety* and the *Autopilot* conditions. This indicated that regardless of the Fault Condition one could expect *Haptic Shared Control* to perform at least as well as the other control sharing conditions.

The improvement in driving performance with *Haptic Shared Control* can be attributed to the more gradual nature of collaboration in *Haptic Shared Control* as compared to the other Control Conditions. In the *Haptic Shared Control* condition, the automation continuously communicated its control efforts to the driver through torque feedback on the steering wheel. The driver used this feedback to adopt a driving responsibility or assign a driving responsibility to the automation by activating or relaxing his/her muscles [13,18,56,115]. For example, as seen in Table 2.4 and Table 2.5, since the Approach Distance of *Haptic Shared Control* was closer to the *Manual* condition than the *Automatic* condition, it can be said that when faced with an obstacle, the human activated his/her muscles and overpowered the automation to deviate earlier from the centerline. Whereas, since the RMS Lateral Deviation of *Haptic Shared Control* was closer to the *Automatic* condition than the *Manual* condition, it can be said that while maneuvering around the obstacle, the human

relaxed and let the automation take control to perform the maneuever efficiently.

Based on the analysis, these results indicate that sharing control under *Haptic Shared Control* promotes safer driving, enhances driver preparedness to take over or give away the driving authority, and promotes more efficient driving maneuvers around obstacles than sharing control between two agents with fixed and predefined primary and secondary driving roles. These results support the benefits of control sharing with haptic shared control that have been previously published in the literature [13,56,59,100,116–118]. Complementing previous research, this study demonstrates how shared driving with continuous transitions involving haptic feedback can help improve driving performance in the event of human errors or automation dropouts over control sharing techniques with discrete transitions that are currently available in production vehicles.

Finally, looking at the differences between the Fault Conditions based on the Control Conditions, I found that for *Autopilot* and *Haptic Shared Control*, the Automation Fault condition produced significantly larger RMS lateral deviation and lower Approach Distance than both the Human Fault and No Fault conditions. In other words, when only the driver could see the obstacle, in *Autopilot* and *Haptic Shared Control*, the automation's inaction was more detrimental to the driver's maneuvering efficiency and the driver's preparedness to take over or give up the driving authority than the automation's action when the driver could not see the obstacle or when both agents could see the obstacle. Since in both *Autopilot* and *Haptic Shared Control*, the automation was active most/all of the time, we can infer that the reduction in driving performance was probably because the participants mistook the Automation Fault obstacle for a No Fault obstacle and relied excessively on the automation system to avoid it. Such an over-reliance on automation or *misuse* of automation system has been referred to as automation-induced "complacency" in the shared control literature in the past [20,47,119].

Lower driving performance during Automation Fault, especially for the *Haptic Shared Control* condition, might also be a function of the high value of control gains that was used to implement the automation's authority (impedance) in the *Haptic Shared Control* design. As mentioned in the literature previously, high automation impedance is detrimental to the shared task performance in the case of Automation Faults [13]. In future studies it would be interesting to examine if these results hold true for other levels of automation impedance (for instance a lower automation impedance) or for an *Adaptive Haptic Shared Control* design [13] where impedance values vary based on the driver's neuromuscular involvement.

2.5 Conclusion

This study investigated the ability of human-automation teams to avoid obstacles missed by an automation system (Automation Faults) and obstacles missed by human drivers (Human Faults)

under three control sharing schemes. I hypothesized that *Haptic Shared Control*, designed to support graded and gradual transitions of control authority and enable the human driver to monitor automation actions through torque feedback on the steering wheel, would outperform the *Autopilot* and *Active Safety* schemes that feature lumped and instantaneous transitions of control authority.

I found the lowest team performance under *Autopilot* for automation faults and under *Active Safety* for human faults. *Haptic Shared Control* supported the best overall team performance. Relative to individual human or automatic driver performance, I found that control sharing improved obstacle hit rates, maneuvering efficiency, and driver's preparedness to take over or give up the driving authority during obstacle encounters. While both human drivers and the automation system were able to avoid most (but still not all) of the obstacles missed by the other when teamed together, forming a team with control transitions also introduced errors in conditions without faults. Obstacle collisions under No-Fault conditions were not observed when human drivers or the automation system drove alone.

While the timing of faults was unpredictable in the current study, the fault rates were constant and rather high. Handling of a seldom occurring fault likely differs significantly from a fault that occurs at an expected high rate of 20%. Also, in the present study, there was barely time to recover from the previous obstacle or fault before another obstacle or fault appeared. Future research could investigate the compounding effects of deteriorating vigilance when faults cannot be anticipated. Future research could also investigate whether announcing a fault through visual, audio, or haptic feedback could improve performance.

Certainly the results in the present study depend on the particular implementation of each control sharing scheme. Additional research will be required to determine the dependence of performance to parameters within a particular scheme. For example, the limited ability of *Active Safety* to wrest control from the human driver while his or her hands remained on the steering wheel would be very different in a steer-by-wire implementation, where automation actions can be executed without backdriving the human. On the other hand, handing back control to the driver after executing such automation actions could require increased time.

CHAPTER 3

Coupled versus Decoupled Steering during Emergency Obstacle Evasion

3.1 Introduction

Control sharing between driver and automation is aimed at improving driving safety by combining the complementary skills of human drivers and vehicle automation [6]. For example, sharing control can combine the speed and tirelessness of automation with the experience and adaptability of a human driver [4]. However, in emergency situations requiring fast and precise responses, control sharing may actually have a negative effect on joint system performance. Automation systems can perform evasive steering maneuvers in emergency scenarios, including scenarios in which braking alone is insufficient to avoid collisions [64,120]. Meanwhile, human drivers may react to emergencies by executing inadequate steering maneuvers. If steering control is shared, the inadequate steering command by the human driver may reduce the efficiency of steering maneuvers undertaken by the automation [61]. Consequently, the driver may be considered a disturbance to automation during emergency scenarios and control sharing can be considered detrimental to driving safety [62,65,66].

To remove the influence of driver disturbance on automation-initiated steering maneuvers, the driver and steering wheel can be decoupled from the tires with the use of a steer-by-wire system [53,61,67,68]. In decoupled driving, the driver typically has no control over the vehicle during obstacle evasion, and automation is solely responsible for avoiding the collisions [121]. While the driver can still turn the steering wheel, only the automation command is transmitted to the tires. The driver is usually also provided torque feedback corresponding to the automation action on the steering wheel, in addition to torque from tire-road interaction [61,122]. Thus decoupled driving gives full reign to the automation system to use evasive steering to avoid collisions.

However, automation systems are not perfect. Despite technological advances, automation is still subject to false activation and dropouts [6,123]. Decoupling the driver during a false activation invokes safety and liability issues as it deprives the driver of the control authority required to prevent an accident [61,124]. Due to these considerations, the present legal system and code of industrial practice dictate that a driver should always maintain some degree of control over the

vehicle [125–127].

Decoupling the driver also invokes issues that are commonly associated with performance breakdowns in human-machine systems. Decoupling the driver while providing torque feedback may mislead the driver to believe that they are in control of the vehicle. Moreover, highly automated driving systems such as decoupled driving may reduce driver vigilance and situation awareness due to a reduced involvement of the driver in the driving task [19,21,128,129]. In particular, drivers who become aware that they have little or no control over the vehicle may fail to intervene if automation fails to activate [18,127]. On the other hand, drivers unaware of their level of control authority might be surprised or confused by an automation-initiated maneuver (or lack thereof) and left wondering why automation behaved in a certain way [17,130].

One paradigm for control sharing that may circumvent issues associated with decoupling the driver is haptic shared control [12,13,56,131]. In haptic shared control, the driver, the automation, and the tires are all three coupled to one another through the steering wheel. The driver has access to both the tire-road interaction and the automation action through haptic feedback. Automation acts on the steering system through a motor with a finite mechanical impedance roughly matching the driver's biomechanical impedance [13,54]. The driver can modulate their impedance through muscle action and can attempt to overpower automation's action whenever they desire. A coupled steering wheel therefore allows the driver to both exert control over the vehicle and extract information about the automation's actions [12,56].

Coupled driving can also be designed to suppress driver disturbance in emergency scenarios [60,131]. Choosing the mechanical impedance of automation to be larger than the impedance of a typical driver will attenuate driver disturbance while still providing the driver some control over the vehicle. However, high impedance automation may cause driver discomfort, and even a reduction in driving performance, because a large driver torque might be required to overpower the automation system [62]. For example, in [131], Mars et al. showed that high impedance automation systems result in reduced lane-keeping performance and reduced driver acceptance. Likewise, Zwaan et al. in [132] found that high impedance automation can result in lower safety margins and larger conflict torques than low impedance automation. However, unlike high impedance automation, low impedance automation might be too easy to overpower and hence might not be able to suppress the driver disturbance to avoid collisions in emergency scenarios [61,133].

A trade-off appears to exist between the control authority provided to an agent (driver or automation) and the fault protection provided by the other agent (as depicted in Fig. 3.1). For high impedance automation, the protection against automation faults provided by the human driver may be low because the automation system has a high relative control authority. At the same time, the protection against driver faults (or misses or inadequate responses) would be high. On the other hand, for low impedance automation, the automation has a lower relative authority and so

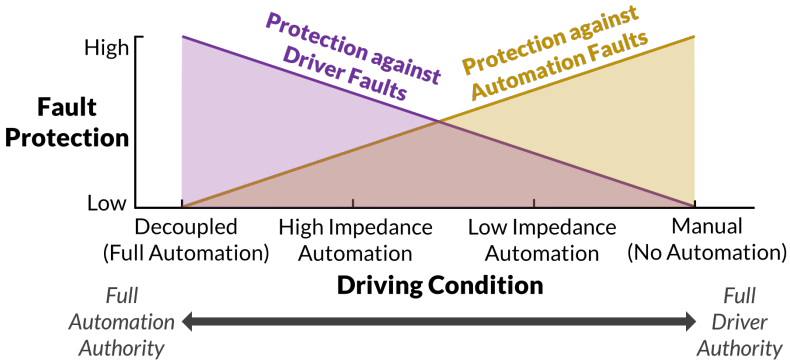

Figure 3.1: Hypothesized fault protection tradeoff. As the control authority provided to one agent (driver or automation) increases, the fault protection provided by the other agent reduces.

protection against automation faults provided by the human driver would be high but protection against driver faults provided by the automation would be low. In decoupled and manual driving, only one agent—automation or driver, respectively—has the full driving authority. These cases represent the extreme ends of the spectrum on protection against faults, as shown in Fig. 3.1.

To understand the influence of authority allocation on driving safety, it is important to compare driving performance between coupled and decoupled steering wheel designs, and likewise to compare the performance of driver/automation teams with low and high impedance automation systems during emergency scenarios. In [61], Heesen et al. presented a comparison of team driving performance between a decoupled and a coupled steering system in emergency situations. However, in this study a very low value of automation impedance was chosen, resulting in a collision with almost every obstacle encountered during the coupled steering case. Other studies testing the performance of emergency obstacle evasion systems have primarily focused on the influence of haptic and auditory warnings in a decoupled driving paradigm (see, for example, studies by Sieber et al. [64] and Hesse et al. [68]).

In this chapter, I compared four evasion schemes—Decoupled, Coupled High Impedance, Coupled Low Impedance, and Manual Driving—in simulated emergency collision avoidance scenarios. By comparing the four evasion schemes in a single study, I attempt to confirm the hypothesized fault protection/performance trade-off during driver and automation faults and investigate the effects of both automation impedance and driver decoupling on driving performance. I induce driver faults by simply simulating scenarios with time-to-collision lower than driver's typical reaction time. Further, I induce automation faults once at the end of each experiment by either making the automation system inactive near an obstacle or by making the automation system activate unjustifiably. I examine driving performance across four evasion schemes by analyzing the excursions around the obstacles and the obstacles hit in each scheme. I also build a driver-automation interaction model to estimate additional performance metrics based on the steering and torque trajectories, such as driver

setpoint, driver torque, and response time, to further obtain insights into the differences in driver behavior across the four evasion schemes.

3.2 Methods

3.2.1 Participants

Sixty-four participants (36 male, 28 female) participated in this study. The participants were between 20 and 30 years old (mean 23.5 years, SD = 3.6 years), had more than two years of driving experience (mean 5.9 years, SD = 3.2 years), and self-reported as having normal or corrected-to-normal vision and normal hearing. All participants provided written informed consent in accordance with a protocol approved by the University of Michigan Institutional Review Board (ID: HUM00164233). Each participant spent about two hours to complete the experiment including testing, training, and survey. Participants were provided a financial compensation of $30 for completing the experiment.

3.2.2 Apparatus

The experimental apparatus was a custom fixed-base driving simulator featuring a motorized steering wheel (Fig. 3.2a). Details pertinent to the steering wheel design, automation motor, encoders, and their assembly can be found in Chapter 2. The simulated driving environment was displayed on three 24-inch LCD widescreen monitors positioned at about 140 cm from the participant. The vehicle dynamics and control and the virtual environment were implemented in CarSim (Mechanical Simulation Corporation, Ann Arbor, MI) and Simulink (Mathworks, Natick MA) and were computed in real-time on a Dell Precision 5820 Tower Workstation computer using an Intel Xeon W-2125 Quad-Core processor. CarSim models and Simulink code were computed at 1000 Hz and the graphical display was rendered at 50 Hz.

The virtual environment was created in CarSim VS Visualizer, and appeared as shown in Fig. 3.2b. It featured a D-Class Sedan vehicle and a two-way road with various landmarks and vehicles that provided motion cues during driving. The vehicle traveled at a constant speed of 60 km/h using 'Constant Target Speed' control in CarSim. The participants were not provided any control over vehicle speed. The two-way road was 8 m wide with 4 m wide lanes and a dashed line separated traffic in two directions. The track width of the vehicle was about 2.1 m. The entire road was 6 km long and the obstacle locations and starting stations on the road were randomized as shown in Fig. 3.2c. Visual notifications and warnings were provided to the participants through a virtual dashboard on the central monitor as shown in Fig. 3.2d. Audio alerts were provided to the participants through a speaker located on the right side of the steering wheel. The visual and audio alerts are further described in section 3.2.6.

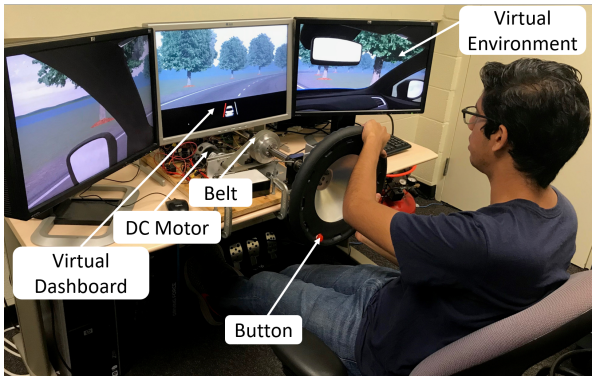

(a)

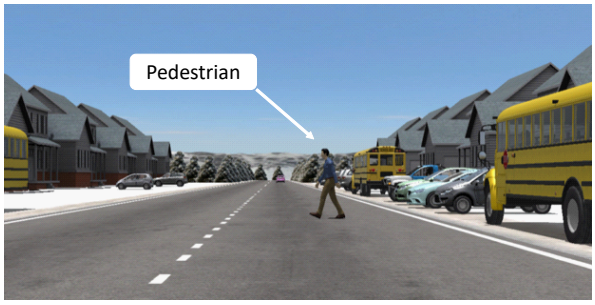

(b)

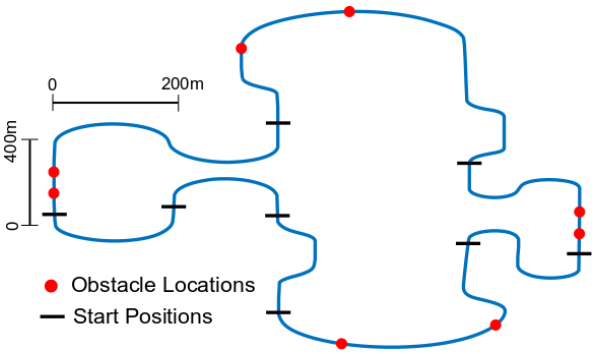

(c)

(d)

Figure 3.2: Experimental setup. (a) A subject performing the test on the fixed-base driving simulator. (b) CarSim virtual environment depicting the scenario in which a pedestrian unexpectedly enters the road. (c) Top view of the driving track (navigated clockwise) indicating the obstacle locations and starting positions. (d) Virtual dashboard that displayed warnings and notifications at the bottom of the middle screen.

3.2.3 Automation System Design

The automation system used a pure pursuit controller to perform lane keeping and obstacle evasion. A pure pursuit controller is a proportional controller that generates a steering angle to reduce the path tracking error of a vehicle at a point located a certain 'look-ahead distance' on the reference path [134]. First, a pilot experiment involving ten human subjects was performed to generate the reference path for the pure pursuit controller. In the pilot study, each subject was instructed to manually drive the simulated vehicle for two minutes and avoid ten obstacles that entered the road at a one second time-to-collision. The successful paths taken by the subjects around the obstacles were then averaged to obtain the reference path. For the controller design, the look-ahead distance was selected by trial and error with the objective to improve the path tracking performance. A look-ahead distance of 3 m was selected as it demonstrated the best tracking performance. Along with the generated reference path, the controller used the longitudinal and lateral coordinates of the vehicle and the heading angle generated by the CarSim vehicle model in real-time to generate the desired automation setpoint that would achieve path tracking. A controller commanded a torque signal to the motor proportional to the difference between the steering wheel angle and automation setpoint. Different proportional gains were used for low and high impedance automation systems as further described in section 3.2.4. A self-aligning (or self-centering) torque was further added to the automation torque feedback. The self-aligning torque arises from the tire-road interaction and is transmitted to the driver through the steering system elements connecting the tires to the steering wheel [135]. The self-aligning torque was designed to be proportional to the steering angle. The proportional gain used in the design was 1.98 N-m/rad.

3.2.4 Evasion Schemes

I compared four human/automation steering interface designs, for their support of successful obstacle evasion by the human/automation team during emergencies. I called these four interface designs *evasion schemes*. The steering wheel was either (1) decoupled from the tires and automation was given full control (*Decoupled with Feedback*), or (2) was coupled to the tires and to an automation system designed with a high impedance (*Coupled High*) or (3) a low impedance (*Coupled Low*), or (4) was coupled to the tires and automation was given no control (*Manual Driving*). (The four schemes in the order of increasing driver authority are shown on the x-axis of Fig. 3.1.) The *Coupled Low*, *Coupled High*, and *Decoupled with Feedback* conditions were further sub-categorized as *shared* evasion schemes, since in these schemes steering control was shared between the driver and automation. All schemes included self-centering torque feedback whereas the shared evasion schemes also included haptic feedback from the automation system during obstacle evasion.

In the *Manual Driving* scheme, there was no automation and participants had full control over the vehicle at all times. On the other hand, in the *Decoupled with Feedback* scheme, participants had no control over the vehicle trajectory during obstacle evasion. Participants could, however, feel the automation torque feedback on the steering wheel. Drivers could also move the steering wheel in the *Decoupled with Feedback* scheme; however, the driver's steering input was ignored and only the steering angle produced by the automation system was passed to the CarSim model to maneuver the vehicle.

In the *Coupled Low* and *Coupled High* schemes, drivers could influence the vehicle trajectory by changing the steering angle. Participants could take over control by increasing their grip (and consequently increasing arm impedance) and imposing a torque on the steering wheel. Conversely, drivers could yield control to the automation system by relaxing their grip (reducing arm impedance) on the steering wheel. In the *Coupled Low* case, the proportional gain used to determine the automation torque feedback was about three times lower and hence the haptic feedback was weaker than in the *Coupled High* case. As a result, it was also easier to take over control and fight the automation system in the *Coupled Low* case than it was in the *Coupled High* case. Also note that since the proportional gain used in the *Coupled Low* and *Decoupled with Feedback* schemes was the same, the torque feedback experienced in the two schemes was similar.

3.2.5 Modeling Physical Driver-Automation Interaction

Characterizing the steering intent of automation is relatively easy, since the automation setpoint is available in the data stream. The steering intent of the driver, on the other hand, must be inferred or estimated. I built a simple model of physical driver-automation interaction to serve as a means to conduct model-based estimation of the steering intent of the drivers. The interaction model developed is shown in Fig. 3.3. Note that although the rotational motion of the steering wheel is of main concern, for convenience an equivalent translational spring-mass-cart system is substituted to represent the driver, steering wheel, and automation system.

The automation setpoint θ_A is transmitted to the steering wheel (of inertia J and self-centering stiffness K_C) through a finite automation impedance K_A which can be represented by a virtual spring (or a combination of a virtual spring and virtual damper) [136]. Therefore, by design, the automation motor does not act as a perfect motion source on the steering wheel. Likewise, the human driver's arms and hands, instead of behaving like a perfect motion source, act with a variable mechanical impedance corresponding to the arm biomechanics. The behavior of arm biomechanics is often characterized by the behavior of a linear mass-spring-damper model whose inertia J_H, stiffness K_H, and damping B_H approximately describe the impedance properties of the arm muscles [76,136]. The driver's arm impedance is further supplemented by a motion source (representing the driver's central nervous system) to describe the driver's volitional action [137,138]. The motion

source generates the human driver's steering intent θ_H, which I call driver setpoint. Note that in the model formulation the mass J captures the combined inertia J_S of the steering wheel and J_H of the driver arms and hands referenced to the steering wheel's axis of rotation (that is, $J = J_S + J_H$). The inertia of automation motor shaft and the transmission mechanism referenced to the steering wheel's axis of rotation were assumed to be negligible.

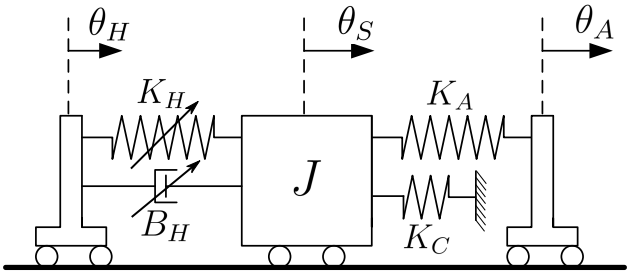

Figure 3.3: Model of physical driver-automation interaction. The human driver on the left imposes a setpoint θ_H with a variable arm impedance (stiffness K_H and damping B_H) on the steering wheel (of mass J). Likewise, automation on the right imposes setpoint θ_A with a fixed automation impedance (proportional gain K_A). A spring (of stiffness K_C) representing the self-centering stiffness of the steering wheel further connects the steering wheel to the ground. The steering wheel moves with an angle θ_S.

Let the automation torque be denoted by τ_A, human driver torque by τ_H, and self centering torque by τ_C, then from Fig. 3.3, we have

$$\tau_A = K_A(\theta_A - \theta_S), \tag{3.1}$$

$$\tau_H = K_H(\theta_H - \theta_S) + B_H(\dot{\theta}_H - \dot{\theta}_S), \tag{3.2}$$

$$\tau_C = -K_C\theta_S. \tag{3.3}$$

The net steering torque τ_S is a sum of the automation torque, human driver torque, and self centering torque, that is,

$$\tau_S = J\ddot{\theta}_S = \tau_A + \tau_H + \tau_C. \tag{3.4}$$

Substituting equations (1), (2), and (3) in (3.4), and rearranging, we get

$$\begin{aligned} K_H\theta_H + B_H\dot{\theta}_H = (K_A + K_H + K_C)\theta_S + B_H\dot{\theta}_S + \\ J\ddot{\theta}_S - K_A\theta_A. \end{aligned} \tag{3.5}$$

The LTI system model represented by the differential equation (3.5) was solved numerically using the Forward Euler method to estimate the driver's setpoint θ_H. The automation setpoint

trajectory θ_A, impedance K_A, and self-centering stiffness K_C were available from the design of the controller. Steering angle θ_S was available from the encoder reading, and the derivatives $\dot{\theta}_s$ and $\ddot{\theta}_s$ were obtained by digitally differentiating and filtering the resulting signals at 5 Hz using a first-order low-pass butterworth filter.

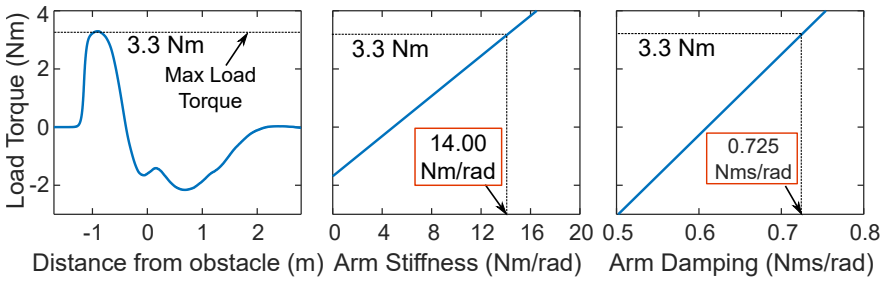

Figure 3.4: Estimation of driver arm stiffness K_H and damping B_H for the *Coupled Low* scheme using the linear models identified in [76]. The maximum value of the automation torque (3.3 Nm) averaged over all subjects was used as the load torque to estimate K_H as 14 Nm/rad and B_H as 0.725 Nms/rad. The values were assumed fixed for the duration of obstacle evasion.

For the values of driver arm stiffness K_H and damping B_H I referred to the results of a system identification experiment performed by Pick and Cole in [76]. In [76], authors identified linear models to describe relationships between the arm stiffness/damping and the load applied on steering wheel when subjects steered against a torque offset. For the 16 participants in each evasion scheme in the experiment, I computed the average of the maximum load (motor torque) that was applied on the steering wheel during obstacle evasion. The applied load was then used to estimate the values of B_H and K_H for each evasion scheme using the models identified in [76]. An example is shown in Fig. 3.4 where B_H and K_H are estimated for the *Coupled Low* evasion scheme. The steering setup in [76] was similar to the fixed base driving simulator setup used in this experiment. Moreover, the torque offset commanded by the motor in [76] was applied similar to the motor torque commanded at the onset of obstacle evasion in this experiment. Though the torque applied in this experiment varied after the initial onset, I have assumed that the impedance parameters stay relatively constant for the duration of obstacle evasion. I have therefore used the maximum value of load torque applied at the onset to estimate the impedance parameters.

For the manual driving scheme, B_H and K_H were obtained by setting the applied load to zero. The driver arm inertia J_H for the four schemes was also obtained from Ref. [76], Table 3, by averaging the measurements reported over all subjects (0.094 kg/m^2). The arm inertia was then added to the inertia of the steering wheel J_S used in the setup (0.048 kg/m^2) to obtain the total inertia J of the steering wheel. The final values of all the parameters are given in Table 3.1. As already mentioned, the value of self-centering stiffness K_C was selected to be 1.98 N-m/rad and was applied to all evasion schemes.

		Evasion Scheme			
		CH	CL	DF	MD
Parameter	K_H (N m/rad)	22	14	14	3.8
	B_H (N m s/rad)	1	0.725	0.725	0.56
	J_H (kg/m^2)	0.094	0.094	0.094	0.094
	K_A (N m/rad)	18.46	5.96	5.96	0

Table 3.1: Values of the impedance parameters used in the analysis. The automation impedance K_A was known from the automation design whereas the arm stiffness K_H and damping B_H were estimated using the commanded load torque as shown in Fig. 3.4. Value for arm inertia J_H was drawn from the literature. K_A was designed to be approximately three times for the *Coupled High* (CH) scheme than for the *Decoupled with Feedback* (DF), and *Coupled Low* (CL) schemes, and was set to zero for the *Manual Driving* (MD) scheme.

3.2.6 Experiment Procedure

The study employed a between-subject design with one factor (evasion scheme) at four levels. The sixty-four participants recruited to the study were randomly divided into four groups (*Coupled Low* (CL), *Coupled High* (CH), *Decoupled with Feedback* (DF)), and *Manual Driving* (MD)) of 16 participants each (9 males, 7 females). Participants were assigned to the four groups based on their age and driving experience to ensure that the average age and driving experience of participants in the four groups were comparable.

The driving task included keeping the vehicle centered in the right lane of the two-way road and avoiding any obstacles that appeared in the lane. To help the driver with lane centering, a lane departure warning appeared on the virtual dashboard (Fig. 3.2d) when the deviation of the vehicle from the center of the right lane exceeded 0.6 m (the lane was 4 m wide). Obstacles in the form of pedestrians, deer, or other vehicles unexpectedly entered the road from the right side of the driving lane (Fig. 3.2b) and stopped at the center of the lane. As soon as the obstacle stopped, the automation system performed an evasive steering maneuver towards the left to help the driver avoid the obstacle. During the obstacle evasion, the lane departure warning disappeared and an 'AUTOMATION IS ON' notification appeared on the virtual dashboard to indicate that the automation system was active. After avoiding the obstacle, the automation system returned the vehicle back to the center of the right lane at which point a take-over-request (TOR) notification 'TAKE OVER CONTROL' appeared on the virtual dashboard. Four seconds after the first appearance of the TOR, monotone auditory alerts (beeps) were sent every two seconds from a speaker to remind the driver to take over. As soon as the driver pressed the red button, automation gave full control of the vehicle back to the driver and turned off the notifications and auditory alerts.

Before the experiment, each participant was given instructions on the screen explaining the virtual environment and dashboard, the lane-keeping task, and the obstacle evasion task. Participants

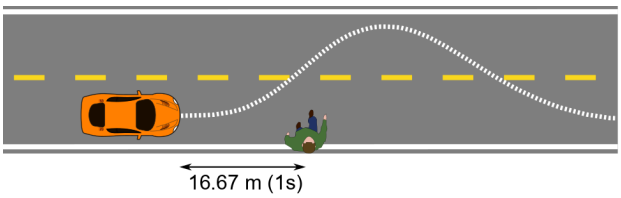

(a) Intended Automation

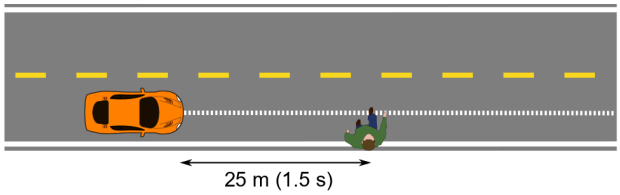

(b) Idle Automation

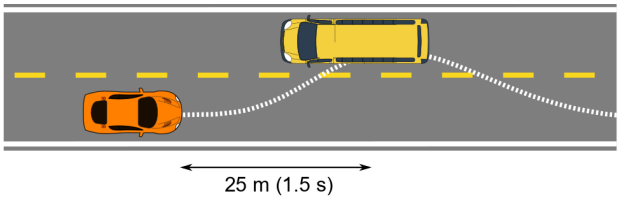

(c) Adversarial Automation

Figure 3.5: Three types of automation behaviors designed and tested in the experiment.

were asked to drive as close as possible to the center of the right lane and mind the lane departure warning. This instruction was given to ensure that all the participants were at the center of their lanes when an obstacle appeared in their lane. Participants were also advised to keep their hands on the steering wheel when the automation performed an obstacle evasion maneuver. In the shared evasion schemes, the participants were told that the obstacles would appear suddenly and that the automation would always turn on and help them avoid the obstacle. In the *Manual* driving scheme, participants were told that they were responsible for avoiding the obstacles themselves.

Next, participants completed two 6-minute training trials with one obstacle in each trial and nine formal trials with eight obstacles in total. There was a minute-long break between trials. The nine formal trials were randomized. Out of these nine trials, three trials had no obstacles, four trials had one obstacle each, and two trials had two obstacles each. Moreover, trials were designed to have different surroundings (weather and time of day varied between trials) and random start positions and obstacle locations. These measures were taken to prevent any learning and adaptation effects.

For the first eight obstacles in the shared evasion schemes, the automation worked as intended; automation attempted to avoid the obstacles without human intervention (see Fig. 3.5a). This resulted in a total of 128 obstacle evasion maneuvers for each of the three shared evasion schemes. Likewise, a total of 128 obstacle evasion maneuvers were also performed in *Manual Driving*, but the maneuvers were performed by the human drivers alone (without automation assistance).

The obstacles were not visible to the drivers until one second time-to-collision. Since drivers typically need at least one second to react to suddenly appearing obstacles [61,62,64], the one second time-to-collision effectively induced a "driver fault".

In the shared evasion schemes, the nine trials were followed by one additional trial. The tenth trial always involved an unexpected "automation fault", either idle automation (automation failed to activate in the presence of an obstacle) or adversarial automation (automation initiated a maneuver into oncoming traffic in the absence of an obstacle), as shown in Fig. 3.5b and Fig. 3.5c. The time available to avoid the obstacles during automation faults was 1.5 seconds; larger than the one second available during driver faults. Half the participants in each scheme experienced idle automation while the other half experienced adversarial automation. This resulted in a total of eight idle automation obstacles and eight adversarial automation obstacles in each shared evasion scheme. The tenth trial with the automation failure was skipped for the participants in the *Manual* driving scheme because there was no automation. For the shared evasion schemes, at the end of each experiment, participants were also asked to fill out a survey that was used to gather participant feedback.

3.2.7 Performance Metrics

The dependent measures used to characterize the behavior and performance of the driver-automation teams were based on the following three categories: (1) the vehicle trajectory around the obstacles, (2) the steering and torque trajectories, and (3) the surveys conducted at the end of the experiments.

Four performance metrics were based on the vehicle trajectory around the obstacles (see Fig. 3.6): (1) Obstacle Hits, simply defined as the total number of collisions with the obstacles in each evasion scheme; (2) Peak Excursion E^{pk}, calculated as the absolute maximum lateral deviation of the vehicle away from the center of the driving lane; (3) Excursion Time T_e, defined as the time between the instant the automation turned on and the instant the TOR was received by the driver; (4) Take-over Time T_t, defined as the time taken by the driver to press the button (and turn automation off) after the TOR was received by the driver. To determine obstacle hits, an elliptical boundary was constructed around the obstacle whose intersection with the trajectory denoted a collision. The actual obstacle boundary circumscribed the obstacle, whereas the expanded obstacle boundary (used to determine collisions) was constructed to account for the dimension of the ego vehicle (as shown in Fig. 3.6). Note that T_e and T_t could only be computed for the three shared evasion schemes because there was no automation in the *Manual Driving* scheme. Moreover, only the Obstacle Hits were analyzed for the idle automation and adversarial automation cases. The other three metrics were only analyzed for the intended automation case.

The following four performance metrics were based on steering and torque trajectories (see Fig.

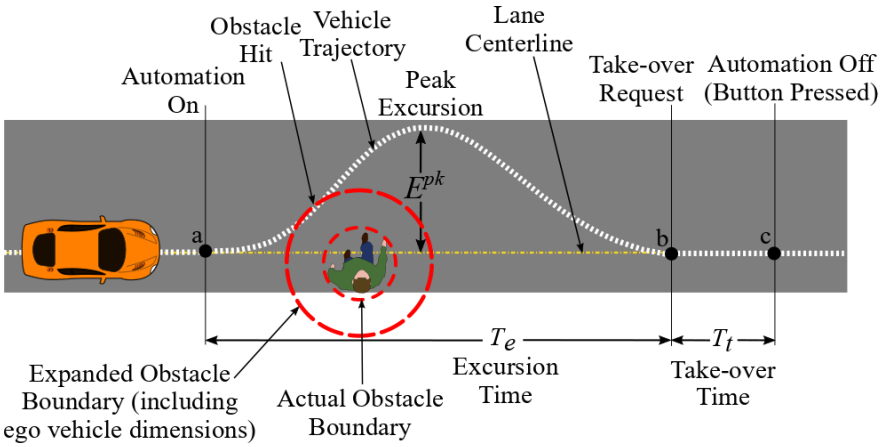

Figure 3.6: Performance metrics based on the vehicle trajectory around obstacles. A sample vehicle trajectory taken by a participant is superimposed on a cartoon of the road. In the trajectory shown, the automation was engaged at point **a** as the obstacle entered the road, the participant received a take-over-request at point **b** as the vehicle returned to the lane center, and the automation turned off at point **c** when the participant pressed the button. The time taken by the vehicle to travel from **a** to **b** was defined as the Excursion Time T_e, and the time taken to travel from **b** to **c** was defined as the Take-over Time T_t. The maximum deviation from the lane center was defined as the Peak Excursion E^{pk}. Any intersection of the expanded obstacle boundary with the vehicle trajectory was counted as an obstacle hit.

3.7): (1) Peak Steering Angle θ_S^{pk}, defined as the maximum steering angle; (2) Peak Driver Setpoint θ_H^{pk}, defined as the maximum driver setpoint; (3) Peak Driver Torque τ_H^{pk}, defined as the maximum *absolute* driver torque; (4) Driver Lag T_H computed as the time difference between the instant the driver setpoint exceeded 5° and the instant the automation setpoint exceeded 5°.

Finally, a survey was administered at the end of the experiment to gather data on: (1) driving satisfaction, (2) trust in automation, (3) awareness of automation actions, and (4) perceived control over the vehicle. The participants rated the four items on a five-point Likert scale (1 - Very Low, 5 - Very High). These subjective ratings were collected only for the three shared evasion schemes.

3.2.8 Statistical Analyses

Obstacle Hits for the idle and adversarial automation cases were analyzed using mixed model binary logistic regression. The Obstacle Hits for the *Manual Driving* scheme and for the intended automation case in the three shared evasion schemes were analyzed using Poisson regression analysis (the data failed the assumptions for a binary logistic regression analysis due to zero hits in one evasion scheme). The survey results were analyzed using univariate analysis of variance (ANOVA) and the remaining metrics were analyzed using linear mixed models. For the analyses, the evasion scheme was chosen as a fixed factor and participant ID as a random factor. The significance level was set at $p < .05$. Post-hoc Bonferroni tests were conducted to perform pairwise comparisons

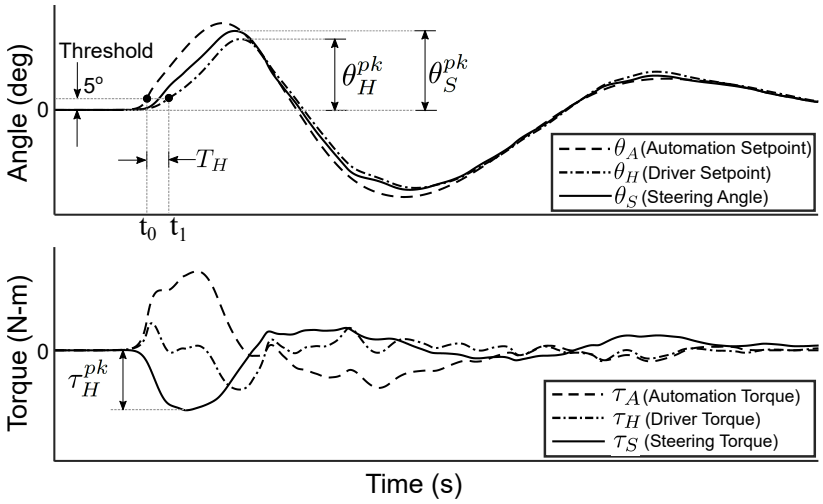

Figure 3.7: Performance metrics based on the steering and torque trajectories. Sample steering and torque trajectories of a participant are shown. The automation setpoint θ_A was recorded from the simulation and steering angle θ_S was measured during the experiment. Driver setpoint θ_H was estimated using Eqn. (3.5), whereas the torque trajectories were created using Eqns. (1), (2), and (3.4). The automation setpoint and driver setpoint exceed 5° threshold at the time instants t_0 and t_1. The Driver Lag T_H was defined as the time difference $t_1 - t_0$. The maximum values of the steering angle and the driver setpoint were respectively defined as the Peak Steering Angle θ_S^{pk} and Peak Driver Setpoint θ_H^{pk}. The maximum *absolute* driver torque was defined as the Peak Driver Torque τ_H^{pk}.

between the evasion schemes.

3.3 Results

3.3.1 Vehicle Trajectory around the Obstacles

Differences in driver behavior across the four evasion schemes were apparent in the vehicle trajectories. Fig. 3.8 shows the vehicle trajectories taken around the obstacles by the 64 participants in four evasion schemes (with 16 participants in each scheme) separated by the type of automation behavior (intended, idle, and adversarial). The trajectories for the *Manual Driving* scheme represent the human driver's performance with no assistance from the automation system. The trajectories in the *Manual Driving* scheme were compared with the trajectories for the intended automation case in the three shared evasion schemes. The obstacles are shown by grey ellipses and the intersections of the trajectories with the ellipses indicate obstacle hits. Insets on the individual plots further provide a zoomed-in view of the obstacle hits. As expected, the largest number of obstacles were hit in the *Manual Driving* scheme that had no automation assistance followed the *Coupled Low* scheme that had only weak automation assistance. The *Decoupled with Feedback* had no obstacle hits in the intended automation case. On the other hand, in the idle and adversarial automation cases, fewer

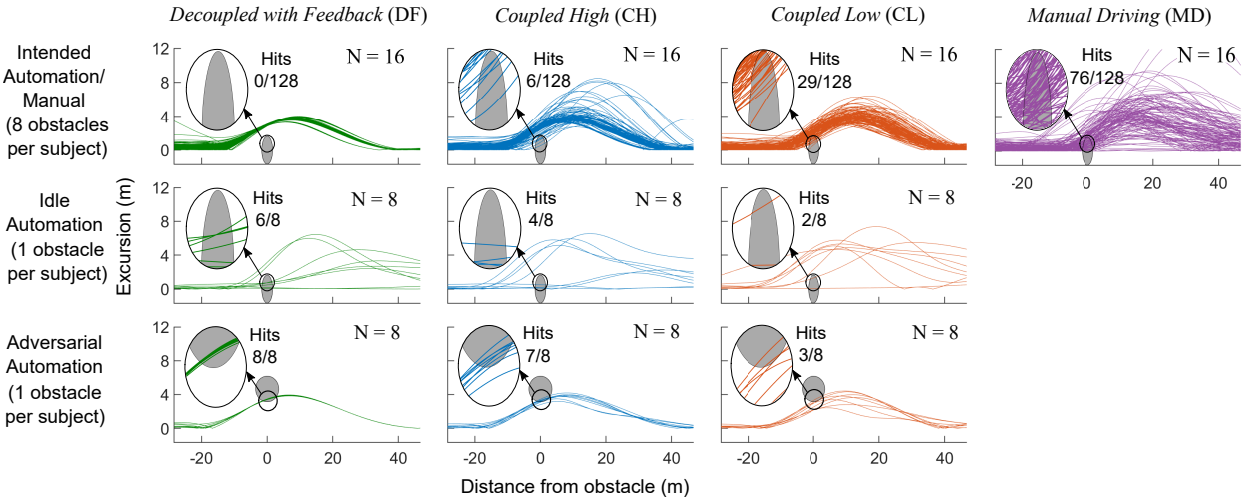

Figure 3.8: Driving trajectories around obstacles for all 64 participants, separated by evasion scheme and automation behavior. Obstacles are depicted to scale by grey ellipses in each plot. Intersection of trajectories with the obstacles indicate obstacle hits. Insets on the plots provide a zoomed-in view of the intersections. Number of hits (out of the obstacles encountered) and the number of subjects (N) in each case are also denoted on each plot. (Note that the obstacle in adversarial automation case had a different size as shown in Fig. 3.5.)

obstacles were hit in the *Coupled Low* scheme compared to the *Coupled High* and *Decoupled with Feedback* scheme. In terms of excursions around the obstacles, *Manual Driving* resulted in the largest excursions followed by the *Coupled High* scheme, whereas the *Decoupled with Feedback* scheme resulted in the smallest excursions.

3.3.1.1 Obstacle Hits

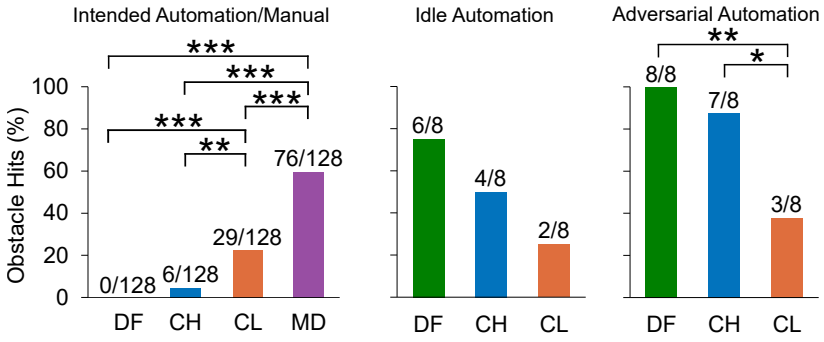

Figure 3.9: Percent obstacle hits for the three types of obstacles separated by evasion scheme. Figures on the top of each bar (X/Y) indicate the number of hits (X) out of the number of obstacles encountered (Y) in each case. Asterisks indicate significant differences: $p < .05$ for *, $p < .01$ for **, $p < .001$ for ***.

3.3.1.1.1 Intended Automation/Manual A total of 128 obstacle evasion maneuvers were performed during manual driving and during the intended automation case in the shared evasion schemes. Out of these 128 obstacles, the *Decoupled with Feedback* scheme resulted in no obstacle collisions (Fig. 3.9). On the other hand, the *Coupled High* scheme resulted in 6, the *Coupled Low* scheme in 29, and the *Manual Driving* scheme in 76 collisions.

Analysis on the Obstacle Hits metric indicated a main effect of evasion scheme ($\chi^2(2, N = 64) = 48.8,\ p < .001$). Post-hoc comparisons further revealed that the likelihood of a hit for the *Manual Driving* scheme was significantly higher than all the other schemes ($p < .001$ for all the comparisons). Moreover, the likelihood of a hit in the *Coupled Low* scheme was significantly higher than for the *Coupled High* scheme ($p = .001$) and the *Decoupled with Feedback* scheme ($p < .001$). The *Coupled High* and *Decoupled with Feedback* schemes showed no significant differences in terms of obstacle hits.

3.3.1.1.2 Idle Automation In the Idle Automation case, the *Coupled Low* scheme resulted in only two hits out of eight obstacles. Six out of eight obstacles were hit in the *Decoupled with Feedback* scheme, while four out of eight obstacles were hit in the *Coupled High* scheme (Fig. 3.9). However, the effect of evasion scheme on hits was not significant ($p = .147$).

3.3.1.1.3 Adversarial Automation Out of the eight obstacle evasion maneuvers performed in the adversarial automation case, the *Coupled High* scheme resulted in seven obstacle hits and *Decoupled with Feedback* scheme resulted in eight obstacle hits. On the other hand, *Coupled Low* scheme resulted in only three hits (see Fig. 3.9). There was a significant effect of evasion scheme in the adversarial automation case ($F(2, 21) = 6.682,\ p = .006$). Post-hoc tests revealed that the likelihood of a hit for the *Coupled Low* scheme was significantly lower than for the *Decoupled with Feedback* scheme ($p = .007$) and the *Coupled High* scheme ($p = .035$). No significant differences were found between the *Decoupled with Feedback* and the *Coupled High* schemes.

3.3.1.2 Peak Excursion

Peak Excursion E^{pk} was used to gauge which evasion scheme produced the largest deviations from the center of the right lane. E^{pk} differed significantly between the four evasion schemes ($F(3, 397) = 16.98,\ p < .001$) (see Fig. 3.10a). Post-hoc tests revealed that the mean E^{pk} for the *Manual Driving* scheme was significantly higher than the *Decoupled with Feedback* (5.21 m vs. 3.70 m, $p < .001$), *Coupled High* (5.21 m vs. 4.12 m, $p < .001$) and *Coupled Low* (5.21 m vs. 4.09 m, $p < .001$) schemes. No other significant differences were found.

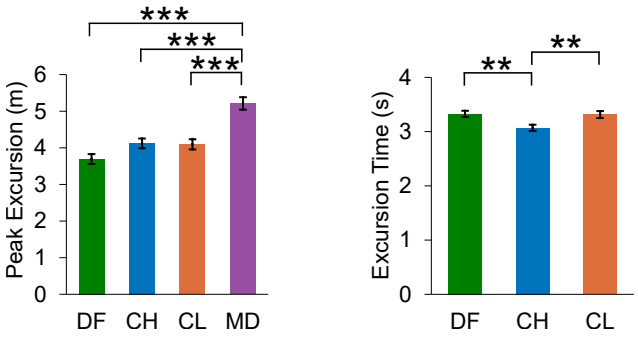

(a) Peak Excursion (b) Excursion Time

Figure 3.10: Mean values of (a) Peak Excursion and (b) Excursion Time for the shared evasion schemes. Error bars indicate standard error. ($p < .05$ for *, $p < .01$ for **, $p < .001$ for ***.)

3.3.1.3 Excursion Time

Excursion Time T_e indicated how much time was spent away from the lane center during obstacle evasion. There was a main effect of evasion scheme on T_e ($F(2, 346) = 4.413,\ p = .003$) (see Fig. 3.10b). Post-hoc tests showed that the *Coupled High* scheme had significantly lower mean T_e than both the *Decoupled with Feedback* scheme (3.07 s vs. 3.33 s, $p = .005$) and the *Coupled Low* scheme (3.07 s vs. 3.32 s, $p = .01$). No other significant differences were found.

3.3.1.4 Take-over Time

Take-over Time T_t was used to measure which evasion scheme encouraged faster automation-to-driver transitions. There were no significant differences between the mean T_t for the three schemes ($p = .348$).

3.3.2 Steering Angle and Torque Trajectories

The steering angle and torque trajectories revealed several differences between the four evasion schemes (see Fig. 3.11). In the three shared evasion schemes, the steering angle lagged the automation setpoint whereas the driver setpoint lagged the steering angle. In the *Manual Driving* scheme, on the other hand, the steering angle lagged the driver setpoint. The driver lag in the *Decoupled with Feedback* scheme was significantly larger than the *Coupled High* scheme and was not significantly different from the *Manual Driving* scheme. The driver torque was the highest in the *Coupled High* scheme, but was the second highest in the *Decoupled with Feedback* scheme. Moreover, the peak steering angle and driver setpoint were the lowest in the *Decoupled with Feedback* scheme.

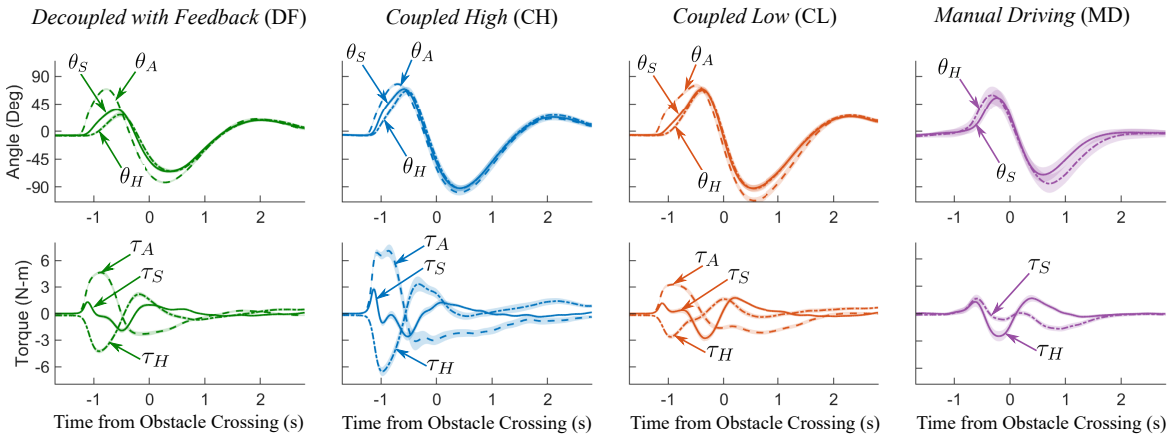

Figure 3.11: Steering angle and torque trajectories during obstacle evasion for all participants separated by evasion scheme. The dash-dot lines represent human driver's setpoint θ_H and torque τ_H that were estimated using the driver-automation interaction model presented in section 3.2.5. The solid lines represent steering angle θ_S measured using encoders and net steering torque τ_S (computed using Equation (4)), and the dashed lines represent automation setpoint θ_A and torque τ_A recorded from the simulation. The trajectories were only analyzed for the intended automation case. Thus, a total of 128 trajectories (8 obstacles each for 16 participants) were analyzed. All the lines represent the mean values of the trajectories and the shaded areas represent 95% confidence intervals.

3.3.2.1 Peak Steering Angle

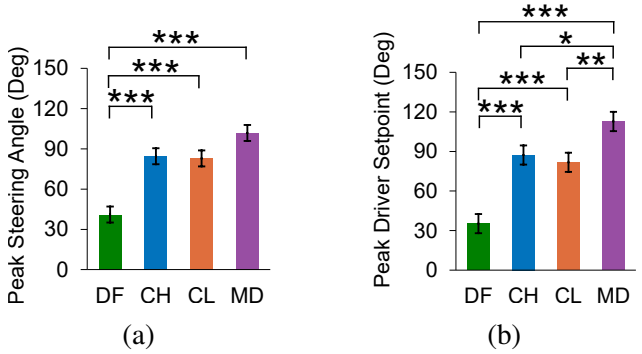

Figure 3.12: Mean values of (a) Peak Steering Angle and (b) Peak Driver Setpoint for the four evasion schemes. Error bars indicate standard error. ($p < .05$ for *, $p < .01$ for **, $p < .001$ for ***.)

Peak steering angle θ_S^{pk} differed significantly between the four evasion schemes ($F(3, 508) = 18.63,\ p < .001$). The *Decoupled with Feedback* scheme had significantly lower mean θ_S^{pk} than the *Coupled High* (41.01° vs. 84.53°, $p < .001$), *Coupled Low* (41.01° vs. 82.87°, $p < .001$), and *Manual Driving* (41.01° vs. 101.77°, $p < .001$) schemes (see Fig. 3.12a). No other significant differences were found.

3.3.2.2 Peak Driver Setpoint

The peak driver setpoint θ_H^{pk} also differed significantly between the four evasion schemes ($F(3, 508) = 19.66,\ p < .001$). The *Manual Driving* scheme had a significantly larger mean θ_H^{pk} in comparison with the *Coupled Low* (112.71° vs. 81.79°, $p = .008$), *Coupled High* (112.71° vs. 87.28°, $p = .028$), and *Decoupled with Feedback* (112.71° vs. 35.28°, $p < .001$) schemes (see Fig. 3.12b). Moreover, the *Decoupled with Feedback* scheme had a significantly lower mean θ_H^{pk} than the *Coupled Low* (35.28° vs. 81.79°, $p < .001$) and *Coupled High* (35.28° vs. 87.28°, $p < .001$) schemes. Only *Coupled Low* and *Coupled High* schemes showed no significant differences.

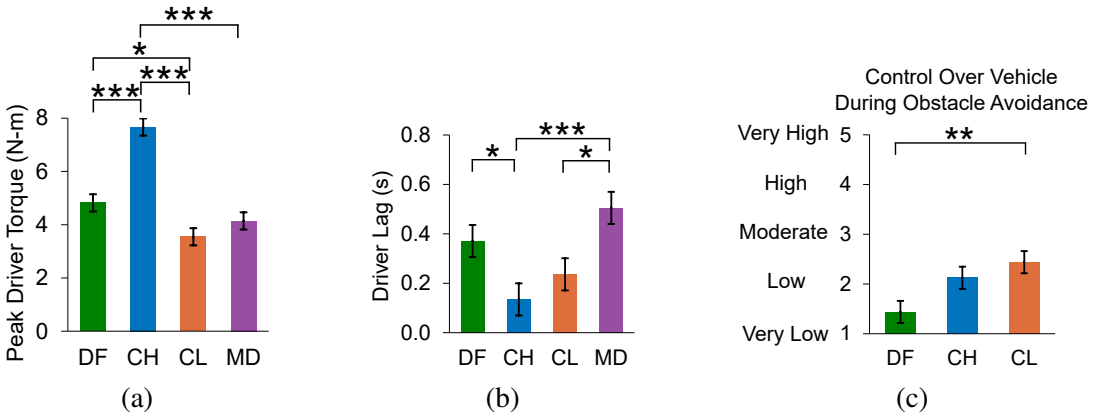

Figure 3.13: Mean values of the (a) Peak Driver Torque, (b) Driver Lag, and (c) Participant rating for "control over vehicle during obstacle avoidance". Error bars indicate standard error. ($p < .05$ for *, $p < .01$ for **, $p < .001$ for ***.)

3.3.2.3 Peak Driver Torque

The evasion scheme also had a significant effect ($F(3, 508) = 32.10,\ p < .001$) on the peak driver torque τ_H^{pk}. The mean τ_H^{pk} was significantly higher under the *Coupled High* scheme than the *Coupled Low* scheme (7.67 N-m vs. 3.55 N-m, $p < .001$), the *Decoupled with Feedback* scheme (7.67 N-m vs. 4.82 N-m, $p < .001$), and the *Manual Driving* (7.67 N-m vs. 4.14 N-m, $p < .001$) scheme (see Fig. 3.13a). Moreover, the mean τ_H^{pk} for *Decoupled with Feedback* scheme was significantly larger than the *Coupled Low* scheme (4.82 N-m vs. 3.55 N-m, $p = .016$).

3.3.2.4 Driver Lag

Driver lag T_H was significantly different between the four evasion schemes ($F(3, 508) = 6.11,\ p < .001$). *Decoupled with Feedback* had a significantly larger mean T_H than the *Coupled High* (0.37 s vs. 0.14 s, $p = .043$) scheme (see Fig. 3.13b). The *Manual Driving* scheme had

significantly larger mean T_H than the *Coupled Low* (0.50 s vs. 0.24 s, $p = .018$) and *Coupled High* (0.50 s vs. 0.14 s, $p < .001$) schemes.

3.3.3 Subjective Ratings

Out of the four subjective measures described in Section 3.2.7, only one metric, control over the vehicle, was significantly influenced by the evasion scheme ($F(2, 45) = 5.289,\ p = .009$) (see Fig. 3.13c). (Participants answered the following prompt on a five-point likert scale: Please rate how much control you had over the vehicle during obstacle avoidance. 1- Very Low, 5-Very High.) Post-hoc tests indicated that participants reported significantly higher mean control over the vehicle in the *Coupled Low* scheme compared to the *Decoupled with Feedback* scheme (2.44 vs. 1.44, $p = .008$).

3.4 Discussion

Whether higher control authority should be provided to the driver or to the automation depends on which agent can outperform the other in a particular driving scenario. In emergency obstacle evasion scenarios, automation can often outperform the driver due to its faster reaction times. However, even in emergency scenarios, the driver might still require the means to override the automation in case the automation system misses an obstacle or activates unjustifiably. This study focused on understanding how the control authority should be allocated between the driver and automation in emergency scenarios, and through what kind of obstacle evasion scheme.

I investigated the relative merits of providing full control authority to the automation by completely decoupling the steering wheel from the road versus sharing the control authority between driver and automation by keeping the steering wheel coupled to the road. With a coupled steering wheel, I further investigated whether a high or a low automation impedance (level of authority) promoted superior driver-automation team performance. In particular, I compared the evasion schemes in their ability to provide protection against driver and automation faults. I created an initially faultless automation system which was designed to provide protection against driver faults by helping the driver avoid obstacles that appeared unexpectedly on the road. I then introduced an automation fault to test which driving scheme allowed the drivers to prevent collisions (and thereby protect against automation faults). I also analyzed performance with purely manual driving to understand the advantages of adding automation to manual driving and the capability of drivers to avoid obstacles on their own.

Adding automation to purely manual driving improved the obstacle evasion performance. When driving manually, the participants hit 59% of obstacles which was significantly higher than the 23%, 5%, and 0% collision rates obtained in the three shared evasion schemes (*Coupled Low*,

Coupled High, and *Decoupled with Feedback* respectively). This indicates that while the protection against driver faults provided in manual driving was not zero, it was still lower than the protection provided in the shared evasion schemes. Moreover, both the peak excursion and driver setpoint obtained in manual driving were significantly larger than the shared evasion schemes, indicating that without automation assistance, participants performed significantly more aggressive and less efficient maneuvers around the obstacles (as also shown in Fig. 3.8). These results establish the baseline obstacle avoidance performance of the participants in emergency scenarios.

The results on collisions across the shared evasion schemes confirmed the hypothesized fault protection tradeoff that was presented in Fig. 3.1: as the authority of an agent (human or automation) increased, the fault protection (obstacle evasion) provided by the other agent was reduced. During driver faults, participants hit significantly more obstacles when they drove alongside the automation system with low impedance. Assuming that impedance directly corresponds to authority (see [13,131]), the low impedance automation provided lower authority to automation and higher authority to the driver. Higher driver authority reduced the automation's ability to suppress the driver's tendency to fight the automation-initiated maneuvers. On the other hand, when automation was provided more authority, driver disturbance was suppressed allowing safer obstacle evasion maneuvers. This observation was further supported by the 0% collision rate obtained in the decoupled driving mode where automation was provided full control authority and driver input was completely suppressed.

On the other hand, during automation faults—in particular when the automation activated unjustifiably—the participants hit significantly more obstacles when they drove alongside the automation system with higher impedance. Participants in the high impedance automation group reported that they recognized the automation failure but found it difficult to overpower the automation in time to prevent the collision (consistent with the observations in [60,131,132]). Clearly, the high impedance automation provided more authority to automation and less authority to the drivers resulting in more collisions during automation faults. For the same reason, decoupling the steering wheel resulted in 100% collision rates because the driver had no authority over the vehicle. These results corroborate the known pitfalls of using higher levels of automation in systems where automation is subject to faults. If the automation system is unreliable, giving automation more authority precludes the driver from covering for automation faults [139].

Driving alongside the automation system with high impedance also caused driver discomfort. Some participants in the high impedance automation group reported that the transitions from manual to automated driving were abrupt and discomforting because the automation system intervened with a large force. These observations were further borne out in the mean driver torque metric, which was found to be the highest for the high impedance automation case. The discomfort experienced by the participants may also have caused significantly shorter excursion times in the high impedance

automation case. It is possible that the struggle for control against the automation system forced the participants to return to the lane center earlier and shorten the duration of excursions.

One of the main objectives of this study was to investigate whether it is reasonable to decouple the driver for the duration of an obstacle evasion. Clearly decoupling the driver avoided causing driver discomfort observed in the high impedance automation case and avoided collisions during driver faults observed in the low impedance automation case. However, decoupling also resulted in the highest number of collisions when automation failed as it took away the driver authority required to intervene and prevent collisions. The lack of driver authority further resulted in the out-of-the-loop problem; decoupled driving degraded driver vigilance and caused collisions when automation did not activate [19]. As shown in Fig. 3.8, six out of eight participants in the decoupled driving scheme were not able to avoid the obstacles when automation was inactive. Being out-of-the-loop also made the drivers significantly less active during obstacle evasion. Decoupled drivers exhibited both significantly lower peak steering angle and driver setpoint than the other evasion schemes, indicating that they did not apply the steering angle necessary to avoid the obstacles. Further, as indicated by the driver lag metric, the drivers reacted slower to the emergencies when they were decoupled and did not attempt to avoid the obstacles in time (consistent with [140]).

Another shortcoming of decoupled driving is the lack of system transparency and the potential for miscommunication with the driver [141,142]. Especially in emergency interventions, where the drivers are decoupled for a short interval but are still provided torque feedback corresponding to automation action, drivers can be misled into believing that they have some control over the vehicle. This tends to reduce driver's awareness of the driving mode (manual or automated driving) and results in "mode confusion" which can be detrimental to the driving performance [62,128,141]. Results on the estimated driver torque revealed that the participants were confused about who was in control at a given point in time. Participants in the decoupled driving mode applied significantly larger driver torque than in the low impedance automation case. This was unexpected because the automation system in the decoupled case and the low impedance automation case were designed with the same mechanical impedance. Moreover, five out of 18 participants in the decoupled scheme reported that they had some control over the vehicle during obstacle evasion when in fact they had no control. Two participants in the decoupled scheme reported that they tried to counteract automation because they thought they could influence the vehicle trajectory.

Note that in terms of obstacle evasion, the decoupled and coupled high impedance automation schemes exhibited similar performance. There were no significant differences in the collision rates obtained in the two schemes either during driver faults or automation faults. None of the subjective ratings collected through the survey were significantly different between the two schemes. Both schemes provided a high authority to the automation system and resulted in performance breakdowns during automation failures and human factors issues. These results indicate that until

automation is fully reliable, an obstacle evasion scheme that provides high authority to automation might cause more issues than a scheme that provides low authority to automation. Decoupling the drivers may result in out-of-the-loop issues and mode confusion and high impedance automation may cause driver discomfort. Such human factors issues were not observed with low impedance automation and manual driving in this study.

One limitation of this study was the absence of speed control. Subjects reported that the lack of brakes and throttle made it difficult to avoid collisions. While in the real world drivers may prefer braking instead of steering away from the obstacles, past research has shown that at the speed and time-to-collision chosen in this experiment, steering maneuvers result in more successful obstacle evasion than braking [61,64,143]. Moreover, adding speed control in the study would have made it difficult to isolate the influence of a driver's steering behavior on obstacle evasion. Another limitation of the study was lack of warnings and alerts prior to obstacle evasions. Some subjects reported that the interventions were too abrupt and startling at times and a warning could have prepared the drivers and improved the obstacle evasion performance (consistent with [64,68]). In future experiments it would be valuable to explore the effectiveness of providing haptic, visual, and audio alerts before the obstacle evasions.

3.5 Conclusions and Future Work

This driving simulator study investigated the performance of four emergency obstacle evasion schemes during driver and automation faults. The evasion schemes differed in the amount of control authority provided to the human drivers. Drivers were either provided no driving authority by decoupling their steering inputs from the tires, or a partial driving authority by keeping them coupled with a low or high automation impedance, or full driving authority by removing the automation assistance. The results revealed a tradeoff between the control authority provided to one agent (driver or automation) and the fault protection provided by the other agent. Higher driver authority reduced automation's ability to prevent collisions during driver faults while higher automation authority reduced driver's ability to prevent collisions during automation faults. Moreover, coupled high impedance automation resulted in driver discomfort, as a significantly larger effort was required to overpower the high impedance automation. Decoupling the drivers prevented driver discomfort and reduced collisions during driver faults by taking the driver out of the loop, but caused more collisions during automation faults. Decoupled driving further reduced driver's vigilance and mode awareness during obstacle evasions.

As long as automation remains only partially reliable, decoupled driving appears unacceptable as it deprives the drivers of the ability to intervene during automation failures. Moreover, decoupled driving may carry human factors issues that can put both the drivers and the surrounding vehicles at

risk. Coupled driving may prevent these issues but may result in collisions during driver faults if designed with a low impedance and may result in collisions during automation faults if designed with a high impedance. Future studies could focus on designing coupled driving schemes that are safe to operate during both driver and automation faults. One potential way forward is to combine the advantages of low and high impedance automation system through an adaptive impedance automation design. An adaptive impedance system would assume a high level of authority during emergency situations in which the automation has high confidence, and a low level of authority during situations in which the automation has low confidence, so as to grant override power to the human [13,132,144]. The design challenge for such a system would be to modulate automation impedance as a function of driver intention, sensor precision, and environment complexity.

CHAPTER 4

Estimating Road Feedback for Driving on Uneven Roads

4.1 Introduction

The torque experienced by a driver at the steering wheel, also referred to as steering feel, significantly influences a driver's perception of a vehicle [73–75]. In modern cars, this torque feedback is primarily regulated by the Electric Power Steering (EPS) system [145]. An EPS system modulates the torque feedback by overlaying controlled amounts of torque on the steering column of the vehicle [69]. The objectives of the EPS system are to make the driving task easier, safer, and more comfortable while keeping the driver aware of road conditions [146,147].

To achieve these objectives, the EPS system uses an estimate of rack force [70,145,148]. Rack force is defined as the force transmitted from the front tires to the steering rack of a vehicle through the tie rods. Tire forces and moments, and hence the rack force, arise from the interaction of tires with the road. Naturally, rack force depends on the road profile, but also on how the road profile is traversed, and thus depends on the steering angle in combination with the road profile. When a driver performs a steering maneuver, the tire forces and moments and hence the rack force generally oppose the effort applied by the driver. The counteracting rack force increases the driver effort needed to steer the vehicle, however it also informs the driver of the vehicle state and the road conditions. Accordingly, EPS uses rack force estimates to attenuate the rack force and assist the driver in performing the maneuver, while leaving a portion of the counteracting force unattenuated to maintain driver awareness [70,71,146].

Apart from the EPS assist torque, rack force estimates are also used to determine the EPS torque needed to reject disturbances arising from elements internal to the steering system [69,71,75]. Lane keeping and steer-by-wire systems also utilize the estimates of rack force [148–150]. Unfortunately, it is expensive to install reliable measurement systems for rack force in commercial vehicles [74,150]. As a result, estimation of rack force using real-time capable techniques has attracted the attention of researchers both in industry and academia [69,73,148,151].

One real-time capable technique used for rack force estimation utilizes system identification (SID) methods. An SID-based estimator uses data generated through driving experiments to

identify a model between the measured output rack force and a measured input signal (such as rack displacement) [151,152]. Such estimators are computationally inexpensive and can be used in vehicles of different configurations [151]. However, current SID-based estimators can only estimate rack force due to the steering angle and ignore the effect of road profile variations on rack force.

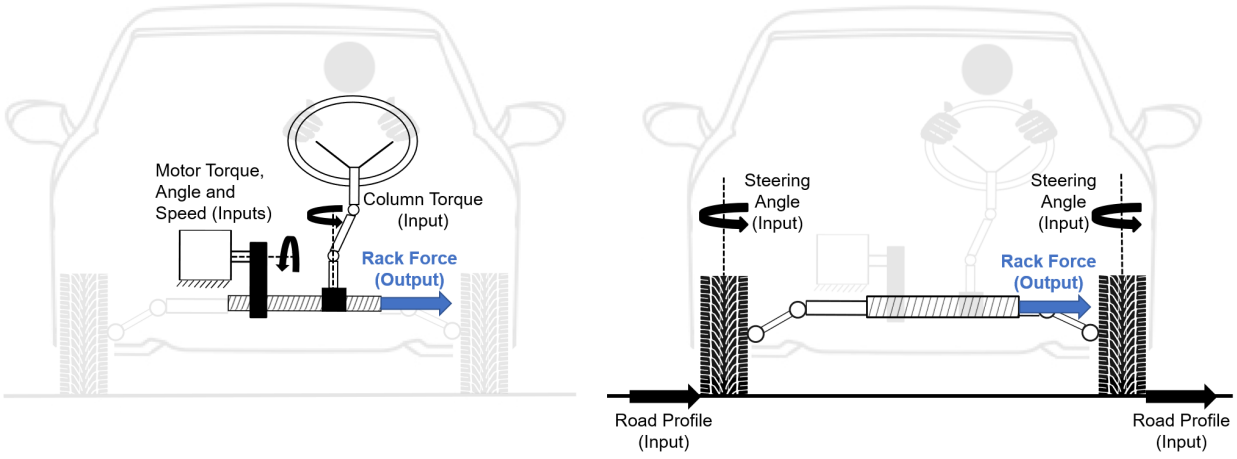

(a) (b)

Figure 4.1: Two common methods to estimate rack force due to steering angle and road profile. (a) In a steering model-based (SM-based) rack force estimator, the sensed EPS motor angular position, speed, and torque along with the steering column torque are fed into an input observer to compute rack force. (b) In a vehicle and tire model-based (VTM-based) rack force estimator, the road profile and the steering angle are fed into a combined vehicle and tire model to compute rack force.

A rack force estimator that disregards the effect of road profile variation can negatively affect the driver's safety. Studies show that any inability to account for road profile variation, such as road bank, road grade, and side-slopes, can result in long periods of unaccounted steering disturbances which might increase the chance of rollover and loss of steering control [153–156]. Therefore, estimators that can account for road profile variation in rack force estimation have the potential to improve both the safety and comfort of the driver. Estimators shown in Fig. 4.1 utilize models of the steering and vehicle systems to estimate the effect of road profile variation on rack force. I call the estimator shown in Fig. 4.1(a) a steering model-based (SM-based) rack force estimator, and the estimator shown in Fig. 4.1(b) a vehicle and tire model-based (VTM-based) rack force estimator.

The SM-based rack force estimator uses a lumped parameter model of the steering system along with the EPS motor torque, position, and speed, and the steering column torque to produce an estimate of rack force [69,70,148,157]. The SM-based rack force estimators have been widely used in EPS applications because of their ability to produce sensor-level-accurate rack force estimates. However, the SM-based estimators do not support decomposition of rack force; the SM-based

estimators cannot estimate the contribution of road profile variation to rack force independent of the contribution of steering angle. The SM-based estimators further require identification of the inertia, damping and stiffness values of steering system components [148].

An estimator that produces estimates of rack force due to road profile independent of the steering angle holds additional advantage for EPS control; two separately estimated components of rack force can be compensated individually to different degrees to enhance the steering feel. Several researchers have adopted the idea of performing decomposition of steering signals such as rack force [71,73], steering angle [158,159], and steering torque [74,147,160,161] with the aim of performing targeted compensation on the signal components and improving the steering feel. Currently, only the VTM-based rack force estimators (depicted in Fig. 4.1(b)) are capable of producing component-wise estimates of rack force. A VTM-based estimator uses sensed steering angle and road profile together with a vehicle model and tire model to produce its estimate of rack force.

VTM-based rack force estimators have appeared in various forms. Software packages such as CarSim and CarMaker use relatively more complex VTM-based estimators to produce highly accurate rack force estimates [162,163]. A disadvantage of the estimators used in these packages is that they are computationally heavy and therefore cannot be used in real-time in production vehicles. They can, however, be used for running simulation studies to verify the estimation performance of other estimators [164,165]. Real-time capable VTM-based estimators appearing in the literature use simpler vehicle and tire models for rack force estimation and are computationally inexpensive. Conventional VTM-based estimators ignore the presence of road profile variations and only consider the steering angle as an input when estimating the rack force (perhaps due to the unavailability of real-time road profile measurements) [69,75,77,78].

In this chapter, I present three VTM-based estimators that I developed to estimate and decompose rack force using sensed steering angle and road profile inputs. I develop the estimators with the same vehicle model but three different tire models to isolate the effect of the tire model on estimation accuracy. I present the results from three driving experiments to comment on which features of the tire models improve or reduce the accuracy of rack force estimation. In addition, I present a CarSim simulation study to test whether the estimates of rack force due to steering angle and rack force due to road profile produced by one of the three estimators can potentially be used to perform targeted compensation.

This chapter is organized as follows. In Section 4.2 I briefly discuss the overall structure of a VTM-based rack force estimator. Section 4.3 presents the details of the vehicle model and the three tire models used to estimate the rack force. In Section 4.4 I describe the driving experiments which were used to compare the model fidelity of the three estimators, and the simulation setup that was used to produce the component-wise estimates of rack force. Section 4.5 presents the results and discussion for the driving experiments and the simulation study followed by Section 4.6 that

presents the conclusions of the chapter.

4.2 Modeling Framework

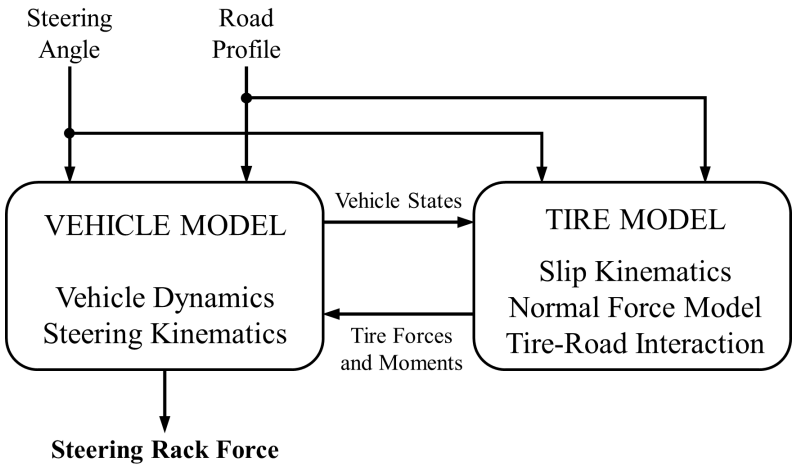

Figure 4.2: Simplified structure of the VTM-based rack force estimator. The road profile and the steering angle are inputs to a vehicle model and tire model that in combination enable rack force estimation. The tire model includes a slip kinematics model to estimate the tire slip angles, a model to estimate tire normal force, and a tire-road interaction model to estimate tire forces and moments. The vehicle model includes a vehicle dynamics model to estimate vehicle states and a steering kinematics model to estimate rack force.

Fig. 4.2 shows the simplified structure of a VTM-based rack force estimator. For a relatively constant non-zero vehicle speed, the two inputs to the estimator are steering angle and road profile. While the steering angle is primarily governed by the driver, the road profile is determined by the environment. Road profile is generally characterized by the slope and the frequency content of the road. Various advanced model-based and sensor-based methods can be used to estimate road profile. The model-based methods include input observers or disturbance observers that work alongside a vehicle model to estimate road profile inputs [166,167], and sensor-based methods include use of cameras [168], radar [169], LiDAR sensors [170], and GPS working alongside on-board vehicle sensors [171]. Certain road profile inputs, especially road slopes, can also be estimated on the fly using on-board sensors (see [135,172], for example). The focus of this study was limited to only two types of road profile variations: road slopes (longitudinal and lateral) and road cleats.

Referring to Fig. 4.2, in a VTM-based rack force estimator, the steering angle and road profile signals are first made available to a vehicle model that generates vehicle states. The same signals along with the vehicle states are then used in a tire model to obtain tire slip angles and tire forces and aligning moments. These forces and moments are in turn used in the vehicle model to generate

vehicle states for the next time instant. Meanwhile, the tire aligning moments are used to determine the steering rack force using a steering kinematics model that relates tire aligning moments to the rack force.

4.3 Modeling

In this section I present three VTM-based estimators that I developed to determine rack force. The three estimators are only distinguished by their tire models. The first estimator has a Linear Tire model [173], and is called the LT Model. The second estimator has a nonlinear Brush Tire model (also known as the elastic foundation model) [113], and is called the BT Model. The third estimator has a Rigid Ring tire model [174], and is called the RR Model. All the estimators are based on the same vehicle dynamics given by the 2DOF bicycle model presented in [135].

The following assumptions apply to all rack force estimators presented in this chapter:

1. The tire parameters such as tire stiffness and damping and tire radius were assumed constant.
2. Tire inertia and wheel camber were assumed negligible. Tire-road friction μ was assumed constant: $\mu = 1$.
3. The components of the steering system were assumed mass-less. The vehicle's mass was assumed constant.
4. The influence of the suspension system on rack force was assumed negligible.

In the following subsections, I first describe the vehicle model common to the three estimators followed by a description of the three tire models that distinguish the estimators. I then present how rack force was estimated using the tire models and briefly describe the assembly of the vehicle and tire models that enable rack force estimation. I conclude the section by describing how VTM-based estimators can be used to produce component-wise estimates of rack force and how the component-wise estimates can be used to perform targeted compensation to improve steering feel.

4.3.1 Vehicle Model

Consider a vehicle of mass m and yaw inertia I driven with steering angle δ and speed u. Let the the vehicle yaw angle be ψ, and let the forces on the vehicle's front (f) and rear (r) tires in the longitudinal (x) and lateral (y) directions respectively be denoted by F_{xf}, F_{xr} and F_{yf}, F_{yr} (see Fig. 3). Likewise, let the tire aligning moments for the front and rear tires be denoted by M_{zf} and M_{zr}. Then the two degrees of freedom of the vehicle, namely, lateral speed v and yaw rate $\dot{\psi}$, or the lateral dynamics of the vehicle for driving on a flat road are governed by the following differential equations [135]

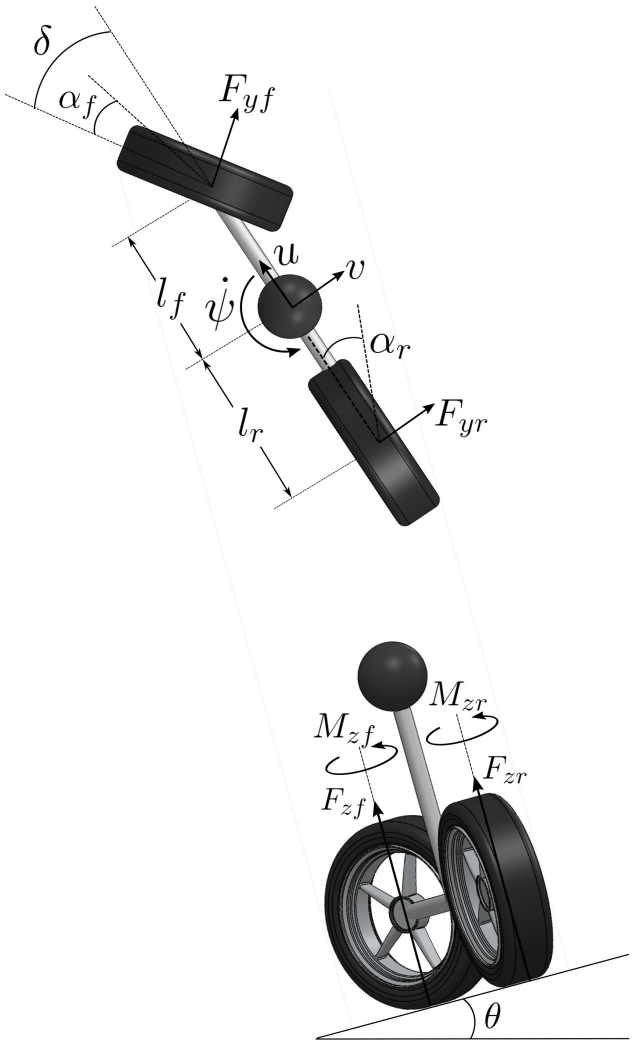

Figure 4.3: Schematic of a 2DOF bicycle model. In the configuration shown, the bicycle drives along a road with lateral slope θ with speed u and steering angle δ . The two degrees of freedom are lateral speed v and yaw rate $\dot{\psi}$. The vertical tire forces, slip angles, tire lateral forces, and tire aligning moments are denoted by F_{zi}, α_i, F_{yi}, and M_{zi}, respectively, where $i \in \{f, r\}$ denotes the front and rear tires.

$$\begin{aligned} m\dot{v} + mu\dot{\psi} &= F_{xf}\sin\delta + F_{yf}\cos\delta + F_{yr} \\ I\ddot{\psi} &= l_f F_{xf}\sin\delta + l_f F_{yf}\cos\delta - l_r F_{yr}, \end{aligned} \tag{4.1}$$

where the distance between the center of mass of the vehicle and the centroid of the front tire contact patch is l_f and the distance between the center of mass of the vehicle and the centroid of the rear tire contact patch is l_r.

Assuming the steering angle δ remains small, the differential equations governing the lateral

dynamics of the vehicle can be rewritten as

$$\begin{aligned} m\dot{v} + mu\dot{\psi} &= F_{yf} + F_{yr} \\ I\ddot{\psi} &= l_f F_{yf} - l_r F_{yr}. \end{aligned} \tag{4.2}$$

Now consider driving on an uneven road. Equation (4.2) also applies for driving on a longitudinal slope or a road grade because the longitudinal slope does not significantly influence the lateral dynamics of the vehicle [135]. Likewise, although driving over a cleat or a pothole changes the tire dynamics considerably, cleats or potholes do not directly influence the vehicle's lateral dynamics. On the other hand, for driving on a lateral road slope or a road bank (simply referred to as road slope in this chapter), the differential equation for the lateral speed is different. If the lateral slope of the road is θ, as shown in Fig. 4.3, and the acceleration due to gravity is denoted by g, the vehicle states are governed by the equations

$$\begin{aligned} m\dot{v} + mu\dot{\psi} + mg\sin\theta &= F_{yf} + F_{yr} \\ I\ddot{\psi} &= l_f F_{yf} - l_r F_{yr}. \end{aligned} \tag{4.3}$$

A detailed derivation of these equations can be found in [135].

4.3.2 Tire Model

The rack force is primarily influenced by the aligning moments acting on the front tires of a vehicle because the movement of the steering rack is linked to the steering angle of the front tires. Therefore, to enable rack force estimation, the primary objective of a tire model is to estimate the aligning moments acting on the front tires. For the bicycle model, since the front tires are lumped into a single tire, the goal of the tire model is simply to estimate the aligning moment M_{zf}.

In order to obtain the aligning moment, it is first required to obtain tire slip angles and tire normal forces. The vehicle states obtained using Equations (4.2) and (4.3) can be used to determine the lateral slip angles α_f and α_r of the front and rear tires using the equations

$$\begin{aligned} \alpha_f &= \frac{v + l_f\dot{\psi}}{u} - \delta, \\ \alpha_r &= \frac{v - l_r\dot{\psi}}{u}. \end{aligned} \tag{4.4}$$

The tire normal forces for the front tires F_{zf} and for the rear tires F_{zr} for driving on the road slope θ

are given by the following equations

$$\begin{aligned} F_{zf} &= \frac{mgl_r \cos\theta}{2(l_f + l_r)}, \\ F_{zr} &= \frac{mgl_f \cos\theta}{2(l_f + l_r)}. \end{aligned} \tag{4.5}$$

The slip angles presented in Equation (4.4) and normal forces presented in Equation (4.5) remain the same in the tire models which are discussed next.

4.3.2.1 Linear Tire (LT) Model

The lateral forces on the front and rear tires with respective cornering stiffness C_{α_f} and C_{α_r} are given by

$$F_{yf} = C_{\alpha_f}\alpha_f; \quad F_{yr} = C_{\alpha_r}\alpha_r. \tag{4.6}$$

To express the lateral forces acting on both the front (f) and rear (r) tires using a single equation, let us rewrite Equation (4.6) in the following form

$$F_{yi} = C_{\alpha_i}\alpha_i, \tag{4.7}$$

where $i \in \{f, r\}$.
The front tire pneumatic trail t_p for the LT Model is given by the expression [175]

$$t_p = t_{p0}\left(1 - \mathrm{sgn}(\alpha_f)\frac{C_{\alpha_f}}{3\mu F_{zf}}\tan\alpha_f\right),$$

where t_{p0} is the pneumatic trail at zero front slip angle.

The aligning moment M_{zf} for the front tire is then given by

$$M_{zf} = -(t_p + t_m)F_{yf}, \tag{4.8}$$

where the front tire mechanical trail t_m is a constant for a given vehicle. For a detailed description of the pneumatic trail t_p and the mechanical trail t_m, the reader is referred to [113].

Note that the tire lateral forces are directly proportional to the slip angles which is why this model is referred to as the "linear tire" model. Such proportionality only applies within a range of slip angles, in particular for low values of slip angles, after which it no longer captures the variation of tire forces accurately [113].

4.3.2.2 Brush Tire (BT) Model

Unlike the LT Model where the tire forces vary linearly with the slip angles, in the BT Model the tire forces are non-linear in the slip angles. Therefore, the BT Model can provide a better estimate of rack force over a larger range of slip angles. According to [113], the lateral tire force for the front (f) and rear (r) tires is given by

$$F_{yi} = \begin{cases} \mu F_{zi}(3\theta_s\alpha_i - 3(\theta_s\alpha_i)^2 + (\theta_s\alpha_i)^3) & \text{if } \alpha_i \leq \frac{1}{\theta_s} \\ \mu F_{zi} & \text{if } \alpha_i \geq \frac{1}{\theta_s}, \end{cases} \tag{4.9}$$

where again $i \in \{f, r\}$ and μ is the coefficient of friction between tire and road. The normal force F_{zi} is given by Equation (4.5), and θ_s is a tire parameter that, for tire tread stiffness of c_p and the contact patch length of $2a$, is defined by

$$\theta_s = \frac{2}{3}\frac{c_p a^2}{\mu F_{zi}}$$

The front tire pneumatic trail t_p for the BT Model is given by the expression [113]

$$t_p = \frac{1}{3}a\frac{1 - 3|\theta_s\alpha_f| + 3(\theta_s\alpha_f)^2 - |\theta_s\alpha_f|^3}{1 - |\theta_s\alpha_f| + \frac{1}{3}(\theta_s\alpha_f)^2}. \tag{4.10}$$

For mechanical trail t_m, the tire aligning moment M_{zf} can then be obtained by using the following expression which is the same as the one used in the LT Model

$$M_{zf} = -(t_p + t_m)F_{yf}. \tag{4.11}$$

4.3.2.3 Rigid Ring (RR) Model

In the LT and BT models, road unevenness is incorporated only in the vehicle model. For instance the road slope θ only influences the vehicle states and the normal force acting on the vehicle which in turn influence the slip angles and hence the tire aligning moment M_{zf}. Any tire deformation due to road unevenness is not taken into account in the LT and BT tire models. This simplification may work when the vehicle travels over low frequency road profile variations such as smooth road grades or banks. However, as the frequency of road profile variations increase, the tires start deforming significantly making it crucial to estimate the influence of tire deformation on tire moments.

The Rigid Ring (RR) tire model can estimate tire forces and moments due to tire deformation on high frequency road profile variations such as road cleats and potholes [113,174,176]. To estimate

the forces and moments, the RR model utilizes the road profile inputs generated by an "enveloping model" [174]. The enveloping model uses the measurements of the actual road profile to produce an "effective road profile" that the deformed tires effectively experience on uneven roads. Enveloping models are discussed in detail in [174,177]. In this study, I used a double track, three-dimensional, tandem tire enveloping model presented in [174] that takes as inputs the dimensions of the cleats (length, height, and angle) and the location of cleats. The 3D enveloping model produces an effective road profile in terms of three road geometry parameters: effective tire height w, effective tire lateral slope β_x, and effective tire longitudinal slope β_y. For a tire with vertical stiffness C_z, the effective road profile is used to estimate the radial deflection of the tire ρ_z as

$$\rho_z = \left(w - \frac{mgl_r \cos\theta}{2C_z(l_f + l_r)} \right) \cos\beta_y, \tag{4.12}$$

which in turn is used to estimate the radial tire force F_z^{rad} using the following equation

$$F_z^{rad} = q_{Fz1}(1 + q_{Fz3}(\beta_x)^2)\rho_z + q_{Fz2}\rho_z^2. \tag{4.13}$$

Given the effective road profile, and the radial tire force F_z^{rad}, the RR model estimates the contact patch normal force F_{cN} as follows (see [178] for a detailed derivation):

$$F_{cN} = \frac{1}{\cos\beta_x}(F_z^{rad} + ((D_N \sin(C_N \arctan(B_N\beta_x))) \cos\beta_x - F_z^{rad} \sin\beta_x) \sin\beta_x) \tag{4.14}$$

Using F_{cN}, the tire lateral forces F_{yi} ($i \in \{f, r\}$) can then be estimated using [174]

$$F_{yi} = D_y \sin(C_y \arctan\{B_y\alpha_{yi} - E_y(B_y\alpha_{yi} - \arctan(B_y\alpha_{yi}))\}) + S_{Vy}. \tag{4.15}$$

The front tire pneumatic trail t_p for the RR Model is given by

$$t_p = D_t \cos(C_t \arctan\{B_t\alpha_{tf} - E_t(B_t\alpha_{tf} - \arctan(B_t\alpha_{tf}))\}),$$

and the resulting aligning moment M_{zf} acting on the front tire can be estimated using

$$M_{zf} = -t_p F_{yf} + D_r \cos(\arctan B_r\alpha_{rf}), \tag{4.16}$$

where the slip angles (α_{yi}, α_{ti}, and α_{ri}) are given by

$$\alpha_{yi} = S_{Hy} + \tan\alpha_i, \qquad \alpha_{ti} = S_{Ht} + \tan\alpha_i, \qquad \alpha_{ri} = \tan\alpha_i.$$

The coefficients B_y, B_r, B_t, C_y, C_t, D_y, D_r, D_t, E_y, E_t, S_{Hy}, and S_{Ht} are either constants or

are functions of slip angles (α_{yi}, α_{ti}, and α_{ri}) and contact patch normal forces F_{cN}, and tire normal forces F_{zi} [174,178].

4.3.3 Rack Force Estimation

The aligning moment M_{zf} obtained using each model was used to estimate the resultant road feedback or the rack force RF using the expression

$$RF = i_p M_{zf}, \tag{4.17}$$

where the constant ratio i_p defines the tire moment to rack force transmission ratio for a given vehicle, and is determined using steering kinematics.

4.3.4 Model Assembly

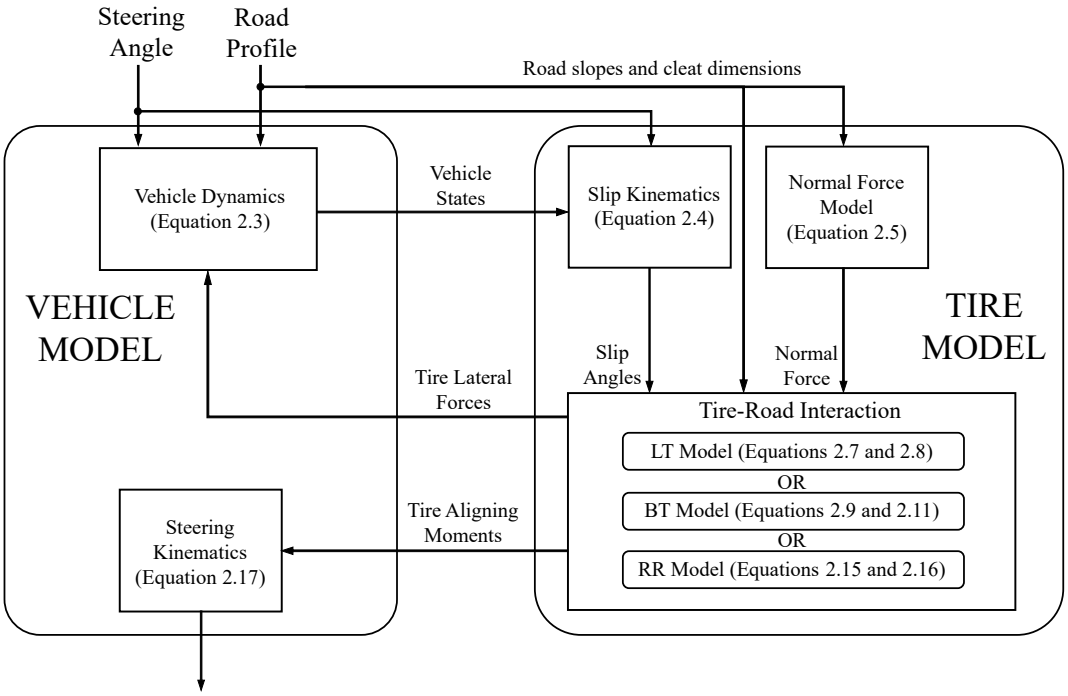

Figure 4.4: An expanded version of Fig. 4.2 is used to describe the rack force estimation process with references to the equations presented in Section 4.3.

Referring to Fig. 4.4, the vehicle states (lateral speed v and yaw rate $\dot{\psi}$) are produced using the vehicle dynamics represented by Equation (4.3) for sloped roads. Independently, the vehicle's mass and dimensions and the road slope are used to compute normal tire forces using Equation (4.5). In the tire model, the vehicle states are used to find the tire slip angle for the front and rear

tires using Equation (4.4). Tire slip angles and normal forces are then used to find tire forces and aligning moments using Equations (4.7) and (4.8) for the LT Model, Equations (4.9) and (4.11) for the BT Model, and Equations (4.15) and (4.16) for the RR Model. The tire forces are fed back into the vehicle model in Equations (4.2) and (4.3) to generate the vehicle states for the next time instant. During this process, the rack force for each time instant is obtained through Equation (4.17) using the aligning moment estimated in Equation (4.8) for the LT Model, in Equation (4.11) for the BT Model, and in Equation (4.16) for the RR Model.

4.3.5 Targeted Compensation using Rack Force Components

VTM-based estimators can be utilized to determine the rack force due to steering angle independent of the rack force due to road profile. The components can then be used to compensate for the individual effects of steering angle and road profile on the steering feel. However, there are some preliminary requirements for performing such a targeted compensation. In this subsection, I attempt to outline these requirements.

Consider rack force RF obtained in Equation (4.17). RF is clearly a nonlinear function of steering angle and road profile, and can be expressed using a generic function f as

$$RF = f(\delta, \theta). \tag{4.18}$$

Now let us denote rack force due to steering angle by $RF_{Steering}$ and rack force due to road profile by RF_{Road}. Using Equation (4.18), $RF_{Steering}$ and RF_{Road} can be obtained by using one input at a time in function f as follows

$$RF_{Steering} = f(\delta, 0), \quad RF_{Road} = f(0, \theta). \tag{4.19}$$

Since rack force is nonlinear, $RF_{Steering}$ and RF_{Road} may not be the only components of rack force. Rack force may consist of additional nonlinear components arising from the interaction of steering angle and road profile inputs. Let us combine the additional components of rack force into a single variable ΔRF which I call the residual rack force. The rack force RF can then be decomposed into three components

$$RF = RF_{Steering} + RF_{Road} + \Delta RF \tag{4.20}$$

Clearly, to properly perform targeted compensation it is important to verify whether the residual rack force ΔRF is small in comparison to $RF_{Steering}$ and RF_{Road}. If $RF_{Steering}$ and RF_{Road} are not the primary components of rack force, compensating only for the effect of steering angle and

road profile may not be sufficient. The unknown and uncompensated residual rack force may result in incorrect compensation which in turn may result in a substandard or undesirable steering feel. According to Equation (4.20), ΔRF can be obtained by subtracting the sum of the components of rack force, that is $RF_{Steering} + RF_{Road}$, from the total estimated rack force RF. In Section 4.5, I therefore compare $RF_{Steering} + RF_{Road}$ with rack force RF to verify whether ΔRF is small and whether the rack force is primarily composed of only $RF_{Steering}$ and RF_{Road}.

To perform targeted compensation, it is also important to verify whether the estimates of rack force due to steering angle $RF_{Steering}$ and rack force due to road profile RF_{Road} obtained using the estimator accurately represent the contributions of steering angle and road profile to rack force. Unfortunately, unlike the total rack force RF, the component-wise estimates of rack force $RF_{Steering}$ and RF_{Road} cannot be validated using the force measurements available from strain gauges mounted on the steering rack. However, estimates produced by higher DOF VTM-based rack force estimators, such as those available in commercial vehicle dynamics packages, can still serve as a reference to compare the estimates produced by low DOF VTM-based rack force estimators. In the next section I discuss how the component-wise estimates produced by one of the estimators were compared with the estimates produced by a higher DOF rack force estimator available in CarSim.

4.4 Methods

In this section I describe the experimental setup and the simulation setup used to test the performance of the three rack force estimators developed in this chapter. I first describe the three driving experiments and the hardware setup that were used to determine and compare the real-time estimation accuracies of the rack force estimators. After that, I explain the simulation setup that was used to verify whether the component-wise estimates of rack force can be used to perform targeted compensation.

4.4.1 Experimental setup

Driving experiments were performed at test tracks with known road profile variations. The test tracks were located at Ford's Dearborn Development Center (formerly Dearborn Proving Grounds) in Dearborn, Michigan. The results from the following experiments are described in this chapter:

1. *Experiment 1: Driving on a road with varying lateral slope*
   Driving experiment 1 was performed on a crowned road with 11° slope on the two sides of the road crown. The vehicle was driven from one side to the other side with a speed of about 20 km/h.

2. *Experiment 2: Aggressive slalom driving on a road with constant lateral slope*

Experiment 2 was performed on a road with constant lateral slope of about 11°. The steering angle was varied between approximately -60° and 60° to perform a slalom maneuver with a speed of about 15 km/h.

3. *Experiment 3: Slalom driving on a road with cleats of varying heights*
   Experiment 3 was performed on a road with thirteen metal cleats of known dimensions: the first four cleats were 1 cm tall, the next five cleats were 2 cm tall, and the remaining cleats were 3 cm tall. All cleats were 4 cm long and were oriented transverse to the road. Driving speed was maintained at about 30 km/h. The steering angle was varied between approximately -30° and 30° so that the vehicle impacted the cleats at an angle (roughly equal to the steering angle). This maneuver was performed to test the performance of the estimators for driving over arbitrary high frequency unevenness, such as oblique cleats, on the road. Moreover, hitting the cleats straight with zero impact angle did not significantly influence the tire aligning moment and therefore did not induce much rack force.

(a)

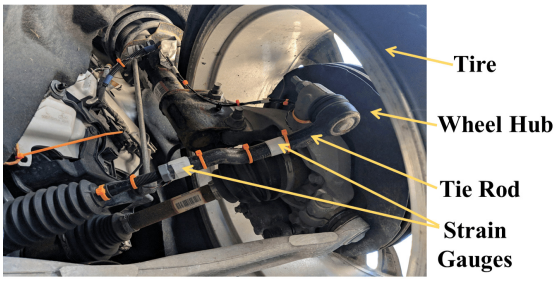

(b)

(c)

Figure 4.5: Experimental setup. (a) Lincoln MKX test vehicle. (b) Tie rod instrumented with strain gauges to measure the steering rack force. (c) Inertial measurement unit (IMU) mounted inside the car used to measure the road slopes during driving.

The experiments were performed using the Lincoln MKX vehicle equipped with Pirelli (Scorpion

Verde AS) tires shown in Fig. 4.5 (a). The tire model specific parameters used in the models were taken from Table A3.1, Appendix 3, in [113] and from Table B.1, Appendix B, and Table 3.5 (section 3.7), in [174]. The tests required to identify the parameters of the RR model are further discussed in Section 3.7 in [174] and Appendix 3 in [113]. Other tire and vehicle specific parameters can be found in [135]. To evaluate the estimation performances of the models, the rack force estimates produced by the three models were compared to the measurements from strain gauges installed on the tie rods of the test vehicle (shown in Fig. 4.5 (b)). The steering angle and the vehicle speed were measured using steering angle and tire speed sensors, respectively. The vehicle speed was calculated by multiplying the tire rolling circumference with the angular speeds of the left and right rear tires and then averaging the two resulting products. The vehicle acceleration was computed by digitally differentiating and filtering the vehicle speed.

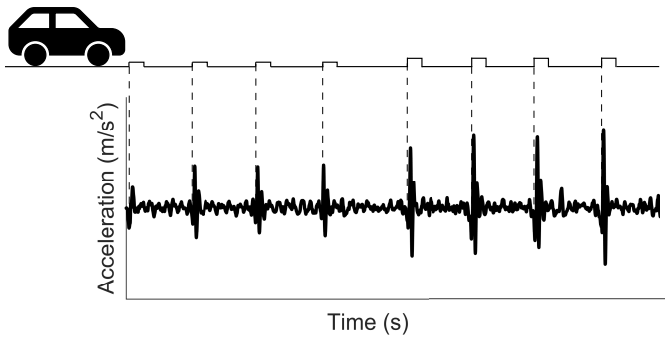

Figure 4.6: Vehicle acceleration was used to determine the location of cleats during the experiments. Each impulse marked the beginning of a cleat. The vehicle speed and cleat lengths were used to estimate the duration of each tire-cleat interaction.

During the driving tests, a rapid control prototyping platform (dSPACE MicroAutoBox) was used to link sensed steering angle, road profile, and vehicle speed signals with an online simulation of the three rack force estimators (integrated in real-time Simulink), using CAN-bus communications at 250 Hz. Five road profile parameters were used in the models: lateral road slope, longitudinal road slope, cleat height, cleat length, and cleat locations. The road slopes (both longitudinal and lateral) were obtained using the pitch and roll measurements obtained from a high fidelity IMU (OXTS RT3003 v2) installed in the vehicle (shown in Fig. 4.5 (c)) that transmitted signals at 100 Hz. The pitch and roll measurements were assumed to be roughly equal to the longitudinal and lateral slopes of the road. The cleat dimensions (height and length) were physically measured on the test track and were fed into the estimator models in Simulink. The vehicle acceleration was used to determine the location of cleats. When tires hit the cleats, the vehicle acceleration showed finite impulses. The impulses were used to synchronise the cleat measurements with the real-time simulation of the RR model in Simulink; each impulse marked the beginning of a cleat (see Fig. 4.6). The length of the cleat and speed of the vehicle were then used to estimate the duration of

tire's impact with the cleats. Ideally the cleat dimensions and locations would be estimated using road preview sensors.

4.4.2 Simulation Setup

The BT Model was used to produce the component-wise estimates of rack force: rack force due to steering angle $RF_{Steering}$ and rack force due to road profile RF_{Road}. Unlike the estimates of total rack force, the component-wise estimates of rack force could not be measured using sensors available in the vehicle. Therefore, a higher DOF VTM-based estimator available in CarSim was chosen as a reference to validate the component-wise estimates of rack force produced by the BT Model. The VTM-based estimator in CarSim had a four-wheel vehicle model that had 15 mechanical degrees of freedom (DOF) in comparison to the bicycle model with only two DOF used in the BT Model. The math model for the 15 DOF model vehicle in CarSim had over 250 state variables. For tire models, CarSim provided various options for tire models that had higher complexity than the Brush Tire model used in the BT Model. I used the semi-empirical tire model called "Internal Table Model with Simple Camber" which used combined slip theory [179] and similarity method [180] to compute tire forces and moments [181].

To perform the simulation experiment, I recreated Experiment 1 described in Section 4.4.1 in the CarSim environment. I fed the recorded steering angle from Experiment 1 into the CarSim Simulink Model and re-created the same road profile in the CarSim driving environment that was traversed while performing Experiment 1. Moreover, I performed the simulation on an SUV vehicle with the parameter values, such as vehicle dimensions, mass, yaw inertia and tire sizes, exactly the same as the parameter values for the Lincoln MKX vehicle on which the actual test was performed.

The CarSim simulation setup is summarized in Fig. 4.7. The first simulation experiment was used to estimate RF_{Road} where the steering angle was set to zero but the driving was simulated on a sloped road (shown in Fig. 4.7 (a)). The second simulation experiment was used to estimate $RF_{Steering}$ where the steering angle was non-zero but the driving was simulated on a flat road (shown in Fig. 4.7 (b)). The vehicle speed remained the same in both simulation experiments. The component-wise estimates obtained using CarSim were then compared with the estimates obtained using the BT model. Finally, the sum of component-wise estimates obtained using the BT Model was compared with the total rack force estimate to determine the contribution of residual rack force to the total rack force.

4.4.3 Performance Analysis

To quantify the performance of a given estimator, I used the normalized root mean square error (NRMSE) between the rack force estimate produced by the estimator RF and the rack force

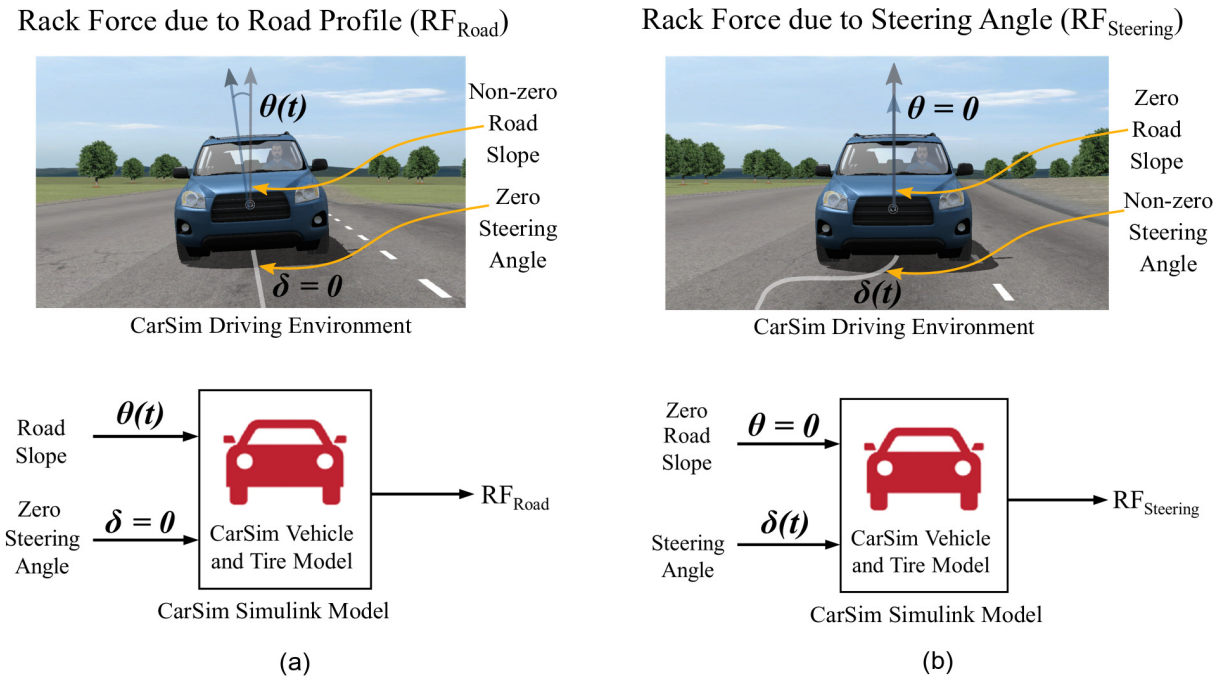

Figure 4.7: CarSim setup for component-wise rack force estimation. (a) RF_{Road} was estimated by setting the steering angle to zero in the CarSim Simulink model and by creating a sloped road profile in the driving environment. (b) $RF_{Steering}$ was estimated by making the steering angle non-zero in the CarSim Simulink model and by creating a flat road profile in the driving environment.

estimated using a reference estimator RF_{ref}. NRMSE was expressed as a percentage and was obtained using the following equation

$$\text{NRMSE}(\%) = \frac{\sqrt{\text{mean}((RF_{ref} - RF)^2)}}{\max(RF_{ref}) - \min(RF_{ref})} \times 100 \tag{4.21}$$

For the driving experiments the sensors mounted in the vehicle served as the reference, whereas for simulation experiments the rack force estimates produced using CarSim served as the reference. I also compared the rack force estimation performance of the estimators to each other to find out which estimator had the highest relative accuracy.

4.5 Results and Discussion

4.5.1 Effect of Model Complexity on Rack Force Estimation

The differences between the three VTM-based estimators were readily apparent in the comparison of estimation errors between the estimators as shown in Table 4.1.

While driving on the road with large slope variation in Experiment 1, no differences were seen between the estimation performances. Despite the significant distinction between the tire models

Table 4.1: Estimation errors (NRMSE %) for the three experiments

Estimator/Experiment	Experiment 1	Experiment 2	Experiment 3
LT (Linear Tire)	5.08%	10.70%	11.36%
BT (Brush Tire)	5.16%	8.57%	11.06%
RR (Rigid Ring)	5.01%	8.18%	7.37%

used in the estimators, all estimators seemed to agree well with the sensor measurements (Fig. 4.8). The estimation errors were low for the three estimators and were only marginally different between the estimators (see Table 4.1). The results indicated that both the linear and nonlinear tire models were equally capable of estimating the rack force irrespective of the magnitude and variation of road slope.

Driving with an aggressive slalom maneuver in Experiment 2, on the other hand, revealed some differences between the estimator using the linear tire model and the estimator using the nonlinear tire model. Estimators with nonlinear tire models, namely, the BT Model and the RR Model, matched the sensor measurements better than the LT Model (Fig. 4.9). For the LT Model, the estimation performance broke down at large steering angles and large steering angle rates (see Fig. 4.9b) while both the BT Model and the RR Model seemed to match the measurements well throughout the experiment (Fig. 4.9c and Fig. 4.9d). The estimation errors for the RR Model and the BT Model were similar to each other and were both lower than the estimation error for the LT Model (see Table 4.1).

The estimation error for the RR Model was the lowest for driving on the road with cleats in Experiment 3. While driving on the flat part of the road, the performance of all estimators seemed similar (Fig. 4.10). However, only the RR Model captured the rack force well when the vehicle drove on cleats as demonstrated by the insets on the plots in Fig. 4.10. Furthermore, as shown in Table 4.1, the estimation error for the RR Model was lower than both the BT Model and the LT Model. The BT Model and the LT Model, on the other hand, seemed to exhibit similar estimation performance.

Clearly, these results reflect the differences in the complexity of tire models used in the three estimators. For example, for Experiment 2, the RR Model and the BT Model perform better than the LT Model because the nonlinear tire models used in the BT Model and the RR Model are better at capturing the tire forces and aligning moments for higher steering angles and slip angles as compared to the linear tire model used in the LT Model. Likewise, in Experiment 3, the RR Model seems to have better performance than both the BT and the LT Model because only the RR Model accounts for high frequency road profile variations (such as cleats) in the estimation of tire forces and moments. And clearly this capability results in a nontrivial difference between the estimation

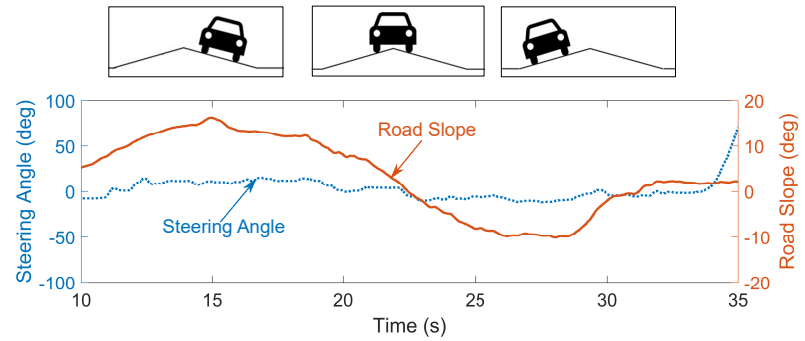

(a)

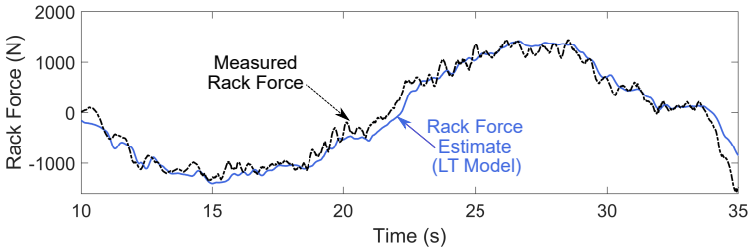

(b)

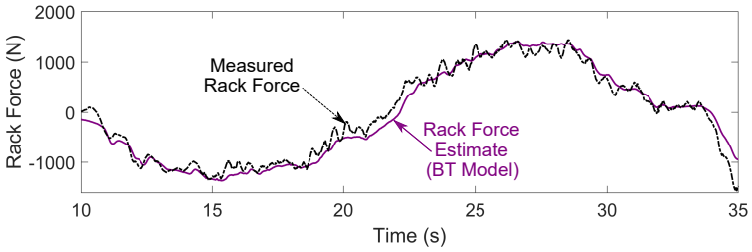

(c)

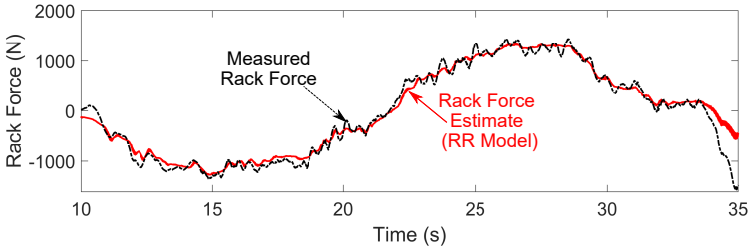

(d)

Figure 4.8: Experiment 1 performed on a crowned road. Vehicle speed was maintained at about 20 km/h. (a) Road profile variation (schematic) and input steering angle and road slope (graph). (b) Rack Force estimated using the LT Model and measured using sensor. (c) Rack Force estimated using the BT Model and measured using sensor. (d) Rack Force estimated using the RR Model and measured using sensor.

errors of the models. On the other hand, all the estimators seem to exhibit satisfactory performance for non-aggressive steering maneuvers regardless of the magnitude and variation of the road slopes as demonstrated by Experiment 1.

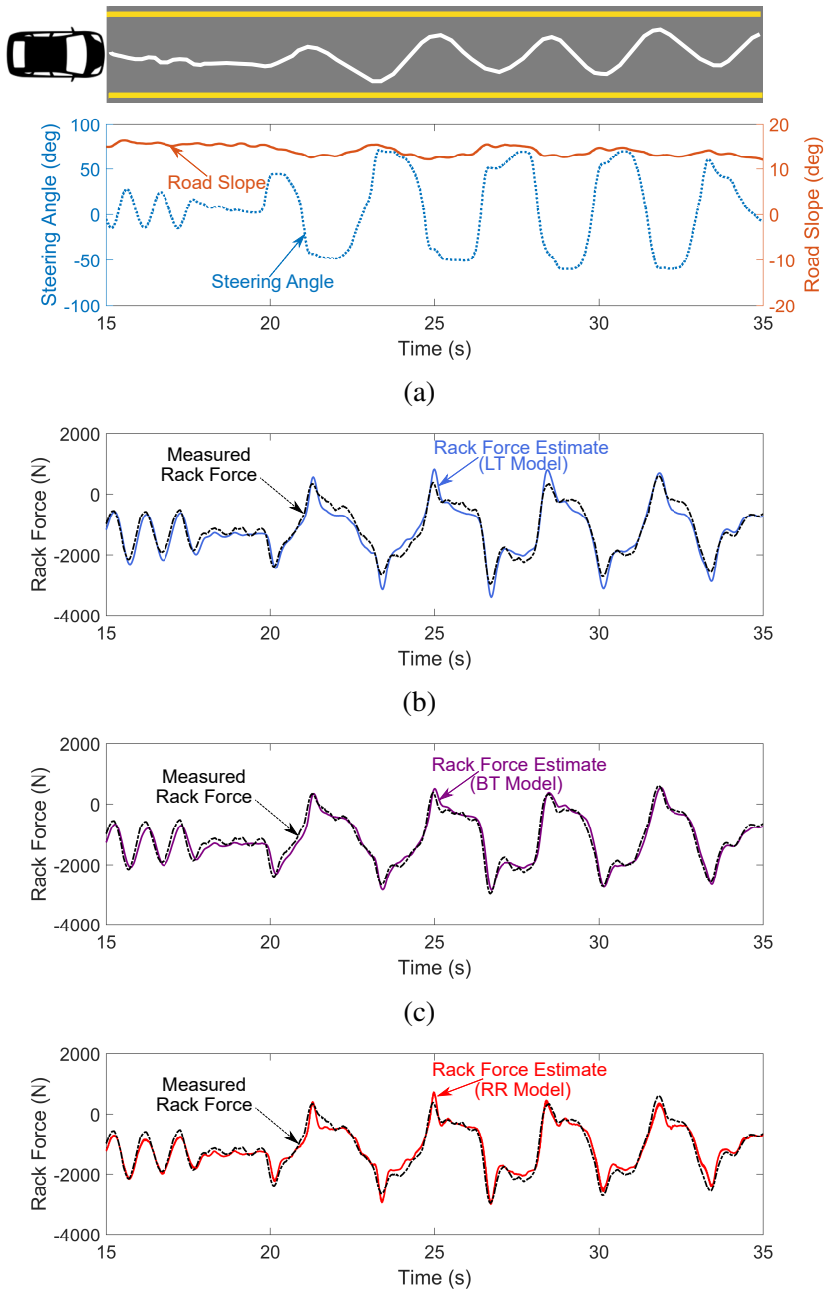

Figure 4.9: Experiment 2 performed with a slalom maneuver on a road with constant lateral slope. Vehicle speed maintained at about 15 km/h. (a) Vehicle maneuver (schematic) and input steering angle and road slope (graph). (b) Rack Force estimated using the LT Model and measured using sensor. (c) Rack Force estimated using the BT Model and measured using sensor. (d) Rack Force estimated using the RR Model and measured using sensor.

In other words, I found that in terms of driving on roads with low frequency profile variations (<8Hz) with non-aggressive steering maneuvers, all three estimators I developed seem to work

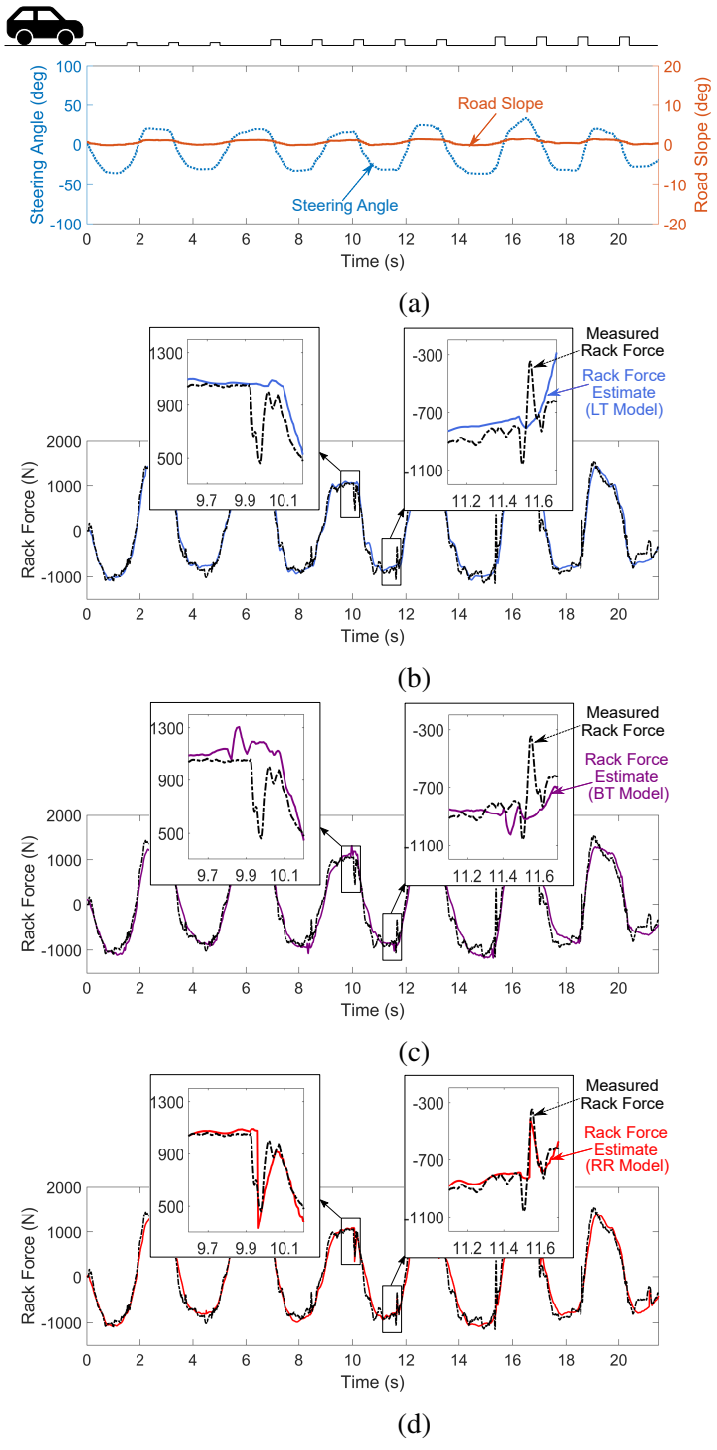

Figure 4.10: Experiment 3 performed with a slalom maneuver on a road with cleats of varying heights. Vehicle speed maintained at about 30 km/h. (a) Road profile variation (schematic) and input steering angle and road slope (graph). (b) Rack Force estimated using the LT Model and measured using sensor. (c) Rack Force estimated using the BT Model and measured using sensor. (d) Rack Force estimated using the RR Model and measured using sensor.

sufficiently well. For driving with slalom steering maneuvers on low frequency road profile variations, however, both the BT Model and the RR Model outperform the LT Model. The BT Model appears to be a better choice for driving on low frequency road profile variations as it is computationally less intensive than the RR Model and produces rack force estimates of accuracy similar to the RR Model. However, for high frequency road profile variation such as produced while driving on road cleats, the RR Model appears to be a better choice for rack force estimation as it supports better estimation performance than the other models.

The rack force estimators presented in this chapter are capable of estimating rack force for driving on different types of road profiles and can therefore be utilized to develop and improve various driver assist controllers. The estimators can be used in existing driver assist controllers that temporarily deactivate their functions when the vehicle transitions from a flat road to an uneven road (see, for example, controllers designed in [69,75,182,183]). The estimators can also be used in virtual prototyping to analyse ride-comfort and durability of a vehicle and in simulating road feedback in hardware-in-the-loop simulators and simulation experiments [78,144,184]. The RR Model, in particular, can also be used in semi and fully autonomous vehicles equipped with advanced road preview technology. Using the road profile inputs available from road preview sensors, the RR Model can enable pre-emptive estimation of rack force and modulation of steering torque feedback while driving on roads with slopes, cleats, or potholes [185].

4.5.2 Estimation of Rack Force Components

Results from the CarSim simulation study (Fig. 4.11) illustrate the accuracy of rack force estimates due to steering angle and road profile produced by the BT Model. Inputs used to estimate rack force due to road profile (RF_{Road}) are shown in Fig. 4.11a, and to estimate rack force due to steering angle ($RF_{Steering}$) are shown in Fig. 4.11c. Note that, as mentioned in Section 4.4.2, the input steering angle and road slopes for the simulation study were modeled after the original inputs to Experiment 1. Therefore, the higher fidelity RR model was not necessary for component-wise estimation because the BT model and RR model had similar performance in Experiment 1 (see Table 4.1).

The $RF_{Steering}$ estimated using the BT Model agreed well with $RF_{Steering}$ estimated using CarSim (Fig. 4.11b). The normalized root mean square error between the estimate produced by the BT Model and the estimate produced by CarSim was found to be only 4.27%. Likewise, the estimates of RF_{Road} produced using the BT Model also matched the estimates produced using CarSim with an estimation error of only 5.09%.

Next, I investigated how much the residual rack force ΔRF contributes to the total rack force. To this end, I compared the sum of the component-wise estimates $RF_{Steering}$ and RF_{Road} with the total steering rack force estimated by the BT model and to the rack force measured using the rack

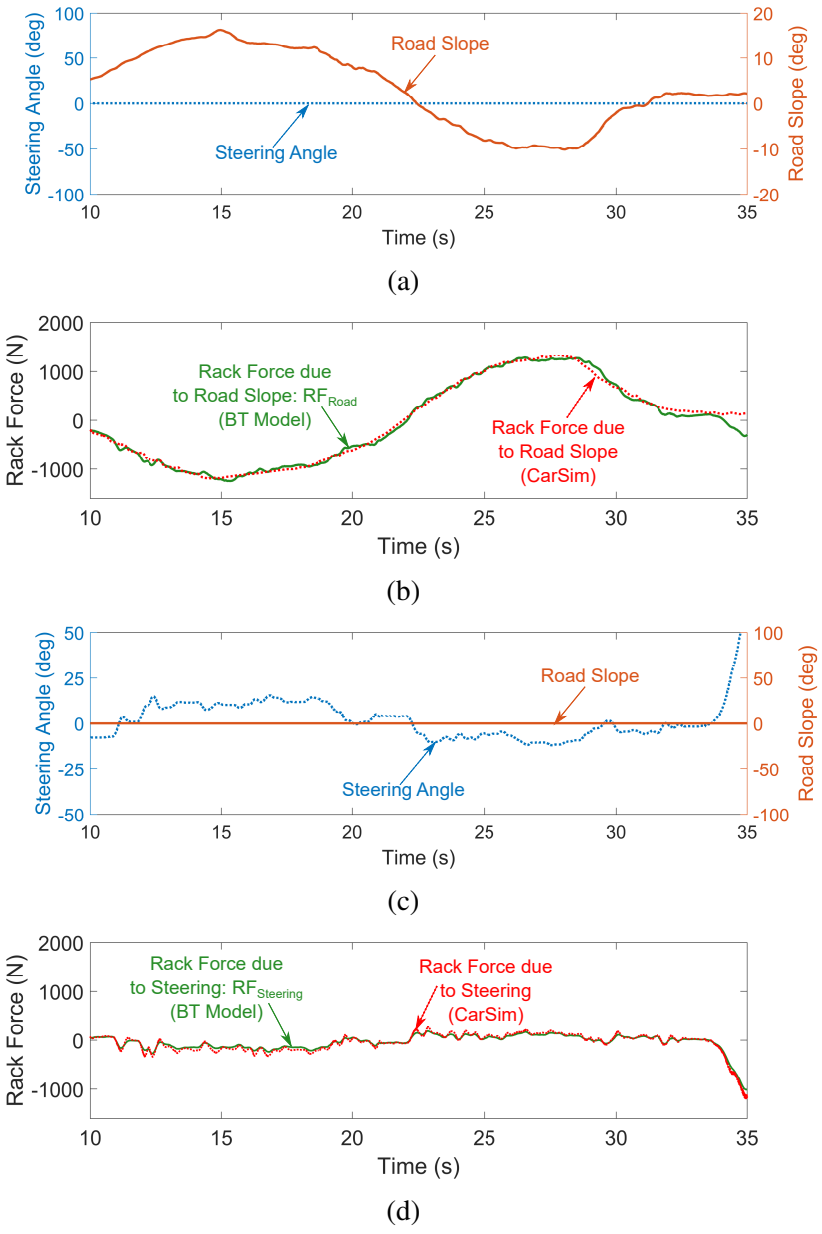

Figure 4.11: Comparison of component wise estimates of rack force generated by the BT Model with the estimates generated by CarSim in Experiment 1. Vehicle speed maintained at about 20 km/h. (a) Input zero steering angle and non-zero road slope. (b) RF_{Road} estimated using the BT Model and using CarSim. (c) Input non-zero steering angle and zero road slope. (d) $RF_{Steering}$ estimated using the BT Model and using CarSim.

force sensor mounted in the vehicle (see Fig. 4.12). The sum of component-wise estimates of rack force matched well with the total steering rack force estimated by the BT Model (Fig. 4.12b). The normalized root mean square error between $RF_{Steering} + RF_{Road}$ and the rack force RF estimated using the BT Model was found to be only 2.49%. In other words, the influence of residual rack

force ΔRF on total rack force was found to be negligible.

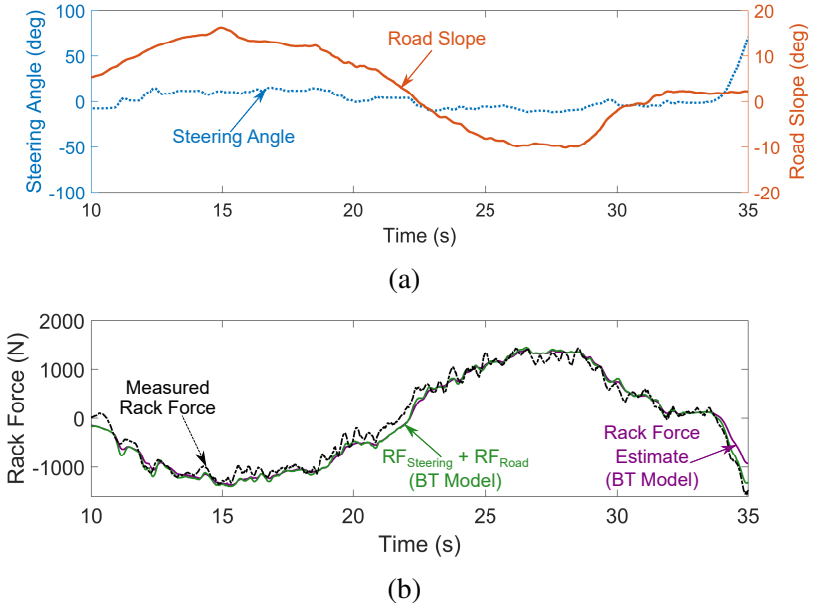

Figure 4.12: Comparison of total rack force estimate as a sum of component-wise rack force estimates generated by the BT Model with the measured rack force and the total rack force estimated using the BT Model. Vehicle speed maintained at about 20 km/h. (a) Input non-zero steering angle and non-zero road slope. (b) Sum of component-wise rack force estimates generated by the BT Model, total rack force generated by the BT Model, and rack force measured using sensor.

The results from the simulation study show that for driving on road slopes with large variations, the BT Model is capable of producing component-wise estimates of rack force to perform targeted compensation. Considering the higher DOF VTM-based estimator in CarSim as a reference, the independent estimates of rack force due to steering angle and due to road profile produced by the simpler BT Model were both found to be accurate. Moreover, at least for the road slope variation of about $-13°$ to $13°$ and steering angle variation of about $-20°$ to $20°$, the residual rack was found to be negligible and rack force turned out to be mostly composed of $RF_{Steering}$ and RF_{Road}.

The results on the component-wise estimates of rack force can be utilized in the design of power steering control algorithms and driver assist features. Using the independent estimates of the rack force components, controllers may be designed to enable targeted compensation for enhanced steering feel (as suggested in [74,158]). Rack force components can also be suppressed entirely to determine a fault or undesirable behavior in the steering system [147]. Targeted compensation may also have critical applications in the steer-by-wire systems, driving simulators, and hardware-in-loop simulators where re-creating road feel and tuning the steering feel have always been an active area of research [78,149]. The individual components of rack force can also be selectively tuned and displayed to the driver to realize different driving modes such as “luxurious” or “sporty” driving as

discussed in [147].

4.6 Summary and Future Work

In this chapter, I presented three vehicle and tire model based (VTM-based) estimators that are capable of estimating rack force for driving on uneven roads. I investigated the level of tire model complexity required to accurately estimate rack force for driving on low and high frequency road profile variations with aggressive and non-aggressive steering maneuvers. I found that the estimators with non-linear tire models produced more accurate rack force estimates for driving with aggressive steering maneuvers. Moreover, out of the three tire models, the most complex tire model (Rigid Ring tire model) demonstrated the highest rack force estimation accuracy for driving on high frequency road profile variations.

In addition, I tested whether the VTM-based estimators can decompose rack force into individual components and enable targeted compensation to enhance steering feel. To this end I showed that for a driving maneuver with large road slope variation, the component-wise estimates of rack force produced by one of the three estimators match the component-wise estimates produced by a higher DOF vehicle and tire model estimator available in a commercial vehicle dynamics package (CarSim). For one driving experiment, I also showed that rack force seems to primarily consist of rack force due to steering angle and due to road profile even though rack force is a nonlinear function of steering angle and road profile.

In the driving experiments presented in this chapter, the speed was maintained consistent in order to highlight the individual effects of steering angle and road profile on rack force. Likewise, the friction conditions were assumed constant, but varying friction conditions could significantly affect rack force estimation [148]. In future, it would be interesting to explore the effects of varying speed and friction on the rack force estimates. The tire model presented in this chapter could be also supplemented with friction estimators like those presented in [186,187] to estimate friction coefficient in real-time and improve the estimation performance.

This study also assumed that an accurate estimate of road profile was always available. Since the study was limited to only two types of road profile variations (road slopes and cleats) I only used/developed methods that could estimate those specific types of road profile changes. Road profile estimation using advanced methods, such as disturbance observers [166] and road preview [168], was considered outside the scope of the study. I believe that in future it would be interesting to explore the effects of using advance road profile estimation methods on the accuracy of rack force estimation. Future work can also focus on studying the effects of varying friction conditions, vehicle speeds, and road profiles on residual rack force and rack force decomposition.

In comparison to other existing estimation techniques, the VTM-based rack force estimators use

significantly more tire and vehicle specific parameters. Future studies can investigate robustness of VTM-based estimators against the uncertainty in the values of the parameters. It will also be worthwhile to explore other tire models such as the Dugoff, LuGre, and Buckhardt models in the future. Future work can also focus on using VTM-based estimators to support development and improvement of EPS control algorithms and advanced driver assist functions, and to perform pre-emptive estimation and rejection of road disturbances using advanced road preview. Finally, the estimators presented in this chapter can be used to produce component-wise estimates of rack force due to steering angle and road profile and perform targeted compensation on the rack force components to improve steering feel.

CHAPTER 5

Modeling Haptic Communication in Physical Human-Human Interaction

5.1 Introduction

A team of two humans, or a *dyad*, is generally more capable than either human performing the same task individually. Experiments have shown that dyads demonstrate higher performance in completing point-to-point movements [82,188], cyclical and continuous aiming movements [84], and tracking moving targets [83,189] when compared with individual agents. The results seem to hold true regardless of the performance and skills of either partner [87]. Investigating the means by which a human-human dyad leads to an increased performance can help design robotic partners that can collaborate efficiently with humans [83,190].

Common explanations for the performance improvement associated with a dyad include load sharing, social facilitation, and haptic communication. Load sharing, that results in lowering the individual forces required to perform a collaborative task, is often not a factor and can be eliminated by halving the load for the single agent (see, for example, [82,83]). Social facilitation, or the effect that people work harder with someone present in the room [191], can also be controlled in the experiment design [82].

Haptic communication is believed to be one of the primary reasons for the performance improvement observed in dyads [54,82,83,85,87]. Haptic communication involves exchange of force or velocity signals between the partners who are simultaneously engaged in perception (including haptic perception) and motor action. When interacting through a physical link, the members of a dyad grasp the common object or linkage, which then acts as a haptic channel between them. Through the haptic channel, the members can coordinate contributions, communicate intentions, negotiate roles, or adapt behaviors. Thus, haptic communication is thought to facilitate the development of a cooperative strategy and a shared action plan that is not available to dyad members when they work alone [82,83].

While the literature provides significant evidence on the utility of haptic communication in establishing the performance improvement enjoyed by dyads, the evidence remains overwhelmingly empirical. There exists limited knowledge about the interpretation of haptic signals in human-

human dyadic interaction, making it difficult to extend the insights derived from existing studies to designing intuitive human-robot collaboration [86,190]. We are thus motivated to develop models of haptic communication among dyad members that can describe how a human-human dyad, by virtue of haptic interaction, can outperform a single human.

Existing models of haptically interacting dyads focus primarily on human-robot collaboration [85,192]. For example, Evrard and Kheddar [85] presented a model to describe interaction behaviors of human-robot dyads in collaborative physical tasks. Wang et al. [193] presented a Hidden Markov Model approach to enable intuitive handshaking between a human and a robot. Inga et al. [194] proposed an optimal control approach to identify human behavior when haptically collaborating with an automation system. The majority of the existing methods do not describe the behavior of physically interacting human-human dyads.

Haptic human-human interaction has been studied by Feth et al. in [86] where they presented control-theoretic models to describe dyadic interaction in a pursuit tracking task. They showed that the McRuer crossover model [88] describes the behavior of humans working alone as well as when working as human-human dyads. Interestingly, they showed that the crossover model cannot describe the behavior of an agent within a dyad, indicating that haptic communication changes individual behavior. However, the authors did not offer a mechanistic explanation for how the individual behavior changed due to haptic interaction. Moreover, their models did not explain how haptic interaction improved the performance of a dyad.

In this chapter, I present a simplest competent model for haptic communication that is aimed at describing the performance improvement observed in dyadic interaction and the changes in the behavior of an agent within a dyad. Like [86], I adopt the McRuer model to describe human tracking behavior of an individual, but I also explicitly model haptic communication through an object or linkage connecting two agents in the context of a pursuit tracking task. A haptic communication pathway is uncovered that supports a means to describe how two agents acting together can outperform either agent acting alone, even when either agent acts only on half the mass.

5.2 Modeling Haptic Communication

Consider an object of mass m and another of mass $m/2$, each responding with velocity $\dot{y}$ to a force F applied by a single agent (see Figs. 5.1A 5.1B). Let us also consider an object of mass m and velocity $\dot{y}$ responding the forces F_1 and F_2 applied by each of two agents, as shown in 5.1C. Assume $\dot{y}$, F, F_1, and F_2 are all positive when directed to the right. To rule out the possibility of load sharing, that is that two agents can move twice the amount of load that a single agent can move, let us compare the performance of two agents acting on mass m against a single agent acting

on half the mass $m/2$. Through this comparison I aim to show that haptic feedback between the agents will enable a performance that exceeds the additive performance of individual agents. But first a model for haptic communication must be developed and key to that development is to split the mass m into two parts of mass $m/2$ with an intervening spring of stiffness k, as in Fig. 5.1D. The intervening spring may represent a force sensor with large stiffness located at the interaction point between the two masses [190].

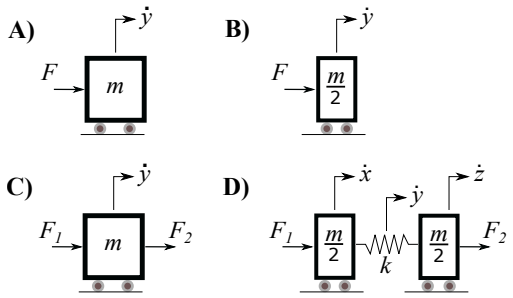

Figure 5.1: A) and B) depict an object manipulated by a single agent; either a full or half-mass respectively. C) and D) depict an object manipulated by two agents. The internal force in a single rigid body (C) can be expressed as the action of an infinitely stiff spring connecting two body halves (D).

As a response to the forces they apply, each agent feels the (common) motion $\dot{y}$ of the object. Yet the agents can communicate with one another through the object. That is, each agent knows what force the other agent is applying even as they modulate their own applied force to produce a desired motion. Intuitively, this haptic communication feels like a reaction force from the object—yet the reaction to an applied force must be a motion. One way to describe haptic communication through the object is by way of internal models: using knowledge of their own applied force and the response motion $\dot{y}$ with a model of mass dynamics $\ddot{y} = \frac{1}{m}(F_1 + F_2)$, each agent can easily figure out the other agent's applied force. In the following, however, I will model haptic communication between the two agents through the internal force $F_k = \frac{1}{2}(F_2 - F_1)$. The internal force can be considered the action of an infinitely stiff spring at the center of the object that holds together the two object halves, each of mass $m/2$ (see Fig. 5.1D). To anticipate a parallel derivation below, I use a block diagram to express F_k as the action of a spring of stiffness k and then "close the loop" to produce an equivalent model.

As shown in Fig. 5.2A, the spring force F_k creates a feedback loop around each of the mass halves. The displacement y is simply the center of the spring, or the average of displacements x and z. The transfer function relating the spring force F_k to the difference $F_2 - F_1$ reads

$$\frac{F_k}{F_2 - F_1} = \frac{1}{\frac{ms^2}{2k} + 2}\bigg|_{k\to\infty} = \tfrac{1}{2}, \tag{5.1}$$

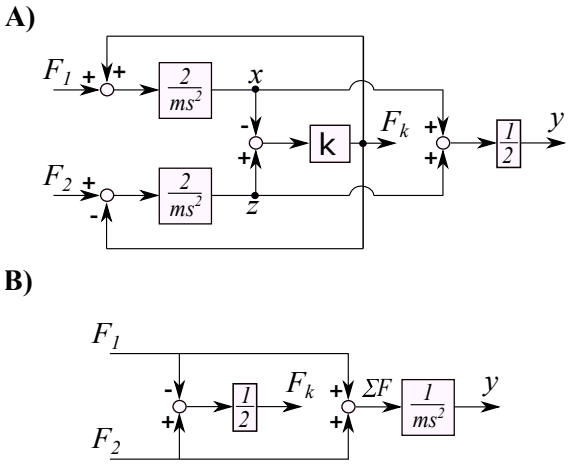

Figure 5.2: As the stiffness k becomes infinitely stiff, it rigidly links the two mass halves. Block diagram (A) may then be replaced by (B), wherein the mass halves are combined and the feedback paths involving the spring force F_k have been eliminated. An internal force computed with the coefficient $1/2$ remains.

where s is the Laplace variable. Thus the block diagram in Fig. 5.2A, with $F_k = k(x - y)$ is equivalent to the block diagram with $F_k = \frac{1}{2}(F_2 - F_1)$ in Fig. 5.2B.

I will adopt the McRuer Crossover model [86,88] to describe the process by which a human operator generates and applies force F to produce object motion y that tracks an unpredictable reference signal r (see Fig. 5.3A). An unpredictable signal does not have a perceptible pattern (for example a large sum of sinusoids) and cannot be addressed with anticipatory control. The McRuer model states that the open loop transfer function $L(s)$, comprising the human controller $C(s)$ and plant dynamics $P(s)$, can be described, within a decade bandwidth centered at ω_c, as an integrator having a crossover frequency ω_c.

$$L(s) = \frac{\omega_c}{s} e^{-\tau s}. \tag{5.2}$$

The pure delay of τ s accounts for neuromotor delay. Thus according to McRuer, the human operator inverts whatever portion of the plant dynamics $P(s) = 1/ms^2$ necessary to produce a loop transfer function $L(s) = \omega_c/s$. For simplicity, the neuromotor delay is ignored. In the case of a simple mass m, human control action becomes a product of mass m, gain ω_c and a differentiator, that is, $C(s) = m\omega_c s$. Assuming $m = 1$kg, human controller reduces to $C(s) = \omega_c s$.

With empirical support from [86], let us assume that each human operator acting as part of a dyad also behaves according to the McRuer model, but acts also on half the mass $m/2$. To model haptic feedback, let us make the internal force F_k available to each human controller as an additional signal input (see Fig. 5.3B). Let us now assume that the response to visual signals r and y that

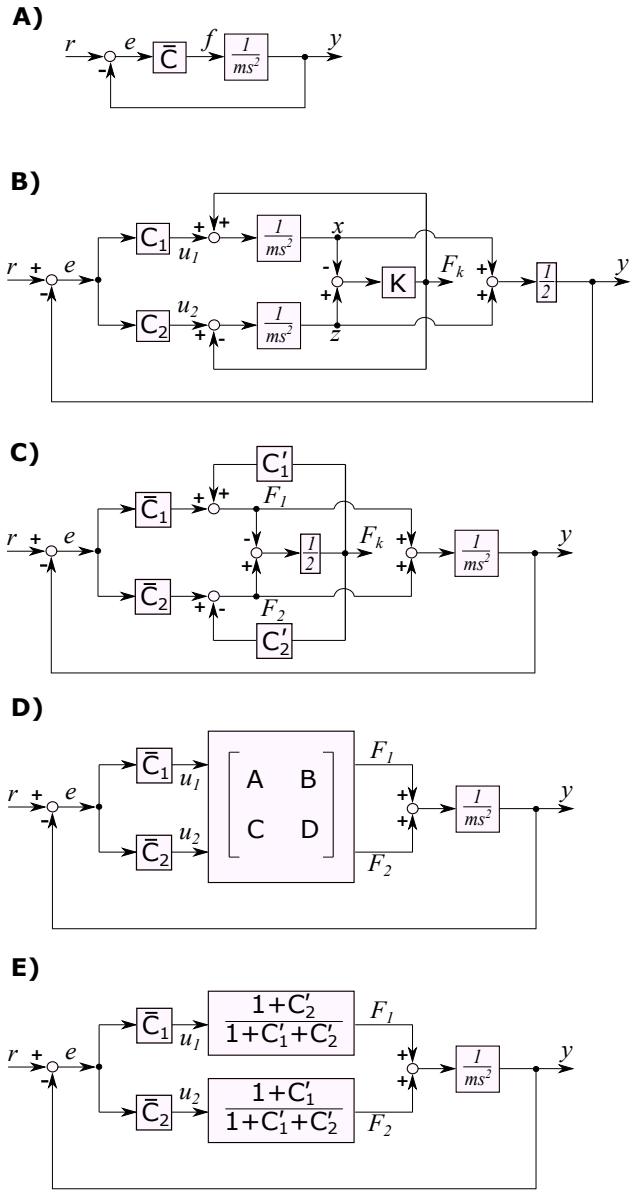

Figure 5.3: Block diagram models of human tracking control in individuals (A) and dyads (B-E) guided by visual and haptic sensory feedback.

follows the McRuer model can be separated from the response to the haptic signal F_k, and call the two parts $\bar{C}_i(s)$ and $C_i'(s)$. In Fig. 5.3C I have both separated $\bar{C}_i$ from $C_i'(s)$ and closed the loop around k (as in Fig. 5.2A). Note that before closing the loop around k, it becomes apparent that $C_i'(s)$ is a signal path in parallel to the spring force F_k for each of the two human operators comprising the dyad. Let us then reduce the block diagram in which $C_1'(s)$ and $C_2'(s)$ appear as feedback operators (assuming they are simply gains). What emerges is a two-port, or 2x2 matrix of transfer functions that relates the applied forces F_1 and F_2 to the control actions u_1 and u_2 (see Fig.

5.3D). A straight-forward reading of the block diagram in Figure 5.3C produces:

$$\begin{bmatrix} F_1 \\ F_2 \end{bmatrix} = \frac{1}{1+\frac{1}{2}(C_1'+C_2')} \begin{bmatrix} 1+\frac{1}{2}C_2' & \frac{1}{2}C_1' \\ \frac{1}{2}C_2' & 1+\frac{1}{2}C_1' \end{bmatrix} \begin{bmatrix} u_1 \\ u_2 \end{bmatrix} \tag{5.3}$$

Note that if $C_1' = C_2' = 0$, the coefficient matrix reduces to the identity matrix, representing the case of no haptic communication between the agents. Otherwise it is quite apparent from Fig. 5.3D that the haptic communication has established a means for the two human agents to cooperate with or compensate for one another. The diagonal entries of the coefficient matrix describe gains that the *other* agent has available to compensate for *each* agent's own control action. For example, C_2' is a gain belonging to agent 2 that multiplies u_1 and appears on the direct path for the applied force F_1 (and vice-versa). The off-diagonal entries of the coefficient matrix add components to each agent's applied force that depend on the other agent's control action. That is, C_1 is a gain belonging to agent 1 that multiplies u_2 and adds to the applied force F_1. Combining the signal pathways yields the alternative expression

$$y = \frac{1}{ms^2}\left[\frac{1+C_2'}{1+\frac{1}{2}(C_1'+C_2')}u_1 + \frac{1+C_1'}{1+\frac{1}{2}(C_1'+C_2')}u_2\right], \tag{5.4}$$

as shown in Fig. 5.3E. From this block diagram and expression it becomes apparent that if $u_1 = u_2$ (the two agents apply perfectly balanced control actions) and either $C_1' = C_2' = 0$ (no haptic communication) or $C_1' = C_2'$ (perfectly balanced compensation), the loop gain $L(s) = C_1' + C_2'$.

Let us assume, in the manner of McRuer, that the signals u_1 and u_2 are produced in response to $e = r - y$ using the control actions $\bar{C}_1(s) = \omega_{c_1} s$ and $\bar{C}_2(s) = \omega_{c_2} s$. The gains ω_{c_1} and ω_{c_2} set the crossover frequencies, and in general they carry different values to represent different skill levels of the two agents. The performance of the dyad acting without haptic feedback will be determined by the parallel configuration of controllers $\bar{C}_1(s)$ and $\bar{C}_2(s)$ and can be characterized by the crossover frequency $\omega_{c1} + \omega_{c2}$. With the addition of haptic feedback, the controllers $C_1'(s)$ and $C_2'(s)$ are made available to the two agents. These control design variables $C_1'(s)$ and $C_2'(s)$ can now be set by each agent to achieve dyad performance that exceeds the performance of either agent acting alone and the performance of the dyad acting without haptic feedback. The new design variables enter the expression for the loop gain in the coefficients u_1 and u_2 appearing in Eq. 5.4. Let us suppose that ω_{c_1} and ω_{c_2} are fixed and further suppose that $C_1'(s)$ and $C_2'(s)$ are simply gains. Essentially *any* performance can be achieved by the dyad with haptic feedback. Dyad performance can be assessed in terms of the crossover frequency ω_c achieved in the loop transfer function $L(s)$ pertaining to the model in Fig. 5.3E. Any loop gain or system crossover frequency can be achieved by setting gain values for C_1' and C_2'. However, to achieve a specific ω_c, the variables C_1' and C_2' must be selected in a coordinated fashion and as functions of ω_{c_1} and ω_{c_2}.

Given a specific desired crossover frequency ω_c for the overall system, and given the baseline performance ω_{c_1} and ω_{c_2} of either agent, Eq. 5.4 can be used to establish a relationship between C_1' and C_2':

$$C_1' = \frac{(\omega_{c_1} - \omega_c)}{\omega_c - \omega_{c_2}} C_2' + \frac{(\omega_{c_1} + \omega_{c_2} - 2\omega_c)}{\omega_c - \omega_{c_2}} \tag{5.5}$$

The values for C_1' and C_2' that together achieve a given dyad performance ω_c lie along a straight line $C_1' = mC_2' + b$ with slope $m = \frac{(\omega_{c_1} - \omega_c)}{\omega_c - \omega_{c_2}}$ and intercept $b = \frac{(\omega_{c_1} + \omega_{c_2} - 2\omega_c)}{\omega_c - \omega_{c_2}}$. These lines are presented in the form of a color map in Fig. 5.4. Interestingly, if the skill levels are the same ($\omega_{c1} = \omega_{c2}$) then there is nothing to be done through haptic communication!

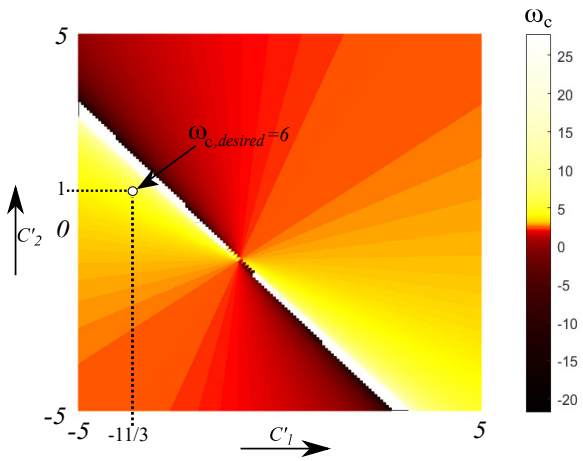

Figure 5.4: The system crossover frequency ω_c is shown as a colormap. The crossover frequency is a function of C_1' and C_2' corresponding to the loop transfer function $L(s)$ of Fig. 5.3E. For the plot shown $\omega_{c_1} = 1$ rad/s and $\omega_{c_2} = 1.5$ rad/s. Note that the frequency ω_c is not defined for the coordinates (C_1', C_2') on the line $C_1' + C_2' = -2$ according to Eq. 5.4.

5.3 Simulation Results

A simulation study was undertaken to visualize the contribution, as predicted by the model, of haptic communication to the performance of a dyad. I aim to validate that with haptic communication the dyad can outperform either agent acting alone, even when either agent acts on only half the mass. In the simulations I supposed that each agent acted to realize a single integrator in the loop transfer function (each agent acted as a pure differentiator), but the second agent used 50% more gain. That is, $\omega_{c_1} = 1$ rad/s and $\omega_{c_2} = 1.5$ rad/s, or $\bar{C}_1 = s$ and $\bar{C}_2 = 1.5s$. I chose 6 rad/s for the desired loop crossover frequency or loop gain ω_c, as indicated in Fig. 5.4. I then selected $C_2' = 1$

and used Eq. 5.5 to obtain $C_1' = -11/3$. The mass m was set to 1 kg.

To visualize the performance of the dyad relative to either agent acting alone, Fig. 5.5A shows the step response of the dyad and each agent acting on the full mass m. Fig. 5.5B shows the dyad and each agent acting on the half mass $m/2$. The dyad outperforms the single agents in both the full and the half mass cases in terms of the response times.

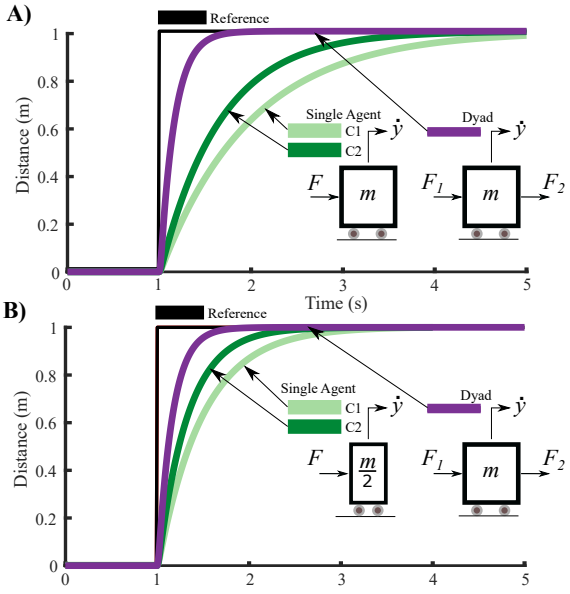

Figure 5.5: Step response of a dyad interacting with a full mass overlaid with the step response of two agents interacting with: A) a full mass and B) a half-mass. The corresponding free-body diagrams for a single agent and a dyad are also shown. The dyad demonstrates faster rise times and outperforms the single agents in both cases.

Fig. 5.6A shows that the dyad attempting to track a unit step reference with the benefit of haptic feedback outperforms a dyad acting without haptic feedback. The response with haptic feedback corresponds to Eq. 5.4 (and Fig. 5.3E) with $C_1' = -11/3$ and $C_2' = -1$, and the response without haptic feedback corresponds to Eq. 5.4 with C_1' and C_2' set to zero. The response is faster (the rise time is lower) with haptic feedback in comparison to the case without feedback. Fig. 5.6B shows the tracking performance for a multi-sine reference. Both the tracking error and the response time of the dyad with haptic feedback are lower indicating higher performance with haptic feedback than without feedback for the multi-sine case as well.

The forces applied by the two agents to track a unit step reference are shown in Fig. 5.7A and Fig. 5.7B respectively. The two agents apply larger individual forces, and hence a larger net force, when haptic feedback is present. Moreover, the magnitude of internal force applied by the agents is larger in the presence of haptic feedback as shown in Fig. 5.7C.

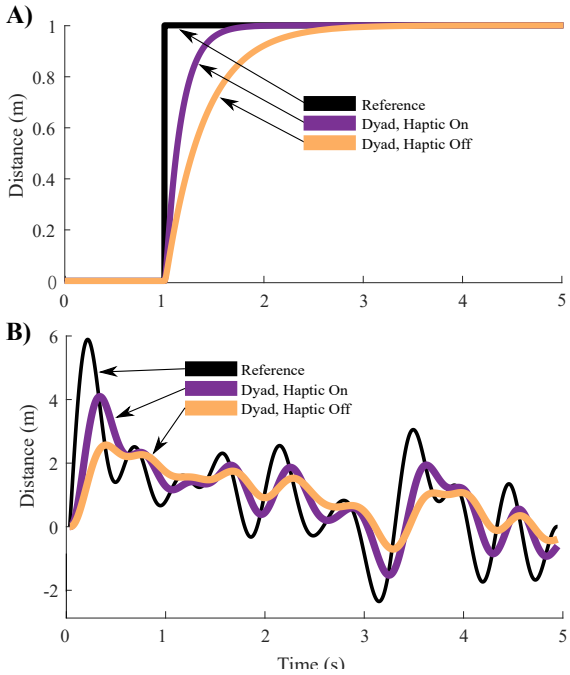

Figure 5.6: The response of single agent and dyad to: A) a step input and B) a multi-sine signal (a sum of sinusoids). The dyad with haptic feedback outperforms the dyad without haptic feedback both in terms of tracking performance and rise times.

5.4 Discussion

Using the internal force as a means to describe haptic communication through an object, I have developed a dyad model that is capable of outperforming either individual acting alone and the same dyad without haptic feedback. Whether the communication pathway that has been modeled actually underlies the performance benefit enjoyed by dyads will have to be empirically validated. A comparison of dyad performance across conditions with and without haptic feedback requires an apparatus capable of rendering the force transmitted across a linkage connecting the two object halves, such as that developed for the experiments presented in [83,86,190]. Indeed, a performance benefit was observed in a tracking task for a dyad with haptic feedback compared to individuals acting on either a half or full mass [83]. It will be interesting to add the dyad acting without haptic feedback and further to determine whether the model predicts the internal forces.

It remains to extract additional testable hypotheses from the developed model. While the signals u_1 and u_2 are not accessible to measurement, one could imagine running a human subject experiment and monitoring the motion y in relation to the reference r along with the applied forces F_1 and F_2 to estimate values for the gains C_1' and C_2' of the model. The force plots in Fig. 5.7 indicate that the dyad members apply larger individual forces and larger internal force ($(F_2 - F_1)/2$) to improve performance when haptic feedback is available, an observation that is already corroborated

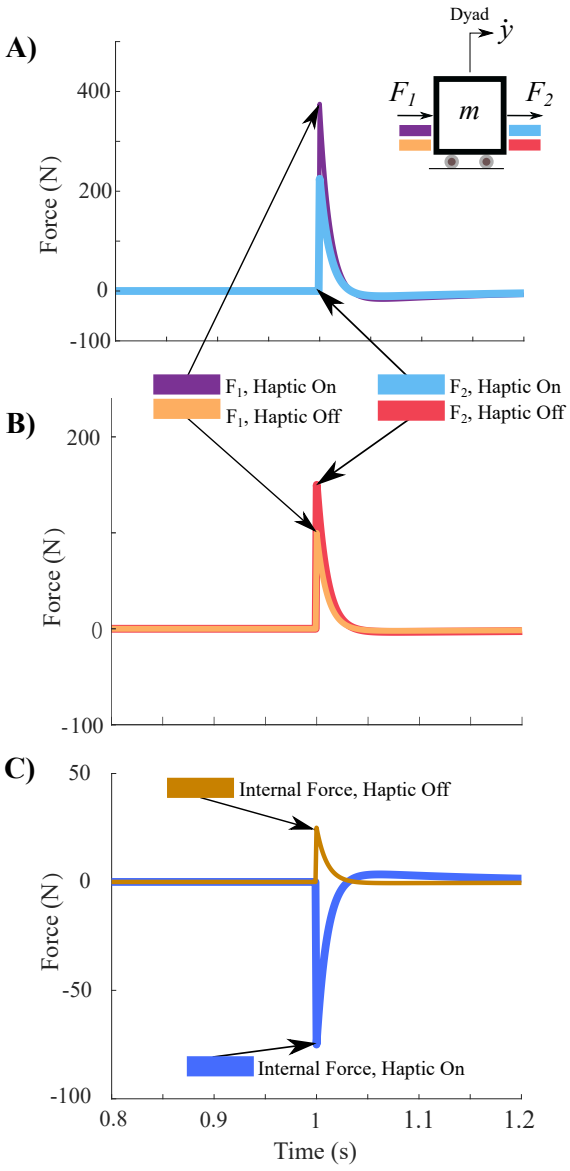

Figure 5.7: The forces F_1 and F_2 applied by each member of a dyad to track a unit step reference A) with haptic feedback and B) without haptic feedback. The resulting internal force is shown in C). Without haptic feedback the dyad members apply lower individual forces and an internal force of lower magnitude when compared with the forces with haptic feedback.

by experiments [86,195]. Thus one way to validate the model would be to compare predicted and observed internal forces and check their correlation with performance improvements. The relationship to cognitive load would also be worth exploring.

As previously highlighted in [82,83], the performance advantage conferred on the dyad does not accrue because of load sharing. As highlighted in Fig. 5.5, the dyad can reach a level of performance that exceeds either agent acting alone, even when the agents move only half the mass. The dyad

performance can in fact be specified in terms of the loop gain ω_c, and with the use of the relationship in Eq. 5.5 and Fig. 5.4, values for C_1' and C_2' can be found to satisfy the desired system loop gain. I showed that it is precisely haptic communication through the object, or awareness of the other agent's actions in addition to one's own actions that enables new feedback loops to be closed around the manipulation goal.

The adaptation that each dyad member undertakes in response to the other member is not a dynamic process in the current model. Nor have I used an adaptive control framework to describe mutual accommodation, though such a treatment might be profitable. A model that includes support for adaptive processes would be necessary to describe negotiation, the adoption of distinct roles, and specialization in dyads. Such processes have been the theme of several conjectures and empirical demonstrations of dyad superiority [196]. Members of specialized dyads may adopt the distinct roles of accelerating and decelerating the shared object [82], of executing and initiating object motion [190], and of controlling and stabilizing the object [197]. While currently there seems to be no interpretation of the feedback gains C_1', C_2' as roles adopted by the members of a dyad, I believe that insights derived from the model can be used to understand how specialization occurs in dyadic interaction.

I have neglected sensorimotor delay in the current model, which would be an important part to any competent model of human behavior. Certainly sensorimotor delay is part of the base McRuer model and could easily be incorporated into the present treatment. I have also not covered dynamic compensation, perhaps derivative compensation that has a physical equivalent in the form of a damper. I would also like to test whether the findings remain the same if I add a damping (and/or a stiffness) term to the plant model which currently only consists of a mass term. Finally, the model formulation only applies to reference tracking for moving targets as presented in [83,189] but I believe it can easily be modified to cover point-to-point movements. Either optimal control approaches or relationships between the information-theoretic basis of Fitt's law [198,199] and its control-theoretic counterparts could possibly be used as starting points.

CHAPTER 6

Conclusion

Semi-autonomous vehicles aim to combine the capabilities of human and automation to improve driving safety and performance. However, developing a combination scheme that preserves the individual strengths of human and automation yet allows them to cover for each other's faults remains a challenge. A majority of existing schemes require the driver to monitor automation actions and take over control in safety-critical scenarios. However, taking over control from an automation system in unexpected scenarios usually requires additional cognitive rather than manual skills, and skills that may be hard to develop and maintain. Drivers left with the task of supervising automation tend to experience a reduction in vigilance, situation awareness, and even skills, and are prone to becoming overreliant on automation. These issues can expand instead of reducing problems for the human driver, especially when faults occur. Guidelines for human-automation interaction design dictate that such issues can be mitigated by designing a human-automation interface that keeps the drivers engaged in the driving task through constant interaction and keeps the driver aware of automation's actions and the external environment through continuous feedback.

This dissertation investigated the potential benefits of incorporating haptic feedback into the human-automation interface for improving driver engagement and human-automation interaction in semi-autonomous driving. I presented findings demonstrating that haptic feedback facilitates smoother authority transitions and improves driver engagement in comparison to the available alternative methods, presented models to estimate haptic feedback from the road for driving on uneven roads, and presented a model for haptic communication aimed at describing how haptic feedback improves shared task performance. These contributions are further described below.

6.1 Contributions

1. **Findings demonstrating that schemes supporting continuous authority transitions, such as haptic shared control, outperform schemes with discrete or instantaneous transitions:** Human-automation teams are particularly prone to errors during control authority transfers. Depending on the driving scenario, drivers may either need to use a discrete control sharing scheme,

where the authority transfers as a lumped whole between human and automation at discrete instants of time, or a continuous control sharing scheme, where authority transfers gradually over a period of time. Knowing which control sharing scheme supports smooth and intuitive transfers of control authority requires directly comparing the schemes with one another. This dissertation presented a driving simulator study that compared the obstacle avoidance performance between continuous and discrete control sharing schemes during human and automation faults. One continuous and two discrete control sharing schemes were implemented in a single driving simulator featuring a motorized steering wheel. In one discrete scheme the transitions were initiated by the driver and in the other by the automation. The continuous control sharing scheme (HSC) supported the best overall driving performance, in terms of obstacle avoidance, maneuvering efficiency, and driver engagement. Team performance suffered most under the discrete control sharing scheme with automation-initiated transitions during automation faults. On the other hand, during human faults, the performance was the lowest under the discrete scheme with driver-initiated transitions. These results were published in [54].

2. **Findings demonstrating the existence of a 'fault protection tradeoff': as the control authority provided to one agent increases, the protection against that agent's faults provided by the other agent reduces:**
Determining how to allocate control authority between human and automation during emergency scenarios is critical to driving safety, especially when both human and automation are subject to faults. However, existing studies do not investigate the influence of different levels of automation authority on emergency obstacle avoidance performance. This dissertation presented a driving simulator study which compared four schemes in their ability to enable successful obstacle evasion in emergency scenarios during driver and automation faults. The steering wheel was either decoupled from the tires and the automation was given full authority, or was coupled to the tires with HSC and the automation was provided high or low mechanical impedance (amount of control authority). A model to describe physical driver-automation interaction was also developed to derive insights into driver behavior. The results highlighted the fault protection tradeoff. Additional results showed that decoupling the drivers invoked out-of-the-loop issues and misled the drivers to believe that they were in control. Moreover, coupled drivers in the high impedance HSC group applied larger steering effort than the other conditions. Low impedance HSC resulted in more obstacle hits during driver faults but prevented more collisions during automation faults. These results were published in [133,200].

3. **Development and validation of road feedback estimators for driving on uneven roads:**
Haptic feedback from the road, or road feedback, is critical to maintaining a driver's awareness of the state of the vehicle and road conditions. Estimates of road feedback are used in a wide

variety of driver assist systems to reduce driver effort and improve steering feel. Conventional road feedback estimators ignore the presence of road profile variations and only consider the steering angle as an input when estimating rack force. In this dissertation, I developed three vehicle and tire dynamics based estimators that enable road feedback estimation on uneven roads. I tested and compared the performance of these three estimators by performing driving experiments on different road profile variations such as road slopes and cleats. I also presented results from a simulation study to demonstrate that the developed estimators are capable of separately estimating the primary components of road feedback: road feedback due to steering angle and road feedback due to road profile. These results were published in [135,178,201].

4. **Simplest competent model for haptic communication to describe the performance improvement observed in physical human-human interaction:**
While the literature provides significant evidence that haptic communication improves the shared performance of two human agents working together, the evidence remains mostly empirical. There exists limited knowledge about the interpretation of haptic signals in human-human physical interaction, making it difficult to extend the insights derived from existing studies to automation design. This dissertation presented a simulation study where internal force was used to model human-human haptic communication through an object. The simulation results uncovered a haptic communication pathway that supported a means to describe how two agents acting together could outperform the two agents acting without haptic feedback or either agent acting alone, even when either agent acted only on half the mass. The results also provided a mechanistic explanation for how the individual behavior could change due to haptic interaction. These results were published in [202].

6.2 Limitations

Following are the main limitations of the work presented in this dissertation:

- **Experimentation on a fixed base driving simulator**: The experiments presented in Chapters 2 and 3 were both performed on a low fidelity fixed base driving simulator in a lab setting. A human driver's response to emergencies on a driving simulator is likely quite different from their response in an actual vehicle where the risk is much higher. While drivers were provided financial compensation for participating in the experiments, they were not provided any reward for avoiding the obstacles which could have influenced their performance. The results in the two experiments also depend on the particular implementation of each control sharing scheme, which might be quite different in actual vehicles. The readers must take these factors into consideration when evaluating the results presented in Chapters 2 and 3.

- **Automation and human fault rates**: While the timing of faults was unpredictable in the

two human subjects experiments presented in Chapters 2 and 3, the fault rates were fixed and rather high. Especially in the first experiment presented in Chapter 2, the fault rates for both human and automation were set at 20% which is unrealistic to expect in actual driving scenarios. Handling of a seldom occurring fault likely differs significantly from a fault that occurs at an expected high rate of 20%. Learning from the Experiment 1, I reduced the rate of faults in Experiment 2 presented in Chapter 3 to make them more 'surprising' and difficult to anticipate. In Experiment 2, driver faults were induced at uneven rates in the trials during an experiment. There were multiple trials in each experiment, and each trial had different surroundings (the time of day and weather), and the locations of the obstacles. While these measures were taken to discourage any learning or adaptation effects, the driver faults were still induced at a higher and more predictable rates than they would occur in actual driving scenarios. In actual driving, fault rates of automation are variable and are not well established. Likewise, fault rates for humans may also vary considering the ever-changing road traffic and driver assist technologies.

- **Absence of speed control**: The experiments presented in Chapters 2 and 3 also did not provide any speed control. Subjects in both experiments reported that the lack of brakes and throttle made it difficult to avoid collisions. While in the real world, drivers may prefer braking instead of steering away from the obstacles, or some combination of the two, past research has shown that for the speed and time-to-collision chosen in the experiments, steering maneuvers result in more successful obstacle evasion than braking [61,64,143]. Moreover, adding speed control in the study would have made it difficult to isolate the influence of the driver's steering behavior on obstacle evasion which was the focus of this dissertation.

- **Lack of warnings and alerts**: Another limitation of the two experiments presented in Chapters 2 and 3 was a lack of warnings and alerts prior to obstacle evasions. Some subjects reported that a warning could have prepared the drivers and improved the obstacle evasion performance (consistent with [64,68]). Especially in the emergency collision avoidance scenarios presented in Chapter 3, which provided only one second to the drivers to avoid the obstacles, a warning could significantly influence obstacle avoidance performance. However, note that one of the prime objectives of the two experiments was to evaluate the sensitivity of different control sharing schemes to unanticipated faults. Adding warnings to the experiments would have made the faults more predictable and would have made it difficult to evaluate the capabilities of the control sharing schemes independent of the warnings.

- **Influence of varying friction conditions and vehicle speed on road feedback estimation**: In the driving experiments presented in Chapter 4, the speed was maintained constant in order to highlight the individual effects of steering angle and road profile on road feedback.

Likewise, the friction conditions were assumed constant, but varying friction conditions could significantly affect road feedback estimation [148]. The tire model used in the road feedback estimators could be also supplemented with friction estimators like those presented in [186,187] to estimate friction coefficient in real-time and improve the estimation performance.

- **Road profile measurements in estimating road feedback**: Road feedback estimators presented in Chapter 4 assumed that an accurate estimate of road profile was always available. Moreover, since the focus of the work in Chapter 4 was limited to only two types of road profile variations (road slopes and cleats), only the methods that could estimate those specific types of road profile changes were used/developed. However, the problem of estimating the road profile in real-time while driving is quite challenging. To account for any other type of road profile variation in road feedback estimation, more work will have to be done on road profile estimation.

- **Plant model and human controller in the haptic communication model**: Human agents were modeled using a simple McRuer model in Chapter 5. While the McRuer crossover model has been shown to describe the pursuit tracking behavior of an individual, only some evidence exists towards its utility in predicting a human's behavior in human-human interaction [86]. I also neglected sensorimotor delay in the McRuer model, which would be an important part to any competent model of human behavior. Furthermore, the designed human controller did not capture the adaptation that each human agent undertakes in response to the other in human-human interaction. Incorporating an adaptive controller in the model would be necessary to describe negotiation, the adoption of distinct roles, and specialization in human-human teams. I have also not tested whether the findings remain the same if I add a damping (and/or a stiffness) term to the plant model which currently only consists of a mass term.

6.3 Future Work

6.3.1 Adaptive impedance haptic shared control

Chapter 3 presented a design tradeoff between the control authority provided to one agent and the protection against that agent's faults provided by the other agent. This became particularly evident when comparing the results between the high and low automation impedance haptic shared control. Using a high automation impedance in HSC resulted in more collisions during automation faults but fewer collisions during driver faults. High impedance HSC was also perceived as discomforting and difficult to overpower by the subjects. On the other hand, low impedance HSC resulted in significantly fewer hits during automation faults and significantly higher hits during driver faults. Low impedance HSC was easier to overpower but failed to suppress driver input during driver faults.

Future studies should therefore focus on designing haptic shared control with automation impedance that is safe to operate during both driver and automation faults. One potential way forward is to combine the advantages of low and high impedance HSC design through an adaptive impedance HSC system. An adaptive impedance HSC system would assume a high level of authority during emergency situations in which the automation has high confidence, and a low level of authority during situations in which the automation has low confidence, so as to grant override power to the human [13,132,144]. The design challenge for such a system would be to estimate automation confidence and to modulate automation impedance as a function of driver intention, sensor precision, and environment complexity.

6.3.2 Multi-axis haptic feedback at the steering wheel

HSC takes its inspiration from two humans collaborating on a manual task. Just like two humans pushing and pulling on an object can read each other's intention through haptic feedback, the human driver and the automation system in HSC can read each other's control intentions (steering angle command) and control authority (mechanical impedance) by feeling the other agent's torque in the axis of control (at the steering wheel). However, two cooperating humans typically supplement their pushing and pulling with other communication channels, which often leads to significant improvements in performance on the shared task. Likewise, haptic feedback in the axis of control can be further supplemented with additional communication channels to further improve driving performance.

One way to introduce an additional channel of communication in HSC is by providing haptic feedback in the axis of steering grip. Human drivers tend to increase their grip on the steering wheel when they desire more control authority [55]. A steering wheel that can sense driver grip force can immediately communicate to the automation system that the driver is sending a takeover request. Moreover, if the same steering interface provides force feedback in the axis of grip it can communicate to the driver whether their takeover request is accepted or denied. The force feedback on the steering wheel can be further accompanied with shape change to make the feedback more noticeable. For example, a driver squeezing the steering wheel to request greater control authority who feels the steering wheel expand in response can immediately know that the takeover request was not granted. On the other hand, if the steering wheel deflates under an increase in grip, the driver will immediately know that the takeover request was granted and that they are now in control. Advantageously, the axis of grip and shape change will be orthogonal to the axis of control, which will ensure that the shape change is independent of the actual steering task further making the interface information-rich. Moreover, feedback through shape change can communicate both visual (change in shape) and tactile (haptic feedback) information.

6.3.3 Adding speed control and warnings to the driving simulator

As mentioned in section 6.2, one limitation of the two experiments presented in Chapters 2 and 3 of this dissertation is the absence of speed control and collision warnings. In future studies it will be worthwhile to add throttle and brake controls to study how the driver's steering input is influenced and supplemented by the driver's speed input. As demonstrated in [61], input at throttle and brakes can further be used to estimate driver intent of avoiding an obstacle, which can be critical in deriving further insights into driver behavior. Likewise, in future experiments it will be valuable to explore the effectiveness of providing haptic, visual, and audio alerts and warnings before the obstacle evasions.

6.3.4 Driver assistance systems utilizing road feedback components

As shown in Chapter 4, there are two primary components of road feedback—road feedback due to steering angle and road feedback due to road profile—and these components can be estimated independently using the developed rack force estimators. Using the component-wise estimates of road feedback, controllers may be designed to enable targeted compensation for enhanced steering feel (as suggested in [74,158]). Targeted compensation may also have applications in the steer-by-wire systems, driving simulators, and hardware-in-loop simulators where re-creating road feel and tuning the steering feel have been an active area of research [78,149]. Road feedback components can also be suppressed entirely to determine a fault or undesirable behavior in the steering system [147]. Finally, they can also be selectively tuned and displayed to the driver to realize different driving modes such as "luxurious" or "sporty" driving as discussed in [147].

6.3.5 Preemptive road feedback estimation and compensation

The estimators developed in Chapter 4 can be utilized in semi and fully autonomous vehicles equipped with advanced road preview technology to estimate road feedback ahead of time. This is possible because the developed estimators use road profile explicitly as input to estimate road feedback. In contrast, the conventional road feedback estimation methods do not use road profile as input limiting them to only estimate road feedback when or after a road profile is traversed. Using the road profile inputs available from road preview sensors (such as cameras, LiDAR and radar) the developed estimators can preemptively estimate the steering torque feedback that the driver will experience in the future [185]. Such estimates can be used to design smarter driver assist algorithms that would preemptively compensate for any steering torque that might result from driving on uneven roads such as slopes, cleats, or potholes, to further reduce driver effort and enhance steering feel.

6.3.6 Empirical validation of haptic communication model

Chapter 5 described a human-human interaction model which revealed a haptic communication pathway that can describe how two agents acting together with haptic feedback can outperform the same two agents without haptic feedback and outperform either agent acting alone. While our simulation results matched the results obtained in some empirical studies performed in the past, they were still strictly theoretical in nature and were not supported by any new human subject experiments. Future studies can perform a comparison of dyad performance across conditions with and without haptic feedback using an apparatus capable of rendering the force transmitted across a linkage connecting the two object halves, such as that developed for the experiments presented in [83,86,190].

The force plots presented in Chapter 5 indicated that the dyad members apply larger individual forces and larger internal force to improve performance when haptic feedback is available, an observation that is already corroborated by experiments [86,195]. Thus another way to validate the model would be to run a human subject experiment to compare predicted and observed internal forces and check their correlation with performance improvements. One could also imagine monitoring the output in relation to the reference along with the applied forces to estimate values for the gains that are hypothesized to enable performance improvement with haptic communication. These gains can then be utilized to design a robotic partner (or an automation system) that can collaborate more efficiently with the human operator.

BIBLIOGRAPHY

[1] V. V. Dixit, S. Chand, and D. J. Nair, "Autonomous vehicles: disengagements, accidents and reaction times," *PLoS one*, vol. 11, no. 12, p. e0168054, 2016.

[2] D. J. Fagnant and K. Kockelman, "Preparing a nation for autonomous vehicles: opportunities, barriers and policy recommendations," *Transportation Research Part A: Policy and Practice*, vol. 77, pp. 167–181, 2015.

[3] S. Singh, "Critical reasons for crashes investigated in the national motor vehicle crash causation survey," National Highway Traffic Safety Administration, Tech. Rep., 2015.

[4] S. J. Anderson, S. B. Karumanchi, and K. Iagnemma, "Constraint-based planning and control for safe, semi-autonomous operation of vehicles," in *2012 IEEE intelligent vehicles symposium*. IEEE, 2012, pp. 383–388.

[5] B. Brown and E. Laurier, "The trouble with autopilots: Assisted and autonomous driving on the social road," in *Proceedings of the 2017 CHI Conference on Human Factors in Computing Systems*, 2017, pp. 416–429.

[6] A. Nunes, B. Reimer, and J. F. Coughlin, "People must retain control of autonomous vehicles," *Nature*, vol. 556, no. 7700, pp. 169–171, 2018.

[7] D. Petrović, R. Mijailović, and D. Pešić, "Traffic accidents with autonomous vehicles: type of collisions, manoeuvres and errors of conventional vehicles' drivers," *Transportation research procedia*, vol. 45, pp. 161–168, 2020.

[8] F. M. Favarò, N. Nader, S. O. Eurich, M. Tripp, and N. Varadaraju, "Examining accident reports involving autonomous vehicles in california," *PLoS one*, vol. 12, no. 9, p. e0184952, 2017.

[9] F. Favarò, S. Eurich, and N. Nader, "Autonomous vehicles' disengagements: Trends, triggers, and regulatory limitations," *Accident Analysis & Prevention*, vol. 110, pp. 136–148, 2018.

[10] I. Wolf, "The interaction between humans and autonomous agents," in *Autonomous driving*. Springer, 2016, pp. 103–124.

[11] SAE On-Road Automated Vehicle Standards Committee, "Taxonomy and definitions for terms related to on-road motor vehicle automated driving systems," *SAE International*, 2014.

[12] M. Steele and R. B. Gillespie, "Shared control between human and machine: Using a haptic steering wheel to aid in land vehicle guidance," in *Proceedings of the human factors and ergonomics society annual meeting*, vol. 45, no. 23. SAGE Publications Sage CA: Los Angeles, CA, 2001, pp. 1671–1675.

[13] D. A. Abbink, M. Mulder, and E. R. Boer, "Haptic shared control: smoothly shifting control authority?" *Cognition, Technology & Work*, vol. 14, no. 1, pp. 19–28, 2012.

[14] M. A. Goodrich, J. W. Crandall, and E. Barakova, "Teleoperation and beyond for assistive humanoid robots," *Reviews of Human Factors and Ergonomics*, vol. 9, no. 1, pp. 175–226, 2013.

[15] J. Y. Chen and M. J. Barnes, "Human–agent teaming for multirobot control: A review of human factors issues," *IEEE Transactions on Human-Machine Systems*, vol. 44, no. 1, pp. 13–29, 2014.

[16] A. Chialastri, "Automation in aviation," in *Automation*. IntechOpen, 2012.

[17] N. B. Sarter, D. D. Woods, C. E. Billings *et al.*, "Automation surprises," *Handbook of human factors and ergonomics*, vol. 2, pp. 1926–1943, 1997.

[18] M. Mulder, D. A. Abbink, and E. R. Boer, "Sharing control with haptics: Seamless driver support from manual to automatic control," *Human factors*, vol. 54, no. 5, pp. 786–798, 2012.

[19] M. R. Endsley and E. O. Kiris, "The out-of-the-loop performance problem and level of control in automation," *Human factors*, vol. 37, no. 2, pp. 381–394, 1995.

[20] R. Parasuraman and V. Riley, "Humans and automation: Use, misuse, disuse, abuse," *Human factors*, vol. 39, no. 2, pp. 230–253, 1997.

[21] L. Bainbridge, "Ironies of automation," in *Analysis, Design and Evaluation of Man–Machine Systems*. Elsevier, 1983, pp. 129–135.

[22] M. P. Linegang, H. A. Stoner, M. J. Patterson, B. D. Seppelt, J. D. Hoffman, Z. B. Crittendon, and J. D. Lee, "Human-automation collaboration in dynamic mission planning: A challenge requiring an ecological approach," in *Proceedings of the human factors and ergonomics society annual meeting*, vol. 50, no. 23. SAGE Publications Sage CA: Los Angeles, CA, 2006, pp. 2482–2486.

[23] H. Van den Broek, J. M. Schraagen, G. te Brake, and J. van Diggelen, "Approaching full autonomy in the maritime domain: paradigm choices and human factors challenges," *MTEC2017, Singapore, Apr*, pp. 26–28, 2017.

[24] K. Pazouki, N. Forbes, R. A. Norman, and M. D. Woodward, "Investigation on the impact of human-automation interaction in maritime operations," *Ocean engineering*, vol. 153, pp. 297–304, 2018.

[25] A. Fast-Berglund, S. Mattsson, and L. Bligard, "Finding trends in human-automation interaction research in order to formulate a cognitive automation strategy for final assembly," *International Journal of Advanced Robotics and Automation*, vol. 1, no. 2, pp. 1–7, 2016.

[26] A. Börütecene and J. Löwgren, "Designing human-automation collaboration for predictive maintenance," in *Companion Publication of the 2020 ACM Designing Interactive Systems Conference*, 2020, pp. 251–256.

[27] D. Golightly, S. Sharples, H. Patel, and S. Ratchev, "Manufacturing in the cloud: A human factors perspective," *International Journal of Industrial Ergonomics*, vol. 55, pp. 12–21, 2016.

[28] Å. Fasth, J. Stahre, K. Dencker, W. Karwowski, and G. Salvendy, "Level of automation analysis in manufacturing systems," *Advances in human factors, ergonomics, and safety in manufacturing and service industries*, pp. 233–242, 2010.

[29] G. Michalos, S. Makris, N. Papakostas, D. Mourtzis, and G. Chryssolouris, "Automotive assembly technologies review: challenges and outlook for a flexible and adaptive approach," *CIRP Journal of Manufacturing Science and Technology*, vol. 2, no. 2, pp. 81–91, 2010.

[30] S. Mattsson, L.-O. Bligård, A. Fast-Berglund, and J. Stahre, "Using usability to measure interaction in final assembly," *IFAC Proceedings Volumes*, vol. 46, no. 15, pp. 64–69, 2013.

[31] G. Charalambous, S. Fletcher, and P. Webb, "Human-automation collaboration in manufacturing: identifying key implementation factors," in *Proceedings of the International Conference on Ergonomics & Human Factors*, 2013, p. 59.

[32] M. Peruzzini and M. Pellicciari, "A framework to design a human-centred adaptive manufacturing system for aging workers," *Advanced Engineering Informatics*, vol. 33, pp. 330–349, 2017.

[33] T. Megaw, "The definition and measurement of mental workload," *Evaluation of human work*, vol. 3, pp. 541–542, 2005.

[34] M. Zecca, M. Saito, N. Endo, Y. Mizoguchi, K. Itoh, H. Takanobu, and A. Takanishi, "Waseda bioinstrumentation system wb-2-the new inertial measurement unit for the new motion caption system–," in *2007 IEEE International Conference on Robotics and Biomimetics (ROBIO)*. IEEE, 2007, pp. 139–144.

[35] T. Arai, R. Kato, and M. Fujita, "Assessment of operator stress induced by robot collaboration in assembly," *CIRP annals*, vol. 59, no. 1, pp. 5–8, 2010.

[36] J. Jiao, F. Zhou, N. Z. Gebraeel, and V. Duffy, "Towards augmenting cyber-physical-human collaborative cognition for human-automation interaction in complex manufacturing and operational environments," *International Journal of Production Research*, vol. 58, no. 16, pp. 5089–5111, 2020.

[37] A. Bhardwaj, A. Jain, and V. Agarwal, "Preoperative planning simulator with haptic feedback for raven-ii surgical robotics platform," in *2016 3rd International Conference on Computing for Sustainable Global Development (INDIACom)*. IEEE, 2016, pp. 2443–2448.

[38] A. Garcia-Ruiz, M. Gagner, J. H. Miller, C. P. Steiner, and J. F. Hahn, "Manual vs robotically assisted laparoscopic surgery in the performance of basic manipulation and suturing tasks," *Archives of surgery*, vol. 133, no. 9, pp. 957–961, 1998.

[39] J. Rosen, B. Hannaford, M. P. MacFarlane, and M. N. Sinanan, "Force controlled and teleoperated endoscopic grasper for minimally invasive surgery-experimental performance evaluation," *IEEE Transactions on biomedical engineering*, vol. 46, no. 10, pp. 1212–1221, 1999.

[40] D. Nio, W. Bemelman, O. Busch, B. Vrouenraets, and D. Gouma, "Robot-assisted laparoscopic cholecystectomy versus conventional laparoscopic cholecystectomy: a comparative study," *Surgical Endoscopy And Other Interventional Techniques*, vol. 18, no. 3, pp. 379–382, 2004.

[41] K. Catchpole, C. Perkins, C. Bresee, M. J. Solnik, B. Sherman, J. Fritch, B. Gross, S. Jagannathan, N. Hakami-Majd, R. Avenido *et al.*, "Safety, efficiency and learning curves in robotic surgery: a human factors analysis," *Surgical endoscopy*, vol. 30, no. 9, pp. 3749–3761, 2016.

[42] C. G. Cao and G. Rogers, "Robotics in health care: Hf issues in surgery," *Handbook of Human Factors and Ergonomics in Health Care and Patient Safety. Mahwah: Lawrence Earlbaum & Associates*, pp. 411–421, 2007.

[43] A. C. Edmondson, R. M. Bohmer, and G. P. Pisano, "Disrupted routines: Team learning and new technology implementation in hospitals," *Administrative science quarterly*, vol. 46, no. 4, pp. 685–716, 2001.

[44] M. Schäfer, M. Lauper, and L. Krähenbühl, "A nation's experience of bleeding complications during laparoscopy," *The American journal of surgery*, vol. 180, no. 1, pp. 73–77, 2000.

[45] L. W. Way, L. Stewart, W. Gantert, K. Liu, C. M. Lee, K. Whang, and J. G. Hunter, "Causes and prevention of laparoscopic bile duct injuries: analysis of 252 cases from a human factors and cognitive psychology perspective," *Annals of surgery*, vol. 237, no. 4, p. 460, 2003.

[46] M. B. Bešlin, "Bile duct injuries during open and laparoscopic cholecystectomy at sestre milosrdnice university hospital rom 1995 till 2001," *Acta Clin Croat*, vol. 42, no. 3, pp. 217–223, 2003.

[47] D. A. Norman, "The 'problem' with automation: inappropriate feedback and interaction, not 'over-automation'," *Philosophical Transactions of the Royal Society of London. B, Biological Sciences*, vol. 327, no. 1241, pp. 585–593, 1990.

[48] C. E. Billings, *Aviation Automation: The Search For a Human-centered Approach*. CRC Press, 2018.

[49] D. Abbink and M. Mulder, "Neuromuscular analysis as a guideline in designing shared control," *Advances in Haptics*, pp. 499–517, 2010.

[50] P. G. Griffiths and R. B. Gillespie, "Shared control between human and machine: haptic display of automation during manual control of vehicle heading," *In: Proc. 12th International Symposium on Haptic Interfaces for Virtual Environment and Teleoperator Systems (HAPTICS)*, pp. 358–366, 2004.

[51] B. A. Forsyth and K. E. MacLean, "Predictive haptic guidance: Intelligent user assistance for the control of dynamic tasks," *IEEE transactions on visualization and computer graphics*, vol. 12, no. 1, pp. 103–113, 2005.

[52] M. Mulder, D. a. Abbink, and E. R. Boer, "The effect of haptic guidance on curve negotiation behavior of young, experienced drivers," *Conference Proceedings - IEEE International Conference on Systems, Man and Cybernetics*, pp. 804–809, 2008.

[53] S. M. Erlien, "Shared vehicle control using safe driving envelopes for obstacle avoidance and stability," Ph.D. dissertation, Stanford University, 2015.

[54] A. Bhardwaj, A. H. Ghasemi, Y. Zheng, H. Febbo, P. Jayakumar, T. Ersal, J. L. Stein, and R. B. Gillespie, "Who's the boss? arbitrating control authority between a human driver and automation system," *Transportation Research Part F: Traffic Psychology and Behaviour*, vol. 68, pp. 144–160, 2020.

[55] H. Nakamura, D. Abbink, and M. Mulder, "Is grip strength related to neuromuscular admittance during steering wheel control?" in *2011 IEEE International Conference on Systems, Man, and Cybernetics*. IEEE, 2011, pp. 1658–1663.

[56] P. G. Griffiths and R. B. Gillespie, "Sharing control between humans and automation using haptic interface: primary and secondary task performance benefits," *Human factors*, vol. 47, no. 3, pp. 574–590, 2005.

[57] K. K. Tsoi, M. Mulder, and D. A. Abbink, "Balancing safety and support: Changing lanes with a haptic lane-keeping support system," in *2010 IEEE international conference on systems, man and cybernetics*. IEEE, 2010, pp. 1236–1243.

[58] M. Della Penna, M. M. van Paassen, D. A. Abbink, M. Mulder, and M. Mulder, "Reducing steering wheel stiffness is beneficial in supporting evasive maneuvers," in *2010 IEEE International Conference on Systems, Man and Cybernetics*. IEEE, 2010, pp. 1628–1635.

[59] F. Mars, D. Mathieu, and J.-M. Hoc, "Analysis of human-machine cooperation when driving with different degrees of haptic shared control," *IEEE Transactions on Haptics*, vol. 1412, no. c, pp. 1–1, 2014.

[60] S. M. Petermeijer, D. A. Abbink, and J. C. de Winter, "Should drivers be operating within an automation-free bandwidth? evaluating haptic steering support systems with different levels of authority," *Human factors*, vol. 57, no. 1, pp. 5–20, 2015.

[61] M. Heesen, M. Dziennus, T. Hesse, A. Schieben, C. Brunken, C. Löper, J. Kelsch, and M. Baumann, "Interaction design of automatic steering for collision avoidance: challenges and potentials of driver decoupling," *IET intelligent transport systems*, vol. 9, no. 1, pp. 95–104, 2014.

[62] N. Fricke, S. Griesche, A. Schieben, T. Hesse, and M. Baumann, "Driver behavior following an automatic steering intervention," *Accident Analysis & Prevention*, vol. 83, pp. 190–196, 2015.

[63] A. Schieben, S. Griesche, T. Hesse, N. Fricke, and M. Baumann, "Evaluation of three different interaction designs for an automatic steering intervention," *Transportation research part F: traffic psychology and behaviour*, vol. 27, pp. 238–251, 2014.

[64] M. Sieber, K.-H. Siedersberger, A. Siegel, and B. Färber, "Automatic emergency steering with distracted drivers: Effects of intervention design," in *2015 IEEE 18th International Conference on Intelligent Transportation Systems*. IEEE, 2015, pp. 2040–2045.

[65] S. G. Klauer, V. L. Neale, T. A. Dingus, D. Ramsey, and J. Sudweeks, "Driver inattention: A contributing factor to crashes and near-crashes," *Proceedings of the Human Factors and Ergonomics Society Annual Meeting*, vol. 49, no. 22, pp. 1922–1926, 2005.

[66] Y. Seto, K. Minegishi, Z. Yang, and T. Kobayashi, "Research on detection of braking reactions in emergency situations," in *The Dynamics of Vehicles on Roads and on Tracks. Proceedings of the 18th IAVSD Symposium Held In Kanagawa, Japan, August 24-30, 2003*, 2004.

[67] P. Kerschbaum, L. Lorenz, and K. Bengler, "Highly automated driving with a decoupled steering wheel," in *Proceedings of the human factors and ergonomics society annual meeting*, vol. 58, no. 1. SAGE Publications Sage CA: Los Angeles, CA, 2014, pp. 1686–1690.

[68] T. Hesse, A. Schieben, M. Heesen, M. Dziennus, S. Griesche, and F. Köster, "Interaction design for automation initiated steering manoeuvres for collision avoidance," in *6. Tagung Fahrerassistenzsysteme*, 2013.

[69] J. Dornhege, S. Nolden, and M. Mayer, "Steering torque disturbance rejection," *SAE International Journal of Vehicle Dynamics, Stability, and NVH*, vol. 1, no. 2017-01-1482, pp. 165–172, 2017.

[70] K. Yamamoto, O. Sename, D. Koenig, and P. Moulaire, "Design and experimentation of an lpv extended state feedback control on electric power steering systems," *Control Engineering Practice*, vol. 90, pp. 123–132, 2019.

[71] F. Vinattieri, T. Wright, R. Capitani, C. Annicchiarico, and G. Danisi, "Target setting and structural design of an EPS-in-the-loop test bench for steering feeling simulation," SAE Technical Paper, Tech. Rep., 2016.

[72] R. Greul, T. Werner, and J. Strecker, "Method for determining a rack force for a steering apparatus and steering apparatus," Mar. 1 2016, uS Patent 9,272,732.

[73] J. Strecker and T. Werner, "Method for determining a toothed rack force for a steering device in a vehicle," Jul. 22 2014, uS Patent 8,788,147.

[74] T. Yang, "A new control framework of electric power steering system based on admittance control," *IEEE Transactions on Control Systems Technology*, vol. 23, no. 2, pp. 762–769, 2014.

[75] A. J. Pick, T. J. Sworn, A. D. Barton, and J. O. P. Farrelly, "Rack force disturbance rejection," Sep. 25 2007, uS Patent 7,273,127.

[76] A. Pick and D. J. Cole, "Dynamic properties of a driver's arms holding a steering wheel," *Proceedings of the Institution of Mechanical Engineers, Part D: Journal of Automobile Engineering*, vol. 221, no. 12, pp. 1475–1486, 2007.

[77] T. Koch, "Untersuchungen zum Lenkgefühl von steer-by-wire Lenksystemen," Ph.D. dissertation, Technische Universität München, 2010.

[78] M. Segawa, S. Nakano, M. Shino, and M. Nagai, "Preliminary study concerning quantitative analysis of steering system using hardware-in-the-loop (HIL) simulator," SAE Technical Paper, Tech. Rep., 2006.

[79] N. Sebanz, H. Bekkering, and G. Knoblich, "Joint action: bodies and minds moving together," *Trends in cognitive sciences*, vol. 10, no. 2, pp. 70–76, 2006.

[80] N. Sebanz and G. Knoblich, "Prediction in joint action: What, when, and where," *Topics in Cognitive Science*, vol. 1, no. 2, pp. 353–367, 2009.

[81] G. Knoblich, S. Butterfill, and N. Sebanz, "Psychological research on joint action: theory and data," *Psychology of learning and motivation*, vol. 54, pp. 59–101, 2011.

[82] K. Reed and M. Peshkin, "Physical Collaboration of Human-Human and Human-Robot Teams," *IEEE Transactions on Haptics*, vol. 1, no. 2, pp. 108–120, jul 2008. [Online]. Available: http://ieeexplore.ieee.org/lpdocs/epic03/wrapper.htm?arnumber=4624256

[83] D. Feth, R. Groten, A. Peer, S. Hirche, and M. Buss, "Performance related energy exchange in haptic human-human interaction in a shared virtual object manipulation task," in *EuroHaptics conference, 2009 and Symposium on Haptic Interfaces for Virtual Environment and Teleoperator Systems. World Haptics 2009. Third Joint*. IEEE, 2009, pp. 338–343.

[84] S. Gentry, E. Feron, and R. Murray-Smith, "Human-human haptic collaboration in cyclical fitts' tasks," in *2005 IEEE/RSJ International Conference on Intelligent Robots and Systems*. IEEE, 2005, pp. 3402–3407.

[85] P. Evrard and A. Kheddar, "Homotopy switching model for dyad haptic interaction in physical collaborative tasks," *Proceedings - 3rd Joint EuroHaptics Conference and Symposium on Haptic Interfaces for Virtual Environment and Teleoperator Systems, World Haptics 2009*, pp. 45–50, 2009.

[86] D. Feth, R. Groten, A. Peer, and M. Buss, "Control-theoretic model of haptic human-human interaction in a pursuit tracking task," in *RO-MAN 2009-The 18th IEEE International Symposium on Robot and Human Interactive Communication*. IEEE, 2009, pp. 1106–1111.

[87] G. Ganesh, A. Takagi, R. Osu, T. Yoshioka, M. Kawato, and E. Burdet, "Two is better than one: Physical interactions improve motor performance in humans," *Scientific Reports*, vol. 4, pp. 1–7, 2014.

[88] D. T. McRuer and H. R. Jex, "A review of quasi-linear pilot models," *IEEE transactions on human factors in electronics*, no. 3, pp. 231–249, 1967.

[89] Z. Lu, R. Happee, C. D. Cabrall, M. Kyriakidis, and J. C. de Winter, "Human factors of transitions in automated driving: A general framework and literature survey," *Transportation Research Part F: Traffic Psychology and Behaviour*, vol. 43, pp. 183–198, 2016.

[90] J. W. Son, M. O. Park *et al.*, "Situation awareness and transitions in highly automated driving a framework and mini-review," *Journal of Ergonomics*, 2017.

[91] A. P. van den Beukel, M. C. van der Voort, and A. O. Eger, "Towards a framework for testing drivers' interaction with partially automated driving," in *2015 IEEE 18th International Conference on Intelligent Transportation Systems*. IEEE, 2015, pp. 1902–1907.

[92] C. Grover, I. Knight, F. Okoro, I. Simmons, G. Couper, P. Massie, and B. Smith, "Automated emergency brake systems: Technical requirements, costs and benefits," Crowthorne: Transportation Research Library, Tech. Rep., 2008.

[93] M. Heesen, M. Dziennus, T. Hesse, A. Schieben, C. Brunken, C. Löper, J. Kelsch, and M. Baumann, "Interaction design of automatic steering for collision avoidance: challenges and potentials of driver decoupling," *IET Intelligent Transport Systems*, vol. 9, no. 1, pp. 95–104, 2015.

[94] S. M. Erlien, S. Fujita, and J. C. Gerdes, "Shared steering control using safe envelopes for obstacle avoidance and vehicle stability," *IEEE Transactions on Intelligent Transportation Systems*, vol. 17, no. 2, pp. 441–451, 2016.

[95] F. Flemisch, M. Heesen, T. Hesse, J. Kelsch, A. Schieben, and J. Beller, "Towards a dynamic balance between humans and automation: Authority, ability, responsibility and control in shared and cooperative control situations," *Cognition, Technology and Work*, vol. 14, no. 1, pp. 3–18, 2012.

[96] Z. Lu, R. Happee, C. D. Cabrall, M. Kyriakidis, and J. C. de Winter, "Human factors of transitions in automated driving: A general framework and literature survey," *Transportation Research Part F: Traffic Psychology and Behaviour*, vol. 43, pp. 183–198, 2016.

[97] K. L. Mosier, "Automation and cognition: Maintaining coherence in the electronic cockpit," in *Advances in Human Performance and Cognitive Engineering research*. Emerald Group Publishing Limited, 2002, pp. 93–121.

[98] J. S. Rubinstein, D. E. Meyer, and J. E. Evans, "Executive control of cognitive processes in task switching." *Journal of Experimental Psychology: Human Perception and Performance*, vol. 27, no. 4, p. 763, 2001.

[99] M. Goodrich, "On maximizing fan-out: Towards controlling multiple unmanned vehicles," *Human-Robot Interactions in Future Military Operations*, pp. 375–395, 2010.

[100] R. Nishimura, T. Wada, and S. Sugiyama, "Haptic shared control in steering operation based on cooperative status between a driver and a driver assistance system," *Journal of Human-Robot Interaction*, vol. 4, no. 3, pp. 19–37, 2015.

[101] F. Mars and P. Chevrel, "Modelling human control of steering for the design of advanced driver assistance systems," *Annual Reviews in Control*, vol. 44, pp. 292–302, 2017.

[102] R. Molloy and R. Parasuraman, "Monitoring an automated system for a single failure: Vigilance and task complexity effects," *Human Factors*, vol. 38, no. 2, pp. 311–322, 1996.

[103] M. Itoh, F. Flemisch, and D. Abbink, "A hierarchical framework to analyze shared control conflicts between human and machine," *IFAC-PapersOnLine*, vol. 49, no. 19, pp. 96–101, 2016.

[104] C. Guo, C. Sentouh, J.-B. Haué, and J.-C. Popieul, "Driver–vehicle cooperation: a hierarchical cooperative control architecture for automated driving systems," *Cognition, Technology & Work*, pp. 1–14, 2019.

[105] F. Flemisch, D. Abbink, M. Itoh, M.-P. Pacaux-Lemoine, and G. Weßel, "Shared control is the sharp end of cooperation: Towards a common framework of joint action, shared control and human machine cooperation," *IFAC-PapersOnLine*, vol. 49, no. 19, pp. 72–77, 2016.

[106] L. Saleh, P. Chevrel, F. Mars, J.-F. Lafay, and F. Claveau, "Human-like cybernetic driver model for lane keeping," *IFAC Proceedings Volumes*, vol. 44, no. 1, pp. 4368–4373, 2011.

[107] A. Eriksson and N. A. Stanton, "Driving performance after self-regulated control transitions in highly automated vehicles," *Human Factors*, vol. 59, no. 8, pp. 1233–1248, 2017.

[108] P. A. Desmond, P. A. Hancock, and J. L. Monette, "Fatigue and automation-induced impairments in simulated driving performance," *Transportation Research Record*, vol. 1628, no. 1, pp. 8–14, 1998.

[109] Y. Zheng, M. J. Brudnak, P. Jayakumar, J. L. Stein, and T. Ersal, "An experimental evaluation of a model-free predictor framework in teleoperated vehicles," in *IFAC Workshop on Time Delay Systems*, vol. 49, 2016, pp. 157–164.

[110] J. Liu, P. Jayakumar, J. Stein, and T. Ersal, "Combined speed and steering control in high speed autonomous ground vehicles for obstacle avoidance using model predictive control," *IEEE Transactions on Vehicular Technology*, 2017.

[111] H. Febbo, J. Liu, P. Jayakumar, J. L. Stein, and T. Ersal, "Moving obstacle avoidance for large, high-speed autonomous ground vehicles," in *2017 American Control Conference (ACC)*. IEEE, 2017, pp. 5568–5573.

[112] J. Liu, P. Jayakumar, J. L. Stein, and T. Ersal, "A study on model fidelity for model predictive control-based obstacle avoidance in high-speed autonomous ground vehicles," *Vehicle System Dynamics*, vol. 54, no. 11, pp. 1629–1650, 2016.

[113] H. Pacejka, *Tire and vehicle dynamics*. Elsevier, 2005.

[114] E. Hollnagel and D. D. Woods, *Joint Cognitive Systems: Foundations of Cognitive Systems Engineering*. CRC Press, 2005.

[115] D. A. Abbink, D. Cleij, M. Mulder, and M. M. van Paassen, "The importance of including knowledge of neuromuscular behaviour in haptic shared control," in *Systems, Man, and Cybernetics (SMC), 2012 IEEE International Conference on*. IEEE, 2012, pp. 3350–3355.

[116] M. A. Benloucif, A.-T. Nguyen, C. Sentouh, and J.-C. Popieul, "A new scheme for haptic shared lateral control in highway driving using trajectory planning," *IFAC-PapersOnLine*, vol. 50, no. 1, pp. 13 834–13 840, 2017.

[117] H. Boessenkool, D. A. Abbink, C. J. Heemskerk, F. C. van der Helm, and J. G. Wildenbeest, "A task-specific analysis of the benefit of haptic shared control during telemanipulation," *IEEE Transactions on Haptics*, vol. 6, no. 1, pp. 2–12, 2013.

[118] C. Masone, P. R. Giordano, H. H. Bülthoff, and A. Franchi, "Semi-autonomous trajectory generation for mobile robots with integral haptic shared control," in *2014 IEEE International Conference on Robotics and Automation (ICRA)*. IEEE, 2014, pp. 6468–6475.

[119] R. Parasuraman, R. Molloy, and I. L. Singh, "Performance consequences of automation-induced 'complacency'," *The International Journal of Aviation Psychology*, vol. 3, no. 1, pp. 1–23, 1993.

[120] J. Wurts, J. L. Stein, and T. Ersal, "Collision imminent steering at high speed using nonlinear model predictive control," *IEEE Transactions on Vehicular Technology*, vol. 69, no. 8, pp. 8278–8289, 2020.

[121] M. Marcano, S. Díaz, J. Pérez, and E. Irigoyen, "A review of shared control for automated vehicles: Theory and applications," *IEEE Transactions on Human-Machine Systems*, 2020.

[122] A. Balachandran, M. Brown, S. M. Erlien, and J. C. Gerdes, "Predictive haptic feedback for obstacle avoidance based on model predictive control," *IEEE Transactions on Automation Science and Engineering*, vol. 13, no. 1, pp. 26–31, 2015.

[123] D. A. Abbink, T. Carlson, M. Mulder, J. C. de Winter, F. Aminravan, T. L. Gibo, and E. R. Boer, "A topology of shared control systems—finding common ground in diversity," *IEEE Transactions on Human-Machine Systems*, vol. 48, no. 5, pp. 509–525, 2018.

[124] F. Rüger, V. Nitsch, and B. Färber, "Automatic evasion seen from the opposing traffic–an investigation with the vehicle in the loop," in *2015 IEEE 18th International Conference on Intelligent Transportation Systems*. IEEE, 2015, pp. 1041–1048.

[125] I. T. Commitee, "Convention on road traffic," *United Nations Economic Commission For Europe*, 1968.

[126] J. Schwarz, "Response 3-code of practice for development, validation and market introduction of advanced driver assistance systems," *VDI BERICHTE*, vol. 1960, p. 465, 2006.

[127] M. S. Young, N. A. Stanton, and D. Harris, "Driving automation: learning from aviation about design philosophies," *International Journal of Vehicle Design*, vol. 45, no. 3, pp. 323–338, 2007.

[128] N. B. Sarter and D. D. Woods, "How in the world did we ever get into that mode? mode error and awareness in supervisory control," *Human factors*, vol. 37, no. 1, pp. 5–19, 1995.

[129] R. Parasuraman, T. B. Sheridan, and C. D. Wickens, "A model for types and levels of human interaction with automation," *IEEE Transactions on systems, man, and cybernetics-Part A: Systems and Humans*, vol. 30, no. 3, pp. 286–297, 2000.

[130] F. Flemisch, M. Heesen, J. Kelsch, J. Schindler, C. Preusche, and J. Dittrich, "Shared and cooperative movement control of intelligent technical systems: Sketch of the design space of haptic-multimodal coupling between operator, co-automation, base system and environment," *IFAC Proceedings Volumes*, vol. 43, no. 13, pp. 304–309, 2010.

[131] F. Mars, M. Deroo, and J.-M. Hoc, "Analysis of human-machine cooperation when driving with different degrees of haptic shared control," *IEEE transactions on haptics*, vol. 7, no. 3, pp. 324–333, 2014.

[132] H. M. Zwaan, S. M. Petermeijer, and D. A. Abbink, "Haptic shared steering control with an adaptive level of authority based on time-to-line crossing," *IFAC-PapersOnLine*, vol. 52, no. 19, pp. 49–54, 2019.

[133] A. Bhardwaj, Y. Lu, S. Pan, N. Sarter, and B. Gillespie, "The effects of driver coupling and automation impedance on emergency steering interventions," in *2020 IEEE International Conference on Systems, Man, and Cybernetics (SMC)*. IEEE, 2020, pp. 1738–1744.

[134] J. M. Snider *et al.*, "Automatic steering methods for autonomous automobile path tracking," *Robotics Institute, Pittsburgh, PA, Tech. Rep. CMU-RITR-09-08*, 2009.

[135] A. Bhardwaj, B. Gillespie, and J. Freudenberg, "Estimating rack force due to road slopes for electric power steering systems," in *2019 American Control Conference (ACC)*. IEEE, 2019, pp. 328–334.

[136] P. Boehm, A. H. Ghasemi, S. O'Modhrain, P. Jayakumar, and R. B. Gillespie, "Architectures for Shared Control of Vehicle Steering," *IFAC-PapersOnLine*, vol. 49, no. 19, pp. 639–644, 2016.

[137] T. Flash, "The control of hand equilibrium trajectories in multi-joint arm movements," *Biological cybernetics*, vol. 57, no. 4, pp. 257–274, 1987.

[138] J. B. Dingwell, C. D. Mah, and F. A. Mussa-Ivaldi, "Manipulating objects with internal degrees of freedom: evidence for model-based control," *Journal of Neurophysiology*, vol. 88, no. 1, pp. 222–235, 2002.

[139] A. Sebok and C. D. Wickens, "Implementing lumberjacks and black swans into model-based tools to support human–automation interaction," *Human factors*, vol. 59, no. 2, pp. 189–203, 2017.

[140] S. Shen and D. M. Neyens, "Assessing drivers' response during automated driver support system failures with non-driving tasks," *Journal of safety research*, vol. 61, pp. 149–155, 2017.

[141] K. M. Wilson, S. Yang, T. Roady, J. Kuo, and M. G. Lenné, "Driver trust & mode confusion in an on-road study of level-2 automated vehicle technology," *Safety Science*, vol. 130, p. 104845, 2020.

[142] V. A. Banks, A. Eriksson, J. O'Donoghue, and N. A. Stanton, "Is partially automated driving a bad idea? observations from an on-road study," *Applied ergonomics*, vol. 68, pp. 138–145, 2018.

[143] L. Adams, "Review of the literature on obstacle avoidance maneuvers: Braking versus steering (umtri-94-19)," *Ann Arbor, MI: University of Michigan Transportation Research Institute (UMTRI)*, 1994.

[144] V. Izadi, A. Bhardwaj, and A. H. Ghasemi, "Impedance modulation for negotiating control authority in a haptic shared control paradigm," in *2020 American Control Conference (ACC)*, 2020, pp. 2478–2483.

[145] S. Grüner, A. Gaedke, and G. G. Karch, "Control of electric power steering systems-from state of art to future challenges," in *Proceedings of the 17th World Congress The International Federation of Automatic Control*, 2008, pp. 10 756–10 757.

[146] A. Marouf, M. Djemai, C. Sentouh, and P. Pudlo, "A new control strategy of an electric-power-assisted steering system," *IEEE Transactions on Vehicular Technology*, vol. 61, no. 8, pp. 3574–3589, 2012.

[147] R. Greul and T. Werner, "Determining a target steering torque in a steering device," Aug. 21 2012, uS Patent 8,249,777.

[148] S. Fankem, T. Weiskircher, and S. Müller, "Model-based rack force estimation for electric power steering," *IFAC Proceedings Volumes*, vol. 47, no. 3, pp. 8469–8474, 2014.

[149] L. Nehaoua, M. Djemai, and P. Pudlo, "Rack force feedback for an electrical power steering simulator," in *Control & Automation (MED), 2012 20th Mediterranean Conference on*. IEEE, 2012, pp. 79–84.

[150] N. Bajcinca, C. Nuthong, and F. Svaricek, "Road feedback estimation for steer-by-wire control," in *2006 IEEE Conference on Computer Aided Control System Design, 2006 IEEE International Conference on Control Applications, 2006 IEEE International Symposium on Intelligent Control*. IEEE, 2006, pp. 1288–1293.

[151] D. Wang and F. Esser, "EPAS system tests using rack force models," SAE Technical Paper, Tech. Rep., 2016.

[152] M. A. Blommer, P. G. Sanders, H. E. Tseng, and D. Wang, "Systems and methods for decoupling steering rack force disturbances in electric steering," Apr. 3 2012, uS Patent 8,150,582.

[153] H. E. Tseng, "Dynamic estimation of road bank angle," *Vehicle system dynamics*, vol. 36, no. 4-5, pp. 307–328, 2001.

[154] H. Eric Tseng, L. Xu, and D. Hrovat, "Estimation of land vehicle roll and pitch angles," *Vehicle System Dynamics*, vol. 45, no. 5, pp. 433–443, 2007.

[155] J. G. Viner, "Rollovers on sideslopes and ditches," *Accident Analysis & Prevention*, vol. 27, no. 4, pp. 483–491, 1995.

[156] S. C. Peters, "Modeling, analysis, and measurement of passenger vehicle stability," Ph.D. dissertation, Massachusetts Institute of Technology, 2006.

[157] T. Weiskircher, S. Fankem, and B. Ayalew, "Rack force estimation for electric power steering," in *ASME 2015 International Design Engineering Technical Conferences and Computers and Information in Engineering Conference*. American Society of Mechanical Engineers, 2015.

[158] M. Hackl and W. Kraemer, "Method and apparatus for operating a steering system for a motor vehicle," Jul. 11 2000, uS Patent 6,085,860.

[159] D. Karnopp, "Motor-driven servo steering system," Apr. 27 1993, uS Patent 5,205,371.

[160] H. Ikeda, M. Endo, and I. Kezobo, "Electric power-steering control apparatus," Nov. 1 2011, uS Patent 8,050,825.

[161] I. Kezobo, M. Kurishige, M. Endo, and T. Kifuku, "Electric power steering control device," Jan. 7 2014, uS Patent 8,626,394.

[162] A. Honisch, M. Lugert, T. Schöning, and S. Hakuli, "Improvement of steering feel virtual approach with HiL," *ATZ worldwide*, vol. 117, no. 6, pp. 10–13, 2015.

[163] T. Toyohira, K. Nakamura, and Y. Tanno, "The validity of EPS control system development using HILs," SAE Technical Paper, Tech. Rep., 2010.

[164] R. Marino and S. Scalzi, "Asymptotic sideslip angle and yaw rate decoupling control in four-wheel steering vehicles," *Vehicle System Dynamics*, vol. 48, no. 9, pp. 999–1019, 2010.

[165] M. Gadola, D. Chindamo, M. Romano, and F. Padula, "Development and validation of a kalman filter-based model for vehicle slip angle estimation," *Vehicle System Dynamics*, vol. 52, no. 1, pp. 68–84, 2014.

[166] M. Doumiati, J. Martinez, O. Sename, L. Dugard, and D. Lechner, "Road profile estimation using an adaptive youla–kučera parametric observer: Comparison to real profilers," *Control Engineering Practice*, vol. 61, pp. 270–278, 2017.

[167] J. C. Tudón-Martínez, S. Fergani, O. Sename, J. J. Martinez, R. Morales-Menendez, and L. Dugard, "Adaptive road profile estimation in semiactive car suspensions," *IEEE Transactions on Control Systems Technology*, vol. 23, no. 6, pp. 2293–2305, 2015.

[168] J.-K. Lee and K.-J. Yoon, "Temporally consistent road surface profile estimation using stereo vision," *IEEE Transactions on Intelligent Transportation Systems*, vol. 19, no. 5, pp. 1618–1628, 2018.

[169] H. Fritz, A. Gern, H. Schiemenz, and C. Bonnet, "Chauffeur assistant: a driver assistance system for commercial vehicles based on fusion of advanced acc and lane keeping," in *IEEE Intelligent Vehicles Symposium, 2004*. IEEE, 2004, pp. 495–500.

[170] J. J. Dawkins, "Model based off-road terrain profile estimation," in *2014 American Control Conference*. IEEE, 2014, pp. 2792–2797.

[171] H. Jansson, E. Kozica, P. Sahlholm, and K. H. Johansson, "Improved road grade estimation using sensor fusion," *Proceedings of the 12th Reglermöte in Stockholm, Sweden*, 2006.

[172] S. R. Pastor and G. L. Tierney, "Method and apparatus for estimating incline and bank angles of a road surface," Aug. 29 1995, uS Patent 5,446,658.

[173] R. Rajamani, *Vehicle dynamics and control*. Springer Science & Business Media, 2011.

[174] A. J. C. Schmeitz, "A semi-empirical three-dimensional model of the pneumatic tyre rolling over arbitrarily uneven road surfaces," Ph.D. dissertation, Delft University of Technology, 2004.

[175] A. Balachandran, S. M. Erlien, and J. C. Gerdes, "The virtual wheel concept for supportive steering feedback during active steering interventions," in *ASME 2014 Dynamic Systems and Control Conference*. American Society of Mechanical Engineers Digital Collection, 2014.

[176] P. Zegelaar and H. Pacejka, "The in-plane dynamics of tyres on uneven roads," *Vehicle System Dynamics*, vol. 25, no. S1, pp. 714–730, 1996.

[177] P. W. A. Zegelaar, "The dynamic response of tyres to brake torque variations and road unevennesses," Ph.D. dissertation, Delft University of Technology, 1998.

[178] A. Bhardwaj, D. Slavin, J. Walsh, J. Freudenberg, and R. B. Gillespie, "Rack force estimation for driving on uneven road surfaces," *IFAC-PapersOnLine*, vol. 53, no. 2, pp. 14 426–14 431, 2020.

[179] E. Bakker, H. B. Pacejka, and L. Lidner, "A new tire model with an application in vehicle dynamics studies," *SAE transactions*, vol. 98, no. 6, pp. 101–113, 1989.

[180] H. B. Pacejka and R. S. Sharp, "Shear force development by pneumatic tyres in steady state conditions: a review of modelling aspects," *Vehicle system dynamics*, vol. 20, no. 3-4, pp. 121–175, 1991.

[181] M. Sayers, "Tire models," Mechanical Simulation Corporation, www.carsim.com, Tech. Rep., 2018.

[182] J. M. Raad and D. Tuttle, "Pull-drift compensation enhancements," Aug. 5 2014, uS Patent 8,798,865.

[183] J. Shah, "Pull drift compensation using active front steering system," Feb. 3 2011, uS Patent App. 12/848,242.

[184] P. Bosch, D. Ammon, and F. Klempau, "Tyre models–desire and reality in respect of vehicle development," *Darmstadter Reifenkolloquium*, vol. 17, pp. 87–101, 2002.

[185] T. Gordon and M. Lidberg, "Automated driving and autonomous functions on road vehicles," *Vehicle System Dynamics*, vol. 53, no. 7, pp. 958–994, 2015.

[186] S. Khaleghian, A. Emami, and S. Taheri, "A technical survey on tire-road friction estimation," *Friction*, vol. 5, no. 2, pp. 123–146, 2017.

[187] R. Rajamani, N. Piyabongkarn, J. Lew, K. Yi, and G. Phanomchoeng, "Tire-road friction-coefficient estimation," *IEEE Control Systems Magazine*, vol. 30, no. 4, pp. 54–69, 2010.

[188] K. Reed, M. Peshkin, M. J. Hartmann, M. Grabowecky, J. Patton, and P. M. Yishton, "Haptically linked dyads are two motor-control systems better than one?" *Psychological Science*, vol. 17, no. 5, pp. 365–366, 2006.

[189] N. Wegner and D. Zeaman, "Team and individual performances on a motor learning task," *Journal of General Psychology*, vol. 55, no. 1, pp. 127–142, 1956.

[190] N. Stefanov, A. Peer, and M. Buss, "Role determination in human-human interaction," *Proceedings - 3rd Joint EuroHaptics Conference and Symposium on Haptic Interfaces for Virtual Environment and Teleoperator Systems, World Haptics 2009*, pp. 51–56, 2009.

[191] R. B. Zajonc, "Social facilitation," *Science*, vol. 149, no. 3681, pp. 269–274, 1965.

[192] A. Bhardwaj, A. Jain, V. Agarwal, and H. Parthasarathy, "Master slave tracking control using adaptive least squares filter," in *2016 3rd International Conference on Computing for Sustainable Global Development (INDIACom)*. IEEE, 2016, pp. 2481–2486.

[193] Z. Wang, A. Peer, and M. Buss, "An hmm approach to realistic haptic human-robot interaction," in *World Haptics 2009-Third Joint EuroHaptics conference and Symposium on Haptic Interfaces for Virtual Environment and Teleoperator Systems*. IEEE, 2009, pp. 374–379.

[194] J. Inga, M. Eitel, M. Flad, and S. Hohmann, "Evaluating human behavior in manual and shared control via inverse optimization," in *2018 IEEE International Conference on Systems, Man, and Cybernetics (SMC)*. IEEE, 2018, pp. 2699–2704.

[195] R. P. Van der Wel, G. Knoblich, and N. Sebanz, "Let the force be with us: dyads exploit haptic coupling for coordination." *Journal of Experimental Psychology: Human Perception and Performance*, vol. 37, no. 5, p. 1420, 2011.

[196] N. Jarrassé, T. Charalambous, and E. Burdet, "A Framework to Describe, Analyze and Generate Interactive Motor Behaviors," *PLoS ONE*, vol. 7, no. 11, 2012.

[197] S. Sheybani, E. J. Izquierdo, and E. Roth, "Evolving dyadic strategies for a cooperative physical task," in *2020 IEEE Haptics Symposium (HAPTICS)*. IEEE, 2020, pp. 684–689.

[198] P. Gawthrop, M. Lakie, and I. Loram, "Predictive feedback control and fitts–law," *Biological cybernetics*, vol. 98, no. 3, pp. 229–238, 2008.

[199] E. Crossman and P. Goodeve, "Feedback control of hand-movement and fitts' law," *The Quarterly Journal of Experimental Psychology Section A*, vol. 35, no. 2, pp. 251–278, 1983.

[200] A. Bhardwaj, Y. Lu, S. Pan, N. Sarter, and B. Gillespie, "Comparing coupled and decoupled steering interface designs for emergency obstacle evasion," *IEEE Access*, 2021 (Accepted).

[201] A. Bhardwaj, D. Slavin, J. Walsh, J. Freudenberg, and R. B. Gillespie, "Estimation and decomposition of rack force for driving on uneven roads," *Control Engineering Practice*, vol. 114, p. 104876, 2021.

[202] A. Bhardwaj, S. Cutlip, and B. Gillespie, "Modeling haptic communication in cooperative teams," in *2021 IEEE World Haptics Conference (WHC)*. IEEE, 2021.